The automation of vehicles in longitudinal and lateral direction based on path following

W.J.A.C. Wiechert

D&C 2017.034

Master's thesis

Coach(es): dr. ir. A.A.J. Lefeber
dr. ir. J. Ploeg (TNO)
dr. ir. E. Silvas (TNO)
MSc. J. Verhaegh (TNO)

Supervisor: prof. dr. H. Nijmeijer

Eindhoven University of Technology
Department of Mechanical Engineering
Dynamics & Control

Eindhoven, February 14, 2017

Summary

The increasing number of vehicles results in a growing number of traffic jams and an increase of environmental pollution. Vehicles that are produced today are accommodated with partial automation systems such as cruise control and lane-keeping assistance. These applications mainly focus on assisting the driver, but have a limited impact on problems such as traffic jams and pollution. Therefore, cooperative driving is considered where the behavior of the individual vehicle is influenced in order to optimize the collective behavior with respect to road throughput and fuel efficiency. The automation of vehicles in longitudinal direction for cooperative driving has been investigated extensively, where research for automation in lateral direction is ongoing. The main objective of this thesis is the design of a longitudinal and lateral controller for the automation of vehicles in a platoon.

The vehicles in the platoon are modeled by means of a kinematic model of a wheeled mobile robot. Controllers for vehicle automation in longitudinal and lateral direction are derived separately. For the lateral controllers, two Lyapunov based controllers are designed for a path following problem. As a results, it is noted that regardless the velocity of the vehicle the path remains unchanged. Using known stability results, globally asymptotically stability is shown. The longitudinal controller is designed based on a cooperative adaptive cruise controller. The controller is derived using input-output linearization of the spacing error dynamics to obtain a linear time-invariant state space model. The performance of these controllers is defined based on the criteria safety, comfort and tracking performance. The controller gains are determined using pole placement and time simulation, considering the these criteria. The controllers are implemented in Simulink and simulations are performed. From these simulations we notice that the vehicles drive in steady state along the same path as their predecessor and follow this predecessor with a desired intervehicle distance. Furthermore, these results are compared with a simulation performed with a tracking controller. The tracking controller converges as fast as possible to the position of the leading vehicle without considering the already traveled trajectory. While the path following controller does take the path of the leader into account while converging towards the it. As a final assessment, the lateral and longitudinal controllers are implemented on a complex wheeled mobile robot model which is validated by experiments. Considering that the leading vehicle drives along a straight line and with a certain velocity profile, the MB follows the leader with a desired intervehicle distance. The lateral error between the MB and the reference vehicle converges to zero and remains stable.

Nomenclature

Abbreviations

ADAS	Advanced Driver Assistance Systems
(C)ACC	(Cooperative) Adaptive Cruise Control
CC	Cruise Control
MB	Moving Base
MIMO	Multiple-Input Multiple-Output
PID	Proportional-Integral-Derivative
WMR	Wheeled Mobile Robot

Roman symbols

A	system matrix
a	acceleration; controller gain
B	input matrix
C	output matrix
c	controller gain
d	intervehicle distance
e	error
H	spacing policy transfer function
h	time gap
I	identity matrix
K	controller gain vector
k	controller gain
L	vehicle length
q	position
R	radius
r	standstill distance
s	traveled distance
T	torque
t	time
u	desired acceleration; system input
V	Lyapunov candidate function
v	velocity
x	position coordinate; state
y	position coordinate
z	state

Greek symbols

δ	steering angle
θ	orientation angle
κ	curvature
λ	pole
ν	new system input
ξ	new vehicle input
σ	saturation
τ	time constant
Φ	coordinate transformation
Ψ	orientation angle
ω	angular velocity

Subscript and superscript

c_1	lateral controller 1
c_2	lateral controller 2
c_l	closed loop
d	derivative action
dd	double derivative action
e	error
f	following vehicle
i, j	indices
l	leading vehicle; linearization
$long$	longitudinal
MB	moving base
p	proportional action
r	reference vehicle

Miscellaneous

$\dot{x}$	time derivative of x
$\ddot{x}$	second time derivative of x
x^T	transpose of x
$\mathcal{J}$	Jacobian

Contents

Chapter 1

Introduction

The number of vehicles in The Netherlands is increasing rapidly over the last decades [1], which results in an increasing amount of traffic jams. Moreover, most vehicles use fossil fuels which leads to an increase of environmental pollution. The Dutch government is facilitating the development of autonomous vehicles as a solution for these problems [2]. A possible solution for this is the Advances Driver Assistance Systems (ADAS). It is believed the advantages of ADAS are not limited to reduce fuel consumption and increase road capacity, but also enhance an increase in road safety and driver comfort [53].

Many vehicles that are on the road today are equipped with ADAS that are focused on improving the driver's comfort. Examples of these systems are cruise control (CC), adaptive cruise control (ACC) and lane-keeping assistance. The new generation of ADAS is primarily focusing on improving the safety of both passengers and other road users [26]. In addition, ADAS are focusing on optimizing the individual vehicle, employing on-board sensors such as radar and lidar. These sensors register only the vehicle in the line-of-sight. These applications are limited when it comes to solving problems such as traffic jams and reduce pollution. The use of ACC has a small impact on the traffic flow [45]. To optimize the whole road traffic system, information of vehicles beyond the line-of-sight is necessary and therefore, cooperative driving is investigated. By using wireless communication, local information of cooperative vehicles is exchanged, which extends the information received by sensors. Cooperative driving can be described as influencing the individual vehicle behavior, either through advisory or automated actions, so as to optimize the collective behavior with respect to road throughput, fuel efficiency and/or safety [37]. Because the vehicles drive behind each other with a smaller intervehicle distance, the road throughput increases. Moreover, ghost traffic jams can be avoided because the platoon drives with the same velocity. An other positive effect of smaller intervehicle distance is the decrease of fuel consumption, as the air resistance is reduced.

An application of cooperative driving is Cooperative Adaptive Cruise Control (CACC), which is already investigated extensively by TNO [37, 34] and others [41, 11, 27]. When implementing CACC, a smaller distance between two vehicles is realized without increasing the risk of accidents.

A next step of Cooperative Adaptive Cruise Control, where the vehicle is automated in longitudinal direction, is the automation of the lateral motion of the vehicle. In some vehicles, ADAS are implemented that involve automation of steering, such as lane-keep assist. But also this application is only aiming for the optimization of the individual vehicle. This report is focusing on the automation of the vehicle in longitudinal and lateral direction using cooperative driving.

[1] http://statline.cbs.nl/StatWeb/publication/?DM=SLNL&PA=7374hvv&D1=2-11&D2=0&D3=a&HDR=T&STB=G2,G1&VW=T

[2] https://www.rijksoverheid.nl/onderwerpen/mobiliteit-nu-en-in-de-toekomst/inhoud/zelfrijdende-autos

1.1 Research Objectives

The contribution of this thesis is the automation of a mobile robot in lateral and longitudinal direction using cooperative driving. The automation of vehicles in these directions enables them to drive in a vehicle platoon and follow the platoon leader. The main research objective is:

Design a lateral and longitudinal controller for following the predecessor with a desired inter-vehicle distance in a vehicle platoon and for converging to the path of the platoon leader.

For the purposes of this report, a simplification of the vehicle model is used, i.e. a mobile robot. This model is used because it allows to design more complex time-varying controllers. The vehicles are modeled as unicycles where only the kinematics are considered. Furthermore, the platoon consist of two vehicles. To tackle the main research objective, four sub-objectives are defined that are addressed in this thesis:

1. Design of a lateral controller based on a path following problem to follow its predecessor in order to drive along a predefined path.
2. Design of a longitudinal controller to follow its predecessor with a desired distance, according to the so-called constant time-gap spacing policy.
3. Investigate the effect of tuning the lateral and longitudinal controller for comfort, safety and tracking performance.
4. Analysis of the benefits of separation of the lateral and longitudinal controller.

1.2 Outline

The report consist of three parts. In chapter 2 an overview of the literature review of lateral and longitudinal controllers is given. Researches about string stability, CACC, trajectory tracking and path following controllers are discussed. In chapter 3 and chapter 4 lateral and longitudinal controllers are derived and tuned, respectively. In chapter 5 the simulation results are presented. A brief description of each chapter is given below.

In chapter 3, two nonlinear lateral controllers are derived and compared. These controllers are derived for a path following problem. Additionally, a longitudinal controller is derived based on a CACC controller. An extension is made for when the vehicle and its predecessor are not yet driving along the same path. Finally, an observer is derived to estimate the vehicle states that can not directly measured and reduce the effect measurement noise.

In chapter 4, the lateral and longitudinal controllers are tuned. The lateral controllers are tuned in to separate ways, i.e. using time simulation for the nonlinear error dynamics and pole placement for the linearized error dynamics. The longitudinal controller is tuned using pole placement.

In chapter 5, the derived controllers are verified with different simulations. Different scenarios are simulated to determine the response of the vehicle. The derived controllers are compared with an already derived tracking controller [18]. Furthermore, the controllers are implemented on the detailed model of a wheeled mobile robot [40].

In chapter 6, a summary is given of the main conclusions concerning the lateral and longitudinal controller and the tuning of both controllers. Furthermore, the simulation results are presented as well as recommendations for future research in this topic.

Chapter 2

Literature Review

The automation of vehicles is a research objective which has been investigated for many years. Several ADAS have been developed or are still being developed. Some examples of commercially available systems are Adaptive Cruise Control (ACC), automatic parking and collision avoidance system. Most of these ADAS are focused on the individual vehicle. In order to improve overall traffic problems, i.e. traffics jams, research is focusing on the behavior of a group of vehicles. Therefore, applications which use cooperative driving are investigated, i.e. Cooperative Adaptive Cruise Control (CACC). In this literature review two subjects are discussed, different CACC controllers together with string stability. Secondly, three motion controllers are discussed: point stabilization, trajectory tracking and path following.

2.1 Cooperative Adaptive Cruise Control

In most vehicles, Cruise Control (CC) is implemented and in many vehicles the more advanced ACC is available. With a CC controller, a vehicle drives with a desired constant velocity. The ACC controller is an improved version of CC, where the distance between the vehicle and its predecessor is measured with sensors such as radar and scanning laser (LIDAR) [54]. ACC allows the vehicle to regulate its velocity when no predecessor is present and in that case it is identical to CC. When there is a predecessor, the vehicle's velocity is regulated to obtain an intervehicle distance according to a spacing policy. Two main spacing policies can be distinguished: a constant desired intervehicle distance and a constant intervehicle time gap [34]. For the latter, the velocity of the i-th vehicle and is given by

$$d_{r,i}(t) = r_i + hv_i(t), \tag{2.1}$$

where h is the time gap, r_i the standstill intervehicle distance and $v_i(t)$ the velocity of the i-th vehicle in the platoon. Here, the time gap is the time it takes for a vehicle to reach the current position of the preceding vehicle when it is driving with a constant velocity [31]. The ACC controller increases the driver's comfort, but has no influence on increasing road capacity and decreasing fuel consumption, because the intervehicle distance is relatively large. The intervehicle distance between the vehicles must be reduced to positively affect the other objectives. Therefore, an extension is made to ACC, referred to as Cooperative Adaptive Cruise Control (CACC). CACC exchanges data through wireless communication, in addition to the information obtained by radar and LIDAR. For communication between the vehicles, different information flow topologies are used [58]. Many possible communication topologies can be used but are not practical. Since there are limitations on the communication range and the amount of information that can be sent over a wireless link. Therefore, six different topologies are commonly used:

- Predecessor follower topology (PF),
- Predecessor-leader follower topology (PLF),

- Bidirectional topology (BD),
- Bidirectional-leader topology (BDL),
- Two predecessors follower topology (TPF),
- Two predecessor-leader follower topology(TPLF).

In this thesis the PF topology is used. The PF topology is the most often used communication topology for CACC controllers. Furthermore, it reduces the distance of wireless communication. The other topologies are not discussed in this report. For each topology, more information can be found in: PLF [52], BD [14], BDL[57], TPF [38] and TPLF [57].

2.1.1 String stability

As noticed before, CACC is designed to reduce the time gap between vehicles in a platoon. The main challenge hereby is to prevent that disturbances are amplified upstream the vehicle platoon, which is covered by string stability [39]. This is important to avoid collisions between the vehicles in the platoon. String stability can be defined for the lateral and the longitudinal controlled system and is focused on the propagation of systems responses of a cascade of systems, in this case a vehicle platoon.
The notions of string stability in longitudinal direction can be divided in three approaches: a Lyapunov-stability approach [51], a spatially invariant systems approach [1] and a performance-orientated frequency-domain approach [32, 41]. The Lyapunov-stability approach is the most formal approach. In this approach, string stability is discussed as a stability problem. Infinite-length platoons are considered by the spatially invariant systems approach and string stability is analyzed by the eigenvalues of the model. The performance-orientated approach is most frequently adapted and is discussed further. A string stability definition is proposed in [39] for a generalized nonlinear state space model representing a heterogeneous platoon. $\mathcal{L}_2$ and $\mathcal{L}_\infty$ string stability conditions are given for string stability in the performance-orientated approach. Independent from the interconnection topology, $\mathcal{L}_p$ string stability is defined for both linear and nonlinear systems, while accommodating initial condition perturbations and external disturbances.
String stability in lateral direction is discussed in [35, 49]. The platoon is string stable in the lateral direction when the lateral error does attenuate upstream the platoon. This is achieved when

$$\|y_l^{(i)}\|_p < \|y_l^{(i-1)}\|_p, \tag{2.2}$$

where $y_l^{(i)}$ and $y_l^{(i-1)}$ are the lateral errors of the i-th and $(i-1)$-th vehicle in the platoon, respectively.

2.2 Motion controller

In the second part of the literature review, different motion controllers are discussed. Many research is done on the automation of vehicles or robot in lateral, longitudinal or in both directions. Figure 2.1 shows an overview of a global structure of the literature about the automation of robots or vehicles. For the motion control problem three approaches can be distinguished:

- point stabilization, where the robot should be asymptotically stabilized around a point,
- trajectory tracking, where the robot has to track a trajectory. Here, the trajectory is a time parametrized reference path.
- path following, where the robot has to follow a path. Now there is a spatial path without temporal specifications. The vehicle follows a velocity profile which is independent from the path. Usually, a smoother convergence to the path is achieved compared with trajectory tracking.

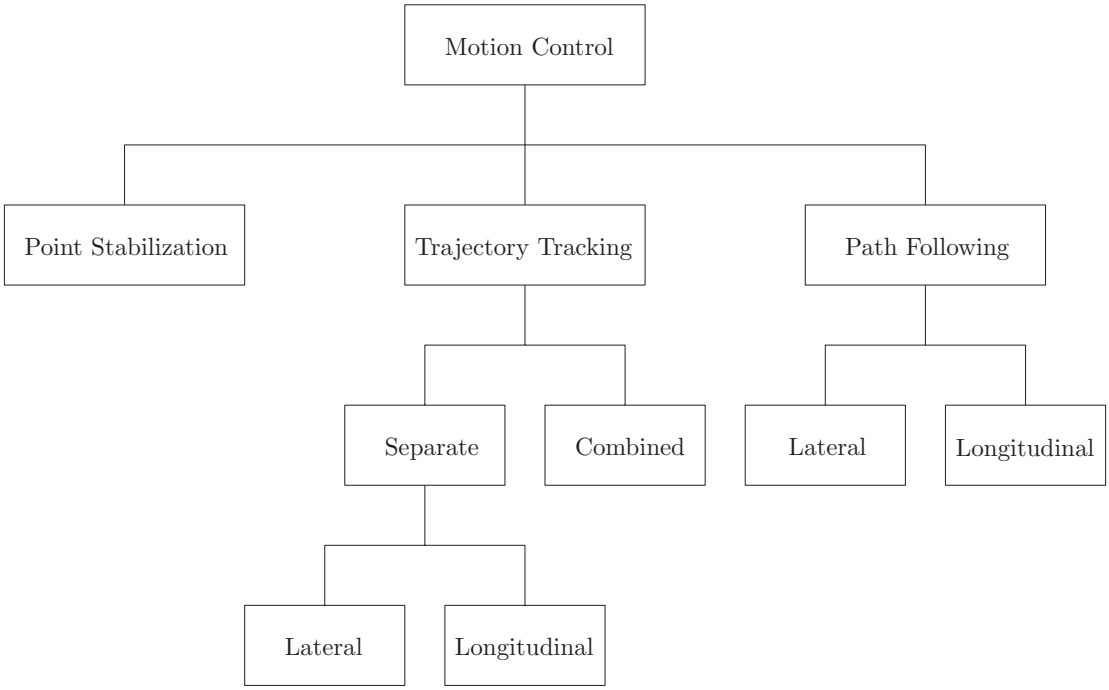

Figure 2.1: The structure of the literature review of motion controllers.

In this report the vehicles are modeled as wheeled mobile robots and only the kinematics are taken into account. This system is characterized by its nonholonomic constraint. Therefore, in the review of the different motion controllers, focus is on the controllers for mobile robots.

2.2.1 Point stabilization

According to Brockett's condition [3], a system with nonholonomic constraints cannot be asymptotically stabilized to a point with a smooth state feedback control law. In literature, several control laws are proposed to asymptotically stabilize a nonholonomic system. These control laws contain time-varying feedback control [43] and discontinuous feedback laws [7]. In [43] time-varying feedback controllers for nonlinear systems are proposed for simple car models. In [7], a piecewise smooth controller for a mobile robot is proposed which exponentially converges to the origin from any initial condition. For this thesis the stabilization problem is not for interest, but the tracking and path following problems are researched more.

2.2.2 Trajectory tracking

With trajectory tracking, the robot must follow a time parametrized trajectory which is defined in a 2D plane. The robot that follows its predecessor is automated in the lateral and longitudinal direction. When designing only a lateral or longitudinal controller, the interaction between the motion in lateral and longitudinal direction is neglected. When designing a control law for the orientation and velocity of the mobile robot, this interaction is taken into account.

Longitudinal controllers

The separate longitudinal controllers are discussed as a CACC controller where the velocity is regulated to maintain a constant intervehicle time gap. The main challenge for the longitudinal CACC controller is to achieve string stability to prevent amplification of disturbances in the upstream direction of the platoon.

A commonly used PD-like CACC controller is designed in [41]. A linear system is considered where the vehicle only communicates with its predecessor and the platoon is homogeneous. The

intervehicle distance is based on the constant time gap spacing policy. To increase the traffic flow safely, string stability is achieved by tuning the controller. The drawback of this controller design is that string stability is not taken into account a priori as control objective for the controller synthesis.
Also a sliding-mode controller is considered because of its robustness properties and the nonlinearities of the vehicle models, but has also the disadvantage of chattering. In [16] a sliding-mode controller is designed for a nonlinear vehicle model with a constant time gap spacing policy. The vehicles communicate with the leader of the platoon to achieve string stable behavior. The same as for the PD-like controller, string stable behavior is achieved by tuning the sliding mode controller. In [11] a Model Predictive Control (MPC) controller is designed for a nonlinear decoupled dynamic model. The vehicle drives in a heterogeneous platoon with a constant intervehicle distance and communicates only with its predecessor. The control problem is to achieve a closed loop stable system and string stable behavior. String stability is achieved by adding a constraint in the optimal control problem. A limitation of this controller is that during initialization all vehicles must communicate with the platoon leader.

Also several optimal control controllers are discussed. A decentralized LQR controller is designed in [50]. The controller is designed for a linearized system with wireless communication with its predecessor. The platoon consists of homogeneous vehicles with a constant time gap spacing policy. The control objective is to design a controller such that an optimal stable system is achieved. Via analysis, additional constraints are derived to obtain string stability. To satisfy these constraints, the weighting matrices are tuned. A mixed $\mathcal{H}_2/\mathcal{H}_\infty$ control problem is discussed in [27]. A linearized vehicle model is used in a homogeneous platoon with a constant time gap spacing policy. The control objective is to avoid collisions by reducing overshoot in velocity and acceleration. This has also a positive effect on the comfort of the passengers. Furthermore, string stable behavior must be achieved. Therefore, string stability is added to the optimization criteria. The drawback of this approach is that it is assumed that all information of the vehicles is known. The limitation of previous discussed controllers is that the string stability is not included in the design specifications as a consequence of which string stability has to be achieved a posteriori, i.e. by tuning the controller gains. Instead of achieving string stability by tuning or adding constraints, string stability is a design specification for the decentralized $\mathcal{H}_\infty$ controller in [38]. A linear vehicle model where the vehicle drives in a homogeneous platoon and communicates with its predecessor is considered. The vehicle is controlled to follow its predecessor with a constant time gap spacing policy. An explicit trade-off can be made between the vehicle-following performance and string stability before the controller synthesis.

Lateral controllers

Different linear and nonlinear lateral controllers are discussed in this section. Also a distinction is made for controllers taking string stability into account and controller that do not.

For a tractor-trailer vehicle, a trajectory tracking control strategy is proposed in [9]. The kinematics of the tractor-trailer vehicle are linearized around the trajectory. For a predefined trajectory, a time-varying Linear-Quadratic Regulator (LQR) controller is designed together with a feedforward signal to track the trajectory. A lateral control following problem for heavy vehicles is discussed in [55]. To follow the trajectory of its predecessor, a yaw rate controller for a linearized system is designed. The vehicles are equipped with LIDAR to measure the relative distance and bearing angle. The goal of the controller is to get good tracking performance. A drawback of this approach is the measurement of the bearing angle. The sensors for this measurement needs a small resolution in order to measure accurately when vehicles drive on a trajectory with a small curvature, i.e. on the highway. Furthermore, there is assumed that the vehicles drive with a constant velocity and the intervehicle distance is not controlled.

A problem using trajectory tracking is that non-smooth steering can appear and the vehicle cuts corners to be in the correct position at the correct time. An alternative to prevent non-smooth steering and cutting corners is presented in [15], where the relative position and the orientation of the vehicle to the trajectory are measured. To prevent that the vehicle cuts corners at low velocities, the look-ahead distance is adjusted for predicting the future curvature and detecting the trajectory error. A feedback controller corrects for deviation at a certain look-

ahead distance and the feedforward controller estimates the necessary steering for the oncoming curve at another look-ahead distance. The feedback controller is a lead-lag controller with a low-pass filter. Small compromises of the tracking performance are made to achieve smooth steering.

In [17], a time-varying state feedback controller is designed. Considering a robot modeled by a nonlinear unicycle model, the controller is designed to track a reference trajectory with saturated inputs. Here the goal is to achieve a stable controlled system and good tracking performance. It is assumed that the velocity of the robot does not converge to zero. A nonlinear adaptive controller is designed in [36] where the second vehicle follows its predecessor. For a platoon consisting of two vehicles, the objective for the last vehicle is to track the trajectory of the leader with a prescribed intervehicle distance. The last vehicle measures the relative distance with sensors. Using a nonlinear controller, the adaptive control law achieves asymptotic stability in the error dynamics and prevents the vehicle from cutting corners in steady state. A drawback of this approach is that the velocity and curvature of the leader has to be estimated. Also the velocity of the leader is assumed constant.

A not broadly discussed subject is string stability in lateral direction. In [35], a PD controller is designed where string stability in lateral direction is taken into account. A platoon of homogeneous linear vehicles is considered. The relative distance and angle between the vehicle and its predecessor is measured with LIDAR. The control problem is to achieve closed-loop stability, comfort, safety and small tracking errors. A definition for string stability in lateral direction is posed. In practical it is hard to realize string stability and satisfactory performance. Another PD controller is designed in [49]. In the platoon of vehicles, information about the predecessor is obtained by sensors and intervehicle communication. The control problem is to achieve a stable closed loop system and to guarantee string stability achieved by tuning. For a system without uncertain vehicle parameters, string stability is guaranteed. When uncertainties are present in the vehicle model, the proof of string stability is conservative. In [25] a $\mathcal{H}_\infty$ controller is designed for a linearized bicycle model. The vehicles in the platoon are equipped with LIDAR and communicate with their predecessors. String stability is achieved by changing the system into a weakly coupled system by intervehicle communication. The advantage of using the $\mathcal{H}_\infty$ controller is its robustness. A drawback is the constant velocity of the vehicles. In [21] a nonlinear globally stable trajectory tracking control strategy is proposed for kinematic models of different mobile robot platforms. The relative distance and bearing-angle to its preceding vehicle are measured by means of on-board sensors. A constant time gap spacing is used for the intervehicle distance and the leading vehicle follows a velocity profile. With the tracking controller, a closed loop stable system and small tracking errors are achieved. The nonlinear error dynamics are linearized to analyze the error propagation. This analysis is only done for a constant reference velocity.

Combined controller

When a combined controller is considered for the automation in lateral and longitudinal direction, the interaction in these directions is taken into account. A decentralized combined controller for a homogeneous platoon is designed in [20]. The vehicles are modeled as a linearized bicycle model. Furthermore, no intervehicle communication is present and only the relative distance and the bearing-angle between itself and its predecessor are measured. A PID controller is implemented for the lateral and longitudinal motion. With this controller, the model is asymptotically stable, small tracking errors are achieved and the vehicles can perform pre-specified tasks. In [24], a combined sliding mode lateral and longitudinal controller, considering a nonlinear vehicle model, is designed. The vehicles drive in a platoon where the vehicles are equipped with sensors. The sliding mode controller is applicable for complex nonlinear models, but can cause chattering. The control problem is to get an asymptotic stable system and to improve the tracking performance. A backstepping controller for vehicles in a platoon is designed in [5]. The objective is to track the predecessor with a predefined intervehicle distance. The vehicles are modeled as a nonlinear system where the lateral and longitudinal dynamics are coupled. Tracking performance and passenger comfort are achieved by tuning the backstepping controller. The advantages of this controller are the robustness properties, small tracking errors

are obtained and the leader of the platoon can vary its longitudinal velocity.

In [40] a time-invariant state feedback controller is designed to realize input-output linearization. For a nonlinear unicycle model, a tracking controller is designed to track a desired position and orientation. By applying a state feedback controller, a linearized system is realized and linear control techniques are applied. The tracking controller is a regular PD-controller with feedforward. Hereby it is important to have stable internal dynamics and a small tracking error. In [8] also a linearization technique is used to design a controller but now for following its predecessor with a constant intervehicle distance and a desired relative angle between the two robots. A feedback control law based on input output linearization for a nonlinear kinematic unicycle is designed. The following robot measures the relative distance and angle of its predecessor and has information about the motion of the leader. Also a combined longitudinal and lateral controller is designed in [4]. It is assumed that the vehicle platoon is homogeneous and no delays are present in the intervehicle communication. A nonlinear bicycle model is chosen to model the vehicles in the platoon. A linearising feedback controller with feedforward is proposed with a constant look-ahead distance, where the error dynamics is linearised. For the angle of this look-ahead vector, two approaches are considered: linked to the yaw angle of the vehicle or to the steering angle. A string stable platoon automation in lateral and longitudinal direction is achieved. A drawback of this approach is that the vehicles cut corners while driving in the platoon.

2.2.3 Path following

The path following problem is studied in multiple fields: ground vehicles [10], marine craft [47], and space crafts [42]. The same as for the trajectory tracking controllers, the controller is separated in a longitudinal and lateral controller. Path following differentiates itself from trajectory tracking with the fact that there are no temporal requirements in path following.

The path following problem is characterized by the separation of the lateral and longitudinal controller. In [47] the path following problem is divided in two subproblems; i) converge to the path and follow this path, and ii) satisfying a desired longitudinal behavior along the path. The two controllers are discussed separately.

Lateral controller

The lateral path following controller can be separated into two approaches: virtual target tracking and set stabilization. Using the virtual target tracking approach, a virtual target is defined and the goal is to converge to this target. By the set stabilization approach, a set corresponding with a desired maneuverer is stabilized to let the vehicle make the desired motion. The set is defined as desired maneuverer the vehicle must travel.

A lateral controller is designed in [29] to steer a unicycle-type robot along the path using a virtual target. A Serret-Frenet frame is considered which moves along the path. The origin of the Serret-Frenet frame is the orthogonal projection on the path. The kinematics of the unicycle-type robot are expressed with respect to the Serret-Frenet frame and is recast to the chained form. It is assumed that the unicycle moves with constant velocity towards the path. The drawback of this controller is the fact that the projection must be unique. This is only satisfied when the distance between the projection and the path is smaller than the smallest radius of the path. Furthermore, the velocity of the robot must be constant and must not be equal to zero. An extension of the work in [29] is done in [48]. The origin of the Serret-Frenet frame is not any more the orthogonal projection on the path, but now moves with its own velocity along the path. Because the frame can now move with a different velocity as the unicycle, the velocity of the frame is an additional input which can be used to achieve faster convergence. Also a dynamic model and parameter uncertainty are considered where a control law in longitudinal direction is assumed that converges the difference in velocity between the actual and desired velocity to zero. A control law is designed using backstepping to let the robot asymptotically converge to the path. An advantage of the extension of an additional input is that the initial condition of the unicycle can now be chosen freely.

When using the approach of set stabilization, the stabilization of sets which correspond with a specific maneuverer is investigated. The set is defined as the desired maneuver for the vehicle. When this set is stabilized, the vehicle moves along the desired path. In [30] a path following approach is provided where neither the robot is projected to the path nor a virtual robot is used. The path is expressed as the equation $f(x, y) = 0$, where this equation describes the set which is stabilized. The distance error is defined as the value $f(x, y)$ when the robot is at position (x, y). With an arbitrary translational velocity and the designed controller for the rotational velocity, asymptotic stability is achieved. An limitation of this approach is that an analytical expression of the path is required to define the set. A sliding mode controller for the path following problem is designed in [6]. A sliding mode controller is chosen because of its robustness properties. A drawback is that also chattering can appear. Controllers are designed for a nonlinear kinematic model and a nonlinear dynamics model. The goal of the controller is to follow a reference angle while the forward velocity of the model follows a velocity profile. The controller is designed to achieve stability, small following errors and reduce overshoot. A drawback of this approach is that only the orientation problem is considered and a constant velocity in the longitudinal direction is assumed. For a nonlinear kinematic model of a unicycle a passivity based controller is designed in [12] to follow a circle with constant radius. The unicycle traverses the circle with a prescribed direction of rotation and a desired velocity. A storage function is defined to asymptotically stabilize a set which describes the circle. An advantage of the passivity based controller is that it can be made compatible with any input saturation constraint. The set stabilization approach is also used for feedback linearization. In [2], sufficient and necessary conditions for feedback linearization of the transverse dynamics are given for a periodic orbit. In [33], the feedback linearization of a nonlinear kinematic unicycle model is discussed to follow a circle. By applying feedback linearization, the control design is simplified. A limitation of this approach is that the velocity in longitudinal direction is assumed to be constant.

Longitudinal controller

In the previous section, the lateral controller is discussed. Most of the times, it is assumed that the velocity in longitudinal direction is constant to separate the lateral and longitudinal controller. In this section, different lateral controllers are discussed. Controllers to regulate the longitudinal direction for a path following problem are mostly used for coordinated path following. Here, different vehicles drive in a desired formation, such as aside each other or in a triangle.

In [56] a coordinated path following controller is designed, based on the lateral controller discussed in [48]. The velocity in longitudinal direction depends on the curvilinear distance of the vehicles. The longitudinal controller for the leader and the followers are the same and based on a proportional controller and a feedforward term of the desired velocity. The desired velocity of the followers depends on the generalized along-path distance between the vehicles. Because of this choice, the follower catches up with the leader when it is far behind and the generalized curvilinear distance converges to zero. The communication between the vehicles is minimal and only the curvilinear distance of the leader is communicated. In [13], also a coordinated path following controller is designed where the lateral controller is the same as discussed in [48]. Decentralized controllers are used where the communication between the robots is kept to a minimum. To drive in formation, the velocity of the robots is adjusted as function of the curvilinear distance. The goal of the longitudinal controller is to let the difference between the curvilinear distances of the robots converge to zero. Constraints in the communication network are discussed using directed graph theory and used to determine a control law to let the difference in curvilinear distance converge to zero.

2.2.4 Conclusion

In the literature, different approaches for string stability are used. In both lateral and longitudinal direction is defined as prevents disturbances upstream the vehicle platoon. For different controller, both lateral and longitudinal string stability is considered. A difference is that string stability can be achieved a posteriori by tuning the controller gains or a priori by taking it into

account by the control synthesis. To make a better trade-off between tracking performance and string stability, the latter is desired.
For the motion control problem, three approaches were discussed. Tracking and path following controller are suitable for the objective in this report. Because implementing the tracking controller for this problem can result in non-smooth steering and in cutting the corners. Therefore, the path following controller is considered. Here the lateral controller has no temporal requirement. This has the advantage that a path can be determine separate from longitudinal motion. In this report the path following controller is used to determine the lateral controller.
For the path following controller discussed here, the longitudinal motion is a prescribed motion. The longitudinal controller derived in this report is based on the CACC controller.

Chapter 3

Lateral and longitudinal controllers

The first step for automating the vehicle is to derive a lateral and longitudinal controller. The cooperative vehicles drive in a platoon where the platoon leader and all vehicles are known. It is assumed that the platoon, considered in this thesis, consist of two vehicles, i.e. the platoon leader and its follower. The leading vehicle is controlled by a driver, while the follower is controlled by the lateral and the longitudinal controllers.
Two lateral controllers are explained in this report and are derived based on a path following problem, because the problem is divided into a geometric task and a dynamic task [46]. The geometric task is considered by deriving the lateral controller. The first lateral controller is proposed in [23], where the curvature of the follower's path is determined in the spatial domain. The controller is transformed to the time domain to implement the lateral controller in simulation. A second lateral controller is proposed in [22], where the curvature of the follower's path is determined in the time domain.
For the dynamic task, a longitudinal controller is derived based on the CACC controller in [37]. Applying the controller, the follower drives with a desired intervehicle distance behind the leading vehicle.
For the lateral and longitudinal controller, a kinematic model of a mobile car with rear wheel drive and front wheel steering, shown in Figure 3.1, is considered:

$$\begin{aligned} \dot{x} &= v(t)\cos\theta(t) \\ \dot{y} &= v(t)\sin\theta(t) \\ \dot{\theta} &= \frac{v(t)}{L}\tan\delta(t). \end{aligned} \tag{3.1}$$

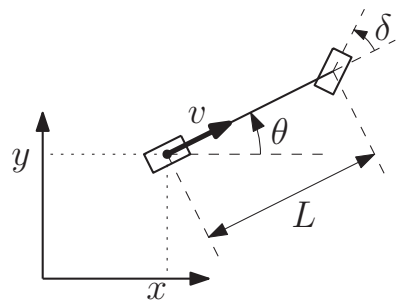

Figure 3.1: The overview of the mobile car.

The forward velocity of the rear wheels $v(t)$ and the angle between the front wheels and the car $\delta(t)$ are considered as inputs. The $(x(t), y(t))$ position of the mobile car is the center of the rear axis, $\theta(t)$ is the orientation of the body of the car and the length of the car $L > 0$ is constant. It is assumed that no slip happens between the vehicle's tires and the road. As a

result of this assumption, the position $(x(t), y(t))$ does not have any lateral velocity component. The curvature is defined as

$$\kappa(t) = \frac{1}{L} \tan \delta(t). \tag{3.2}$$

The remainder of this chapter is organized as follows. In section 3.1 and section 3.2, two lateral controllers are derived to solve the path following problem. In section 3.3, the longitudinal controller is presented to maintain a desired intervehicle distance. In section 3.4, an observer is derived to obtain information of the vehicle's velocity and orientation based on position measurements. This chapter concludes with a summary of the results.

3.1 Lateral controller 1

A lateral controller is designed such that the follower converges to the path of the leader. The controller is derived in the spatial domain such that the lateral controller is not affected by the velocity of the vehicle. The trajectory of the leader is parameterized by the traveled distance of the leader s_l. Now, a path is created that is time-independent and only depends on s_l and is described in the spatial domain. It is assumed that the position coordinates x_l and y_l, the orientation θ_l, the velocity v_l and the curvature of the path of the leader κ_l are measured perfectly. Also the follower is described in the spatial domain by the traveled distance of the follower $s_f(t)$ and all parameters of the follower are measured perfectly. To transform both vehicles to the spatial domain, define

$$\begin{aligned} x_l(t) &= \bar{x}_l(s_l(t)) & x_f(t) &= \bar{x}_f(s_f(t)) \\ y_l(t) &= \bar{y}_l(s_l(t)) & y_f(t) &= \bar{y}_f(s_f(t)) \\ \theta_l(t) &= \bar{\theta}_l(s_l(t)) & \theta_f(t) &= \bar{\theta}_f(s_f(t)) \\ \kappa_l(t) &= \bar{\kappa}_l(s_l(t)) & \kappa_f(t) &= \bar{\kappa}_f(s_f(t)). \end{aligned} \tag{3.3}$$

To design the lateral controller, a reference vehicle is introduced which drives along the path of the leader. This reference vehicle is introduced to separate the leader from the follower for the lateral controller, such that the motions of the leader does not affect the follower. Introducing a reference vehicle provides an additional degree of freedom for the derivation of the controller, namely its "relative velocity", i.e. the displacement of the reference vehicle when the follower displaces with an unit distance. The traveled distance s_r of the reference vehicle as a function of the follower distance s_f is defined as

$$\tilde{v}_r(s_f) = \frac{ds_r}{ds_f}, \tag{3.4}$$

it follows that

$$s_r(s_f) = \int_0^{s_f} \tilde{v}_r(\sigma) d\sigma. \tag{3.5}$$

The "velocity" of the reference vehicle in the spatial domain can be interpreted as the distance covered by this reference vehicle per unit distance covered by the by the follower vehicle. By introducing a variable reference speed, an additional degree of freedom for the controller is introduced, where the benefits will become clear in the next sections. As last step, coordinates of the reference vehicle depending on s_f are defined as

$$\begin{aligned} \tilde{x}_r(s_f) &= \bar{x}_r(s_r(s_f)) \\ \tilde{y}_r(s_f) &= \bar{y}_r(s_r(s_f)) \\ \tilde{\theta}_r(s_f) &= \bar{\theta}_r(s_r(s_f)) \\ \tilde{\kappa}_r(s_f) &= \bar{\kappa}_r(s_r(s_f)). \end{aligned} \tag{3.6}$$

The velocities of the following and reference vehicle are defined as

$$v_f(t) = \frac{ds_f(t)}{dt} \qquad v_r(t) = \frac{ds_r(t)}{dt}. \tag{3.7}$$

Substituting these velocities into (3.1) results in, using (3.3)

$$\begin{aligned}
\frac{d}{dt}\frac{dt}{ds_f}\bar{x}_f(s_f) &= \cos\bar{\theta}_f(s_f) & \frac{d}{dt}\frac{dt}{ds_r}\bar{x}_r(s_r) &= \cos\bar{\theta}_r(s_r) \\
\frac{d}{dt}\frac{dt}{ds_f}\bar{y}_f(s_f) &= \sin\bar{\theta}_f(s_f) & \frac{d}{dt}\frac{dt}{ds_r}\bar{y}_r(s_r) &= \sin\bar{\theta}_r(s_r) \\
\frac{d}{dt}\frac{dt}{ds_f}\bar{\theta}_f(s_f) &= \bar{\kappa}_f(s_f) & \frac{d}{dt}\frac{dt}{ds_r}\bar{\theta}_r(s_r) &= \bar{\kappa}_l(s_r).
\end{aligned} \tag{3.8}$$

Using (3.4) and (3.6), the parameterized kinematic models of the following and reference vehicles are now given by

$$\begin{aligned}
\frac{d}{ds_f}\bar{x}_f(s_f) &= \cos\bar{\theta}_f(s_f) & \frac{d}{ds_f}\tilde{x}_r(s_f) &= \tilde{v}_r(s_f)\cos\tilde{\theta}_r(s_f) \\
\frac{d}{ds_f}\bar{y}_f(s_f) &= \sin\bar{\theta}_f(s_f) & \frac{d}{ds_f}\tilde{y}_r(s_f) &= \tilde{v}_r(s_f)\sin\tilde{\theta}_r(s_f) \\
\frac{d}{ds_f}\bar{\theta}_f(s_f) &= \bar{\kappa}_f(s_f) & \frac{d}{ds_f}\tilde{\theta}_r(s_f) &= \tilde{v}_r(s_f)\tilde{\kappa}_l(s_f).
\end{aligned} \tag{3.9}$$

The path of the leader is characterized by the curvature $\bar{\kappa}_l(s_l)$ where it depends on the traveled distance of the leader. The reference vehicle displaces along the same path with the curvature $\tilde{\kappa}_l(s_f)$, but depends on the displacement of the following vehicle.

3.1.1 Controller design

For the lateral controller, the error between the follower and the reference vehicle are defined in the body frame of the follower as shown in Figure 3.2.
The error coordinates $(\bar{x}_e(s_f), \bar{y}_e(s_f), \bar{\theta}_e(s_f))$ are defined as

$$\begin{bmatrix} \bar{x}_e(s_f) \\ \bar{y}_e(s_f) \\ \bar{\theta}_e(s_f) \end{bmatrix} = \begin{bmatrix} \cos\bar{\theta}_f(s_f) & \sin\bar{\theta}_f(s_f) & 0 \\ -\sin\bar{\theta}_f(s_f) & \cos\bar{\theta}_f(s_f) & 0 \\ 0 & 0 & 1 \end{bmatrix} \begin{bmatrix} \tilde{x}_r(s_f) - \bar{x}_f(s_f) \\ \tilde{y}_r(s_f) - \bar{y}_f(s_f) \\ \tilde{\theta}_r(s_f) - \bar{\theta}_f(s_f) \end{bmatrix}, \tag{3.10}$$

Differentiation with respect to s_f results in the "spatial error dynamics" given by

$$\frac{d}{ds_f}\bar{x}_e(s_f) = \bar{\kappa}_f(s_f)\bar{y}_e(s_f) + \tilde{v}_r(s_f)\cos\bar{\theta}_e(s_f) - 1 \tag{3.11a}$$

$$\frac{d}{ds_f}\bar{y}_e(s_f) = -\bar{\kappa}_f(s_f)\bar{x}_e(s_f) + \tilde{v}_r(s_f)\sin\bar{\theta}_e(s_f) \tag{3.11b}$$

$$\frac{d}{ds_f}\bar{\theta}_e(s_f) = \tilde{v}_r(s_f)\tilde{\kappa}_l(s_f) - \bar{\kappa}_f(s_f), \tag{3.11c}$$

where $\bar{\kappa}_f$ and $\tilde{v}_r$ are the inputs. The control law for the "relative velocity" of the reference vehicle is defined in [23] as

$$\tilde{v}_r(\bar{x}_e(s_f), \bar{\theta}_e(s_f)) = \frac{1 - k_1\bar{x}_e(s_f)}{\cos\bar{\theta}_e(s_f)}, \tag{3.12}$$

where $|\bar{\theta}_e(s_f)| < \frac{\pi}{2}$. From (3.12), it follows that, when the follower is converged to the reference vehicle, i.e. the errors $\bar{x}_e(s_f)$ and $\bar{\theta}_e(s_f)$ are zero, the reference vehicle moves with a "velocity" $\tilde{v}_r$ equal to one, i.e. identical to the follower. Depending on $\bar{x}_e(s_f)$ and $\bar{\theta}_e(s_f)$, the reference vehicle moves forward or backward.

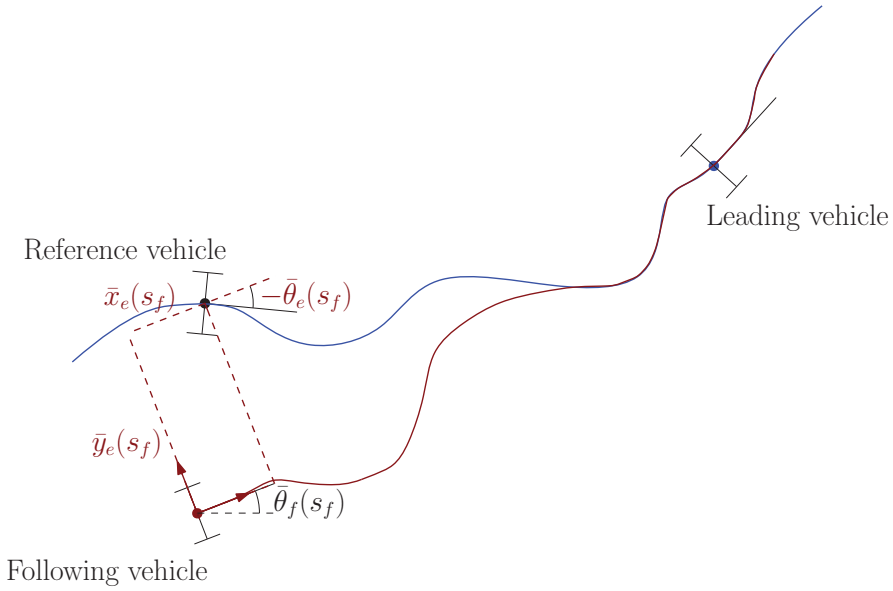

Figure 3.2: A schematic overview of the leading, following and reference vehicle in the spatial domain. The error between the reference and following vehicle with respect to the body frame of the follower is shown.

Proposition 1 ([23]) Consider the "spatial error dynamics" (3.11) in closed loop with the control law

$$\bar{\kappa}_f(s_f) = \tilde{v}_r(s_f)\tilde{\kappa}_l(s_f) + k_2\bar{y}_e(s_f)\left(1 - k_1\bar{x}_e(s_f)\right)\frac{\tan\bar{\theta}_e(s_f)}{\bar{\theta}_e(s_f)} + k_3\bar{\theta}_e, \tag{3.13}$$

where $k_1 > 0$, $k_2 > 0$ and $k_3 > 0$. If $\tilde{v}_r(s_f)$ and $\tilde{\kappa}_l(s_f)$ are bounded and $|\bar{\theta}_e(s_f)| < \frac{\pi}{2}$, then the system (3.11),(3.13) is asymptotically stable.

The proof of Proposition (1) is given in subsection A.1.1.
Because the lateral controller is determined in the spatial domain, the created path does not depend on the velocity of the follower. This is a great advantage because it creates the opportunity to determine an ideal path by only tuning the lateral controller with the gains k_1, k_2 and k_3. This chosen path is not influenced when the follower drives with different velocities along this path.

3.1.2 Extending stability region

An extension for the derived lateral controller is discussed in this section. Let $\sigma(\theta)$ be a locally integrable monotone function on $]-\pi/2, \pi/2[$ which is continuous differentiable satisfying

- $\sigma(0) = 0$,
- $\lim_{\theta\to\pi/2} \sigma(\theta) = \infty$
- $\lim_{\theta\to-\pi/2} \sigma(\theta) = -\infty$
- $\frac{d\sigma}{d\theta}(0) = 1$.

Let $\rho(\theta)$ be a continuous monotone function satisfying $\rho(0) = 0$ and $\rho(\theta)\theta > 0$ for $\theta \neq 0$. Note that $\sigma(\theta)\rho(\theta) > 0$ for all $\theta \neq 0$. The function σ and ρ are chosen as $\sigma(\bar{\theta}_e(s_f)) = \tan\bar{\theta}_e(s_f)$ and $\rho(\bar{\theta}_e(s_f)) = \bar{\theta}_e(s_f)$.

Proposition 2 ([23]) Consider the "spatial error dynamics" (3.11) in closed loop with the control law

$$\bar{\kappa}_f(s_f) = \tilde{v}_r(s_f)\tilde{\kappa}_l(s_f) + k_2\bar{y}_e(s_f)\left(1 - k_1\bar{x}_e(s_f)\right) + k_3\bar{\theta}_e(s_f), \tag{3.14}$$

where $k_1 > 0$, $k_2 > 0$ and $k_3 > 0$. If $\tilde{v}_r(s_f)$ and $\tilde{\kappa}_l(s_f)$ are bounded and $\|\bar{\theta}_e(s_f)\| < \frac{\pi}{2}$, then the system (3.11),(3.14) is globally asymptotically stable.

The proof of Proposition (2) is given in subsection A.1.2.

3.1.3 Implementation in time domain

The implementation of the controller on the vehicle is a drawback of the derived lateral controller. Because the controller depends on the traveled distance of the following vehicle rather than time, it cannot be implemented directly in real time. Therefore, an additional step must be performed to apply the lateral controller in experiments. The first possibility is to perform two simulations. First, $\bar{\kappa}_f(s_f)$ depending on the traveled distance s_f is determined by simulating in the spatial domain. Afterwards a second simulation is performed in the time domain. The traveled distance of the following vehicle is determined and the corresponding curvature $\kappa_f(t)$ is estimated based on the data obtained in the first simulation. A disadvantage is that it is expensive to perform two simulations. Furthermore, the controller cannot be implemented in real time because of this reason. For that reason, a second method to implement the lateral controller is discussed in the section. To do so, the derived lateral controller in (3.14) is recast to the time domain. The kinematic model of the follower and reference vehicle are recasted to the time domain using (3.3) and (3.6)

$$\begin{aligned}
\dot{x}_f(t) &= \frac{d}{ds_f(t)}\bar{x}_f(s_f(t))\frac{ds_f(t)}{dt} & \dot{x}_r(t) &= \frac{d}{ds_f(t)}\tilde{x}_r(s_f(t))\frac{ds_f(t)}{dt} \\
\dot{y}_f(t) &= \frac{d}{ds_f(t)}\bar{y}_f(s_f(t))\frac{ds_f(t)}{dt} & \dot{y}_r(t) &= \frac{d}{ds_f(t)}\tilde{y}_r(s_f(t))\frac{ds_f(t)}{dt} \\
\dot{\theta}_f(t) &= \frac{d}{ds_f(t)}\bar{\theta}_f(s_f(t))\frac{ds_f(t)}{dt} & \dot{\theta}_r(t) &= \frac{d}{ds_f(t)}\tilde{\theta}_r(s_f(t))\frac{ds_f(t)}{dt}.
\end{aligned} \tag{3.15}$$

Given the fact that $\frac{d}{dt}s_f(t) = v_f(t)$ and substituting (3.9) into (3.15) results in

$$\begin{aligned}
\dot{x}_f(t) &= v_f(t)\cos\bar{\theta}_f(s_f(t)) & \dot{x}_r(t) &= v_f(t)\tilde{v}_r(s_f(t))\cos\tilde{\theta}_r(s_f(t)) \\
\dot{y}_f(t) &= v_f(t)\sin\bar{\theta}_f(s_f(t)) & \dot{y}_r(t) &= v_f(t)\tilde{v}_r(s_f(t))\sin\tilde{\theta}_r(s_f(t)) \\
\dot{\theta}_f(t) &= v_f(t)\bar{\kappa}_f(s_f(t)) & \dot{\theta}_r(t) &= v_f(t)\tilde{v}_r(s_f(t))\tilde{\kappa}_l(s_f(t)).
\end{aligned} \tag{3.16}$$

There can be noticed that (3.16) is the same as (3.1) considering that $v_r(t) = v_f(t)\tilde{v}_r(s_f(t))$. The inputs of (3.16) are $v_f(t)$ and $\tilde{\kappa}_l(s_f(t))$. For now, it is assumed that the velocity of the leader v_f is constant and has an arbitrary velocity which is chosen. In section 3.3 a control law for the followers velocity is discussed. The velocity $\tilde{v}_r$ is obtained from (3.12), but $\bar{x}_e(s_f(t))$ and $\bar{\theta}_e(s_f(t))$ are unknown. Therefore, the path following error is recast as

$$\begin{bmatrix} \bar{x}_e(s_f(t)) \\ \bar{y}_e(s_f(t)) \\ \bar{\theta}_e(s_f(t)) \end{bmatrix} = \begin{bmatrix} \cos\bar{\theta}_f(s_f(t)) & \sin\bar{\theta}_f(s_f(t)) & 0 \\ -\sin\bar{\theta}_f(s_f(t)) & \cos\bar{\theta}_f(s_f(t)) & 0 \\ 0 & 0 & 1 \end{bmatrix} \begin{bmatrix} \tilde{x}_r(s_f(t)) - \bar{x}_f(s_f(t)) \\ \tilde{y}_r(s_f(t)) - \bar{y}_f(s_f(t)) \\ \tilde{\theta}_r(s_f(t)) - \bar{\theta}_f(s_f(t)). \end{bmatrix}. \tag{3.17}$$

The derived lateral controller in (3.14) recast to the time domain is finally given by

$$\bar{\kappa}_f(s_f(t)) = \tilde{v}_r(s_f(t))\tilde{\kappa}_l(s_f(t)) + k_2\bar{y}_e(s_f(t))\left[1 - k_1\bar{x}_e(s_f(t))\right] + k_3\bar{\theta}_e(s_f(t)). \tag{3.18}$$

Now the lateral controller $\bar{\kappa}_f(s_f(t))$ is recasted to the time domain, the lateral controller can be implemented directly into the simulation which eliminates the disadvantage of performing two simulations. In this section the lateral controller (3.14) is recasted to the time domain, but also the controller (3.13) can be recast in a similar procedure.

3.1.4 Simulation Results

In this section the derived lateral controller is applied to the follower which is described by the kinematic model (3.1). The leader, also described by (3.1), drives two different trajectories, a straight line and a circle. The leader drives in a circular trajectory with the radius $R = 2m$ and a constant velocity $v_l = 3m/s$. The follower drives with a constant velocity $v_f = 2m/s$. The initial condition of the leader is $[x_l(0), y_l(0), \theta_l(0)] = [0, 1, 0]$ and of the follower is $[x_f(0), y_f(0), \theta_f(0)] = [0, 0, \pi/3]$. The reference vehicle has the same initial conditions as the leader. The controller gains of the lateral controllers are chosen as $k_1 = 1$, $k_2 = 1$ and $k_3 = 1$.

In Figure 3.3, the control input $\bar{\kappa}_f$ are shown for a straight line and a circular path. In each figure, the recast lateral controller (3.18) and (3.14) are shown. To apply (3.14) in this simulation, a simulation in spatial domain and a simulation in the time domain are performed as explained before. As can be seen, no difference is distinguished between the two control inputs for the two different trajectories. For that reason, the recast lateral controller in (3.18) is used in the remaining of this report.

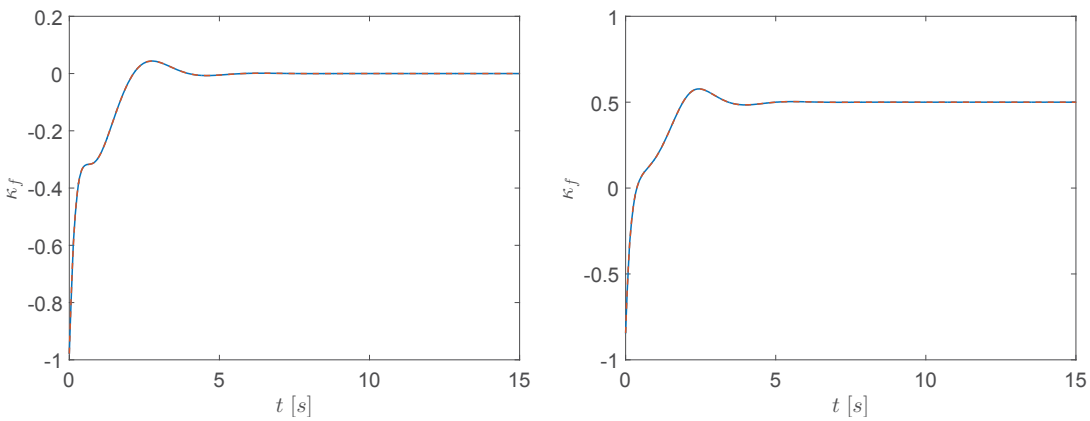

(a) Line (b) Circle

Figure 3.3: The comparison of the control inputs determined by the recast controller $\bar{\kappa}_f(s_f(t))$ (orange) and the control input determined by performing two different simulations (blue).

For the next simulation, the following vehicle drives with two different velocities, i.e. $v_f = 2m/s$ and $v_f = 10m/s$. In Figure 3.4 the paths of the follower and leader are shown for a straight line and a circular path with the corresponding lateral error. For both trajectories, the follower converges to the path of the leader and the lateral error between the follower and the reference vehicle converges to zero. The path of the follower is identical for both velocities as discussed before, which is an advantage of the lateral controller (3.18).
As explained in the previous subsections, the reference vehicle has an additional degree of freedom. To investigate the benefits of this additional degree of freedom, simulations are performed where the following vehicle is placed far from the leader's path. The two different paths are considered. The initial condition of the follower is $[x_f(0), y_f(0), \theta_f(0)] = [-20, 0, \pi/3]$ and the leaders initial conditions are $[x_l(0), y_l(0), \theta_l(0)] = [0, 1, 0]$. Both the leader and the follower drives with the velocity $v_f = 10m/s$. The reference vehicle has the same initial conditions as the leader. The controller gains are $k_1 = 1$, $k_2 = 1$ and $k_3 = 1$.

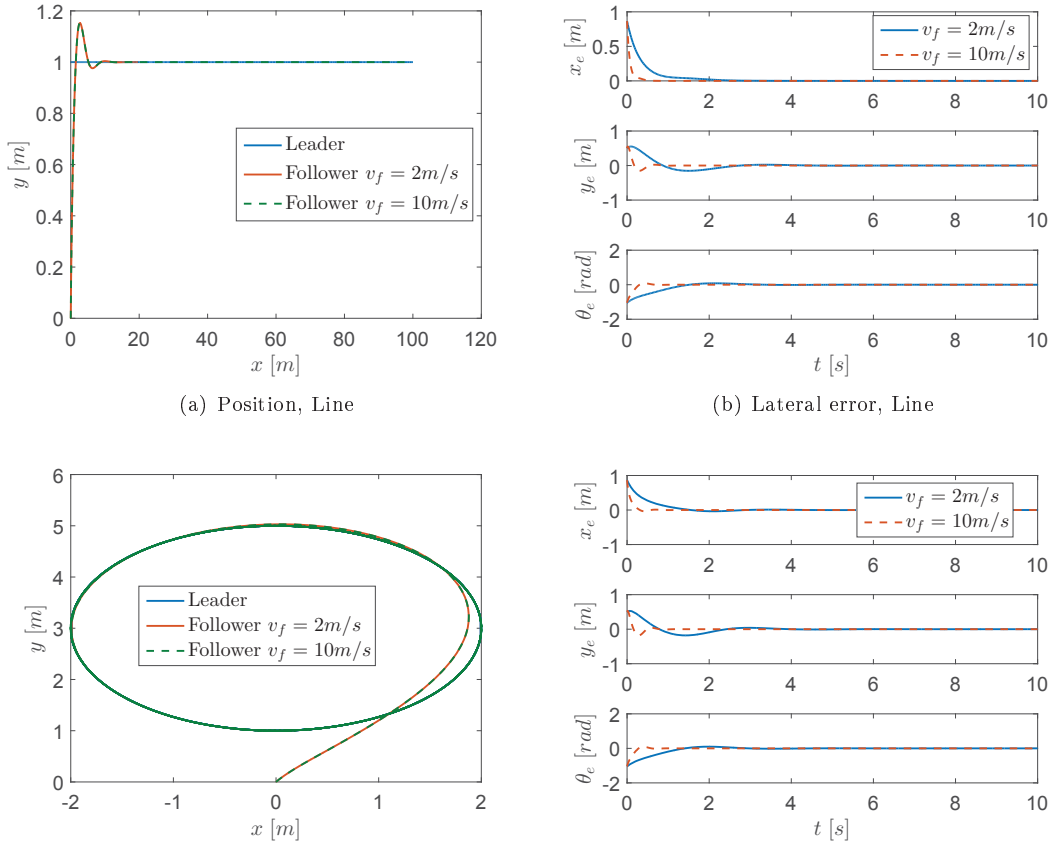

(a) Position, Line

(b) Lateral error, Line

(c) Position, Circle

(d) Lateral error, Circle

Figure 3.4: (a) and (c) show the position of the leader and follower for the two different paths. (b) and (d) show the lateral error between the follower and the reference vehicle.

Figure 3.5 presents the results of the simulations with large initial lateral errors. Based on the motion of the following vehicle shown in 3.5(a) and 3.5(c), the following vehicle makes a detour before it converges towards the leader's path. Figure 3.6 shows the velocity of the reference vehicle. As can be seen, the velocity is large and negative in the beginning. Because the reference vehicle can only moves along the leader's path, i.e. along the line, the reference vehicle moves backwards to reduce the lateral error x_e. Then the errors y_e and θ_e reduces slowly towards zero.

Based on the simulations performed with lateral controller 1, there can be concluded that the advantage of this controller is that the path towards the reference vehicle does not change when driving with different velocities. A disadvantage of this controller is that when large initial lateral errors are present, the following vehicle does not converge towards the path in a desirable way, i.e. moves in a far away towards the path of the leader. A second lateral controller is designed in the next section to prevent that the following vehicle makes a detour when it converges towards the leader's path.

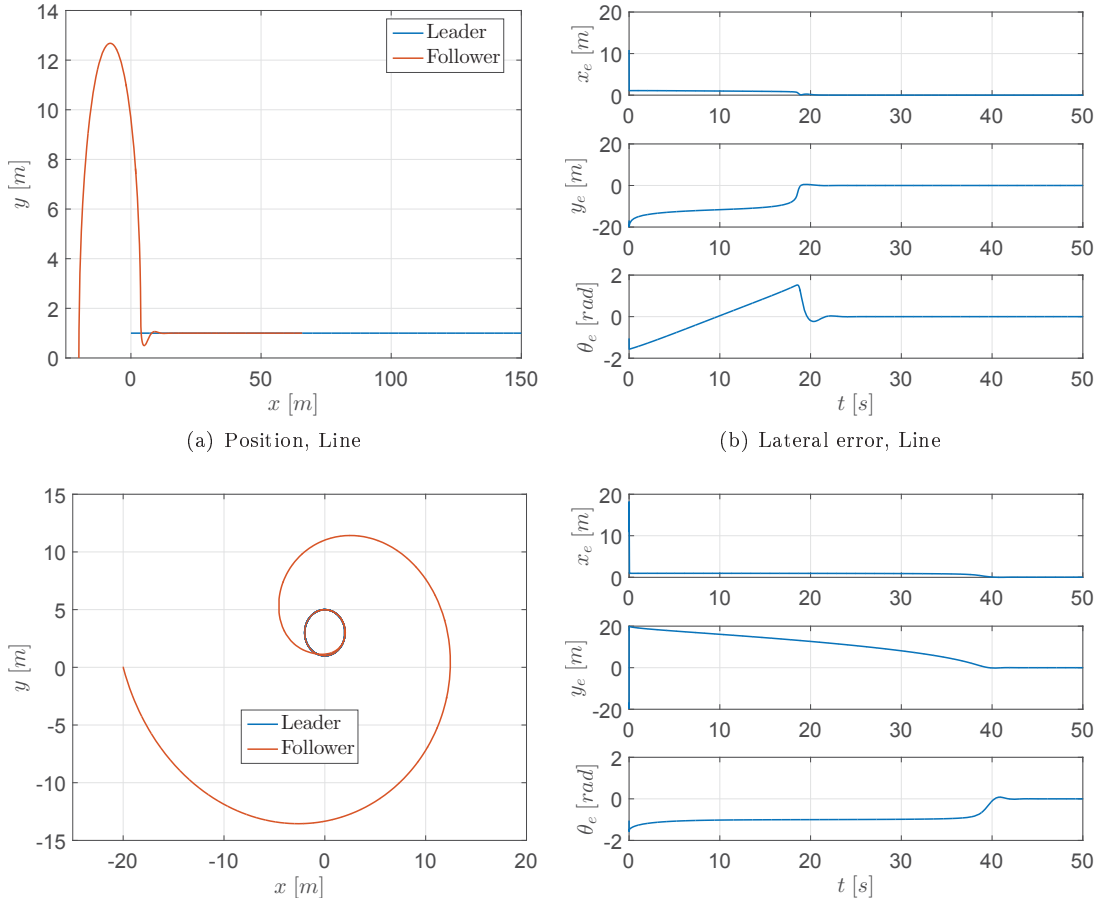

(a) Position, Line

(b) Lateral error, Line

(c) Position, Circle

(d) Lateral error, Circle

Figure 3.5: The simulation results for a large initial lateral error for a straight line and circular path. (a) and (c) show the position of the leader and follower for the two different paths. (b) and (d) show the lateral error between the follower and the reference vehicle.

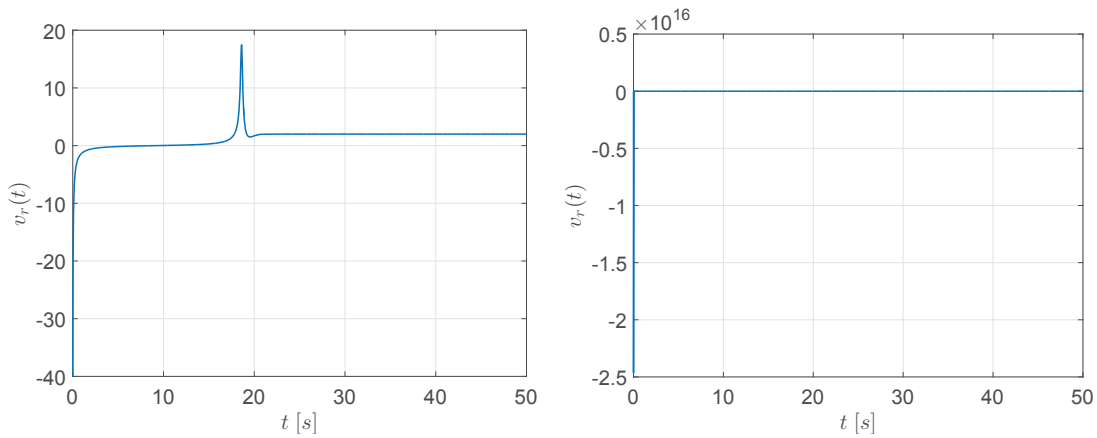

(a) Line

(b) Circle

Figure 3.6: The velocity of the reference vehicle for a straight line and circular path.

3.2 Lateral controller 2

A second lateral controller is designed, because the first lateral controller has the limitation that for large initial lateral errors the following vehicle makes a detour before it converges. The lateral controller designed in this section has two main differences compared with lateral controller 1. Firstly, the implementation of the new controller is easier than before. The lateral controller is designed in the time domain, by determining the error dynamics depending on time. Secondly, more restrictions are given to the motion of the reference vehicle to ensure that the following vehicle moves to faster to the path of the leader compared with lateral controller 1. Identical as for controller 1, a leading and following vehicle are considered. The trajectory of the leader is parametrized by the traveled distance of the leader and the leader can be described in the spatial domain. The following vehicle is positioned at an arbitrary initial position and orientation. Also a reference vehicle is introduced which moves along the leader's path. The velocity of the reference frame can be chosen as an extra input to achieve faster convergence of the follower to the desired path. The objective of the lateral controller remains the same and is to steer the follower towards the leader's path. To do so, the error between the follower and the reference frame is defined in the body fixed frame of the reference vehicle as shown in Figure 3.7.

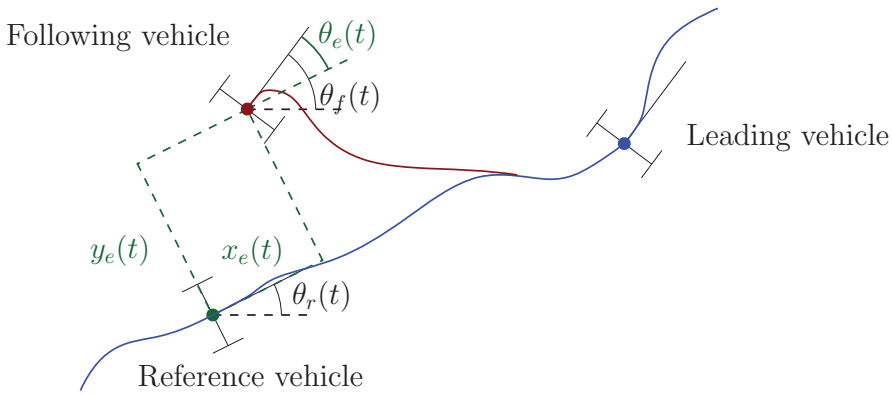

Figure 3.7: A schematic overview of the following and leading vehicle and the reference frame. The error for the lateral controller is defined in the reference frame.

Some differences can be noted compared with Controller 1. First, the lateral error is now defined in the body frame of the reference vehicle, where for Controller 1 the error was defined in the body frame of the follower. Second, the lateral error now depends on time, where the error of Controller 1 depends on the traveled distance of the follower. The position error shown in Figure 3.7 is defined as

$$\begin{bmatrix} x_e(t) \\ y_e(t) \\ \theta_e(t) \end{bmatrix} = \begin{bmatrix} \cos\theta_r(t) & \sin\theta_r(t) & 0 \\ -\sin\theta_r(t) & \cos\theta_r(t) & 0 \\ 0 & 0 & 1 \end{bmatrix} \begin{bmatrix} x_f(t) - x_r(t) \\ y_f(t) - y_r(t) \\ \theta_f(t) - \theta_r(t) \end{bmatrix}. \tag{3.19}$$

The error dynamics are derived in section B.2 and are given by

$$\dot{x}_e(t) = \dot{s}_r(t)\kappa_l(t)y_e(t) + v_f(t)\cos\theta_e(t) - \dot{s}_r(t) \tag{3.20a}$$
$$\dot{y}_e(t) = -\dot{s}_r(t)\kappa_l(t)x_e(t) + v_f(t)\sin\theta_e(t) \tag{3.20b}$$
$$\dot{\theta}_e(t) = v_f(t)\kappa_f(t) - \dot{s}_r(t)\kappa_l(t), \tag{3.20c}$$

where v_f, κ_f and $\dot{s}_r$ are the inputs. Furthermore, $\dot{s}_r$ is the velocity of the reference along the path. It is noted that the error dynamics are now described in the time domain instead of in the spatial domain, as was the case for controller 1. The motion of the reference vehicle is restricted to prevent it from moving backwards, such that the lateral error reduces when the following vehicle moves towards the reference vehicle. The control law of the velocity of the reference vehicle is defined as

$$\dot{s}_r(v_f, x_e) = v_f \left[1 + \sigma(x_e)\right]. \tag{3.21}$$

Here, $\sigma(x_e(t))$ is a saturation which prevents the reference frame from moving backwards. The saturation function satisfies $x_e(t)\sigma(x_e(t)) > 0$ for $x_e(t) \neq 0$ and $\sigma(x_e(t)) \geq -1$, and is defined as

$$\sigma(x_e) = \begin{cases} 1 & \text{for} \quad x_e \geq 1/a \\ ax_e & \text{for} \quad -1/a \leq x_e \leq 1/a \\ -1 & \text{for} \quad x_e \leq -1/a, \end{cases} \tag{3.22}$$

where $a > 0$ is a constant to determine for which value of $x_e(t)$ $\sigma(x_e)$ saturates. When $x_e(t)$ has converged to zero, the velocity of the reference frame is the same as the velocity of the follower but can still move in different directions.
The second lateral controller is derived with help of a Lyapunov function.

Proposition 3 ([22]) Consider the error dynamics (3.20) in closed loop with the control law

$$\kappa_f(x_e, y_e, \theta_e) = \left[1 + \sigma\left(x_e\right)\right]\kappa_l - k_4\frac{\cos\theta_e - 1}{\theta_e}x_e - k_4\frac{\sin\theta_e}{\theta_e}y_e - k_5\theta_e, \tag{3.23}$$

where $a > 0$, $k_2 > 0$, $k_4 > 0$ and $v_f(t) \geq \epsilon > 0$. If $\kappa_l(s_f)$ is bounded, then the system (3.20),(3.23) is globally asymptotically stable (GAS).

The proof of Proposition 3 is given in section A.2.

3.2.1 Simulation results

Simulations are performed for the second lateral controller. The initial condition of the leader is $[x_l(0), y_l(0), \theta_l(0)] = [0, 1, 0]$ and of the follower is $[x_f(0), y_f(0), \theta_f(0)] = [0, 0, \pi/3]$. The reference vehicle has the same initial condition as the leader. The controller gains are chosen as $a = 1$, $k_4 = 1$ and $k_5 = 1$.

In Figure 3.8 the trajectories of the leader and follower with the corresponding lateral error between the follower and reference are shown. Also here, the velocity of the leader is $v_f(t) = 2m/s$ and $v_f(t) = 10m/s$. For both trajectories the follower converges to the leader's trajectory and the lateral errors converge to zero. Furthermore, the path of the follower is identical when it drives with the two different velocities. This result is identical compared with the first lateral controller.
To investigate if the restrictions on the velocity of the reference vehicle results that the follower does not make a detour, simulations are performed where the following vehicle is placed far from the leader's path. The two different paths are considered. The initial condition of the follower is $[x_f(0), y_f(0), \theta_f(0)] = [-20, 0, \pi/3]$ and the leaders initial conditions are $[x_l(0), y_l(0), \theta_l(0)] = [0, 1, 0]$. Both the leader and the follower drives with the velocity $v_f = 10m/s$. The reference vehicle has the same initial conditions as the leader. The controller gains are $a = 1$, $k_4 = 1$ and $k_5 = 1$.

Figure 3.9 presents the results of the simulations with large initial lateral errors. Based on the motion of the following vehicle shown in 4.5(a) and 4.5(c), the following vehicle moves directly towards the leader's path. In 4.5(b) and 4.5(d) the lateral errors are shown. As can be seen, the lateral errors x_e and y_e slowly converge towards zero. The error θ_e converges fast to zero, such that the following vehicle moves in the direction towards the leading vehicle. Figure 3.6 shows the velocity of the reference vehicle. As can be seen, the velocity is zero when the the lateral errors are large. When the lateral error is almost zero, the velocity rapidly increases such that the velocity of the reference vehicle is the same as the velocity of the follower.

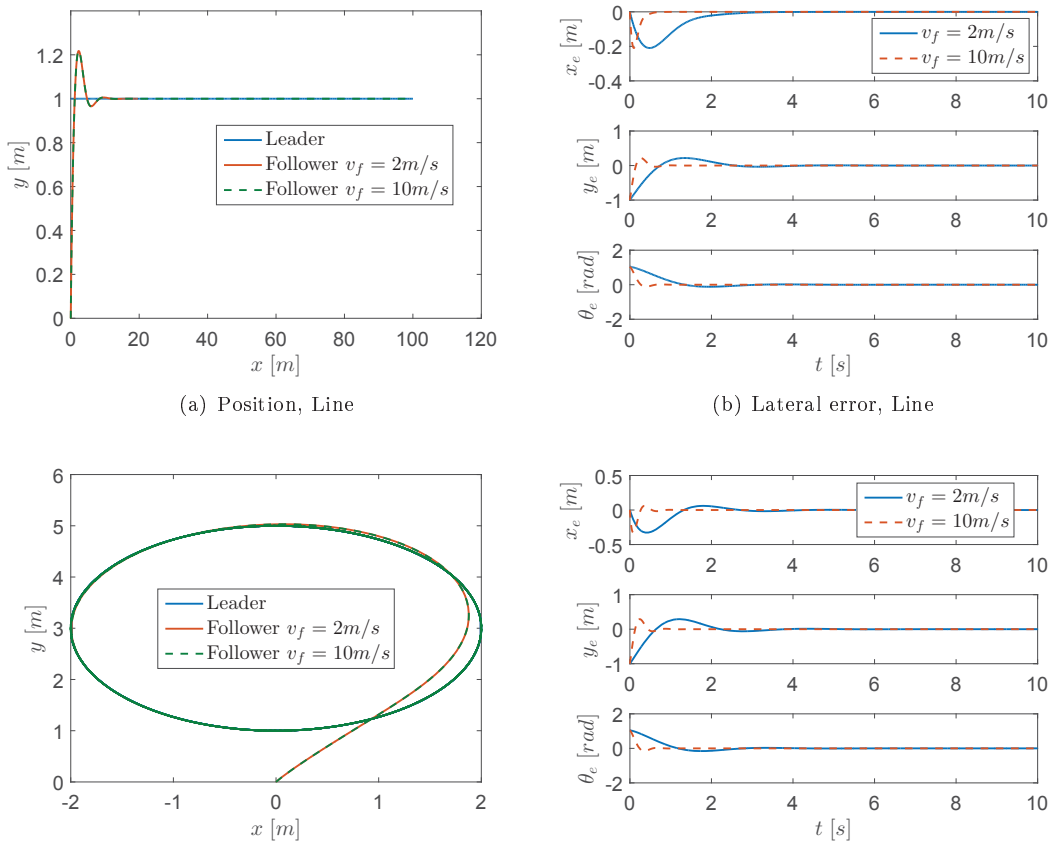

(a) Position, Line

(b) Lateral error, Line

(c) Position, Circle

(d) Lateral error, Circle

Figure 3.8: (a) and (c) show the position of the leader and follower for the two different paths. (b) and (c) show the error between the follower and the reference vehicle.

3.2.2 Comparing lateral controllers

Two different lateral controller are derived in this section and the previous section, respectively. Both controllers have the advantage that the path of the follower is not affected by the follower's velocity. The two controllers are derived using the same principle where a parametrized path of the leader is considered. A difference between the two controllers is the definition of the lateral error "dynamics" between the follower and the reference vehicle. For the first controller the "spatial error dynamics" are defined in the spatial domain, resulting in a lateral controller in the spatial domain. For the second controller, the "spatial error dynamics" are defined in the time domain, resulting in a lateral controller in the time domain. A large difference between the two controller is distinguished for simulations with large initial lateral errors. The restriction on the velocity of the reference vehicle results that the follower converges to the leader's path in a direct way, where the following vehicle with the first lateral controller makes a detour before it converges. Because large differences between the lateral controllers are noticed for large lateral error dynamics, the effect of the controller gains on the path of the following vehicles are further investigated in the next chapter.

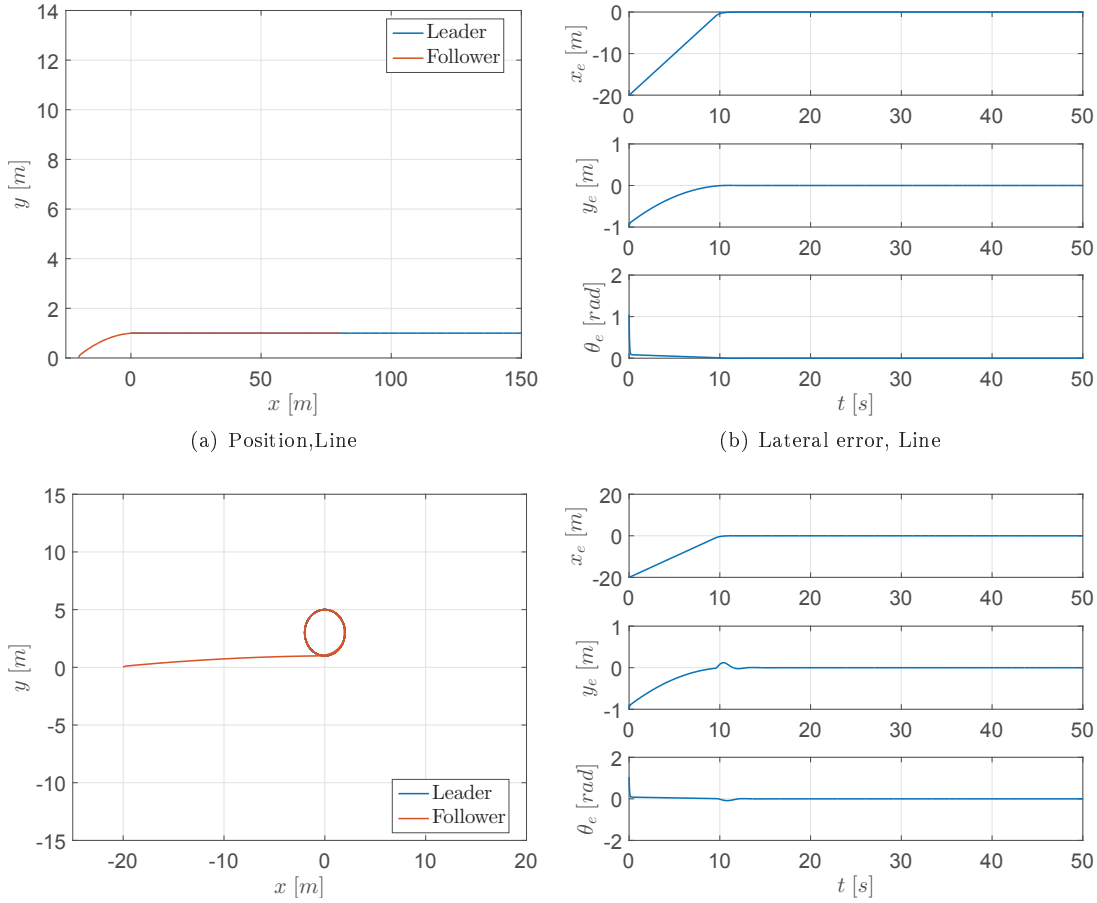

(a) Position,Line

(b) Lateral error, Line

(c) Position, Circle

(d) Lateral error, Circle

Figure 3.9: (a) and (c) show the position of the leader and follower for the two different paths. (b) and (d) show the error between the follower and the reference vehicle.

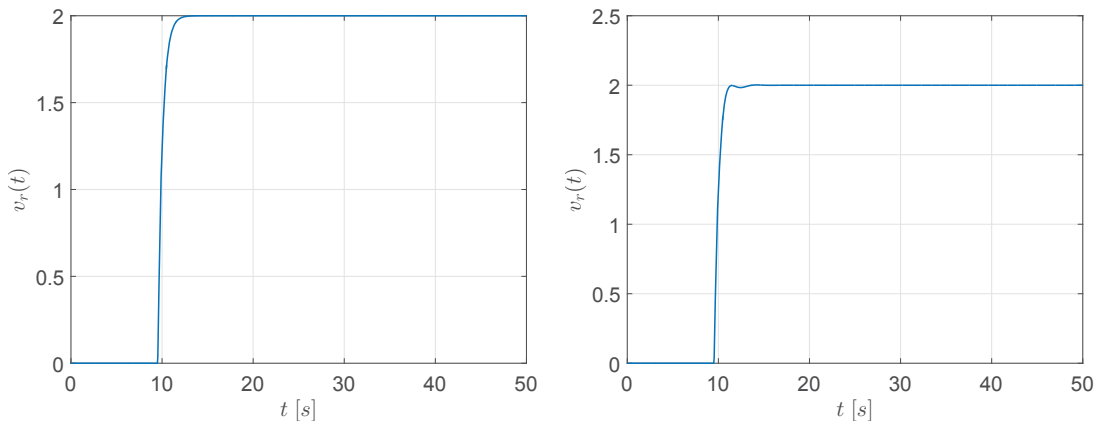

(a) Line

(b) Circle

Figure 3.10: The velocity of the reference vehicle for two different paths.

3.3 Longitudinal controller

Next, a longitudinal controller is derived which is applicable for both lateral controllers. The controller is based on the CACC controller in [37]. The control objective of the longitudinal controller is to regulate the velocity of the follower in order to minimize the spacing error e such that

$$\lim_{t\to\infty} e(t) = 0. \tag{3.24}$$

The longitudinal controller is derived using input-output linearization, where the spacing error e is the output. A control feedback is determined in order to linearize the error dynamics of the spacing error. The already derived CACC controller is designed for the situation in which the vehicle and its predecessor drive along the same trajectory, i.e. a 1D problem. This is not the case for the problem discussed in this report, because the vehicles do not necessarily drive along the same trajectory. As long as the lateral error has not converged to zero, the leader and follower drive along two different paths. For this 2D problem, a longitudinal controller is designed in this section. It is not directly possible to implement the CACC controller, because the leader and follower are not driving on the same path. Ideally, the leader is projected on the path of the follower and the curvilinear intervehicle distance is determined. Because the future path of the leader is not known, this is not possible. In order to apply the 1D problem CACC controller, it is assumed that the leader drives in front of the follower with an estimated curvilinear distance. For the longitudinal controller only the intervehicle distance is needed and the assumption that both vehicles drive along the same path is enough to apply the CACC based controller. In order to estimate the curvilinear intervehicle distance, the longitudinal error is defined in order to determine this distance in longitudinal direction. The error in longitudinal direction with respect to the body fixed frame of the follower, is defined as

$$\begin{bmatrix} x_{e,long}(t) \\ y_{e,long}(t) \\ \theta_{e,long}(t) \end{bmatrix} = \begin{bmatrix} \cos\theta_f(t) & \sin\theta_f(t) & 0 \\ -\sin\theta_f(t) & \cos\theta_f(t) & 0 \\ 0 & 0 & 1 \end{bmatrix} \begin{bmatrix} x_l(t) - x_f(t) \\ y_l(t) - y_f(t) \\ \theta_l(t) - \theta_f(t) \end{bmatrix} \tag{3.25}$$

and shown in Figure 3.11. Now, it is assumed that the curvilinear intervehicle distance between the vehicles is equal to $x_{e,long}$.

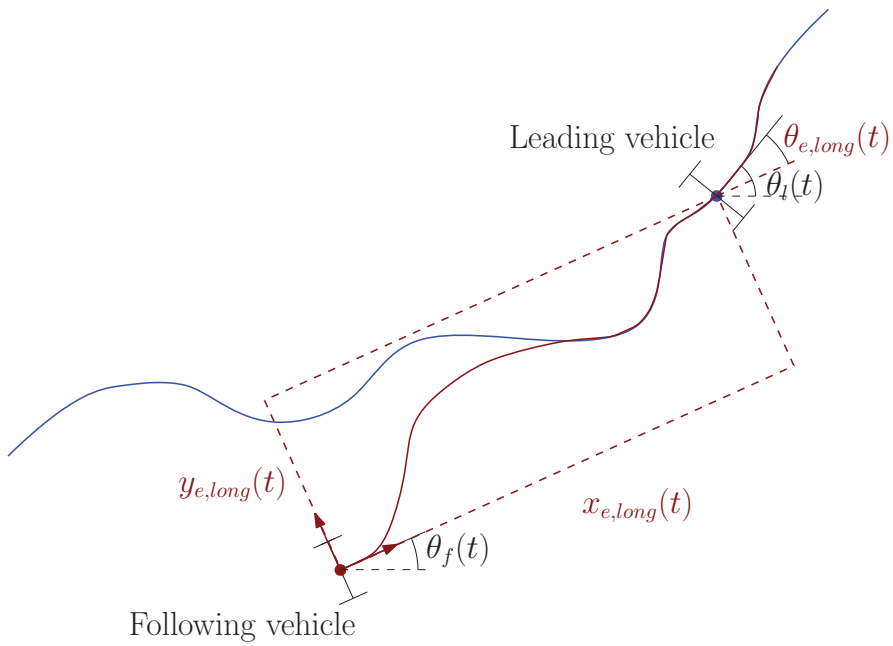

Figure 3.11: A schematic overview of the definition of the error between the follower (red) and leader (blue) for the longitudinal controller in the time domain.

3.3.1 CACC based longitudinal controller

The desired intervehicle distance between the leader and the follower according to a constant time gap spacing policy is defined as

$$d_r = r + hv_f(t), \tag{3.26}$$

where r is the standstill spacing distance and h is the time gap. The spacing error is given by

$$\begin{aligned} e &= d - d_r \\ &= (q_l - q_f - L) - (r + hv_f) \\ &= (x_{e,long} - L) - (r + hv_f)\,. \end{aligned} \tag{3.27}$$

where d is the intervehicle distance from the front bumper of the follower to the rear bumper of the leader, q_l and q_f the curvilinear position along follower's path of the rear bumper of the leader and the follower, respectively. Figure 3.12 shows an overview of the spacing symbols.

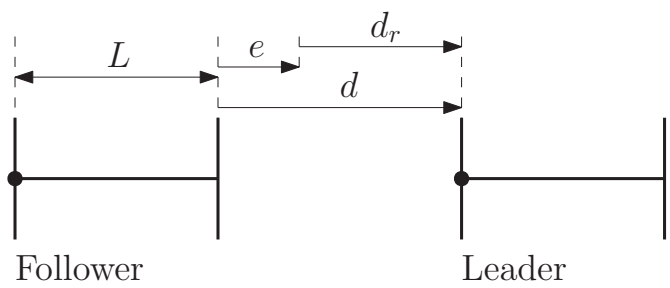

Figure 3.12: A schematic overview of the spacing error.

As a basis for the controller design of the longitudinal controller, the following vehicle model is adopted defined in [37]

$$\begin{bmatrix} \dot{d}(t) \\ \dot{v}_f(t) \\ \dot{a}_f(t) \end{bmatrix} = \begin{bmatrix} v_f\kappa_f\left[\cos\theta_f\left(x_l - x_f\right) + \sin\theta_f\left(y_l - y_f\right)\right] - v_f + v_l\cos\left(\theta_l - \theta_f\right) \\ a_f \\ -\frac{1}{\tau}a_f + \frac{1}{\tau}u_f \end{bmatrix}, \tag{3.28}$$

where $a_f(t)$ is the acceleration of the following vehicle, $u_f(t)$ the desired acceleration of the follower and τ a time constant representing driveline dynamics. The state $\dot{d}$ is determined by taking the derivative of the intervehicle distance d defined in (3.27) and substituting (3.25). The longitudinal controller is derived based on the error dynamics of the spacing error. The states of the error dynamics of the spacing error e are defined as

$$\begin{bmatrix} e_1 \\ e_2 \\ e_3 \end{bmatrix} = \begin{bmatrix} e \\ \dot{e} \\ \ddot{e} \end{bmatrix}. \tag{3.29}$$

By differentiation, the last state of the error dynamics is determined, with the time argument t omitted for readability:

$$\dot{e}_3 = x^{(3)}_{e,long} - \frac{h}{\tau^2}a_f + \frac{h}{\tau^2}u_f - \frac{1}{\tau}\xi + \frac{1}{\tau}u_f, \tag{3.30}$$

with

$$
\begin{aligned}
x_{e,long}^{(3)} = &\left(-3\kappa_f^2 v_f a_f - 3\kappa_f \dot{\kappa}_f v_f^2\right) x_{e,long} + \left(-\kappa_f^3 v_f^3 + 2\dot{\kappa}_f a_f + \frac{1}{\tau}\left[u_f - a_f\right]\kappa_f + v_f \ddot{\kappa}_f\right) y_{e,long} \\
&+ \left(-v_l^2 \dot{\kappa}_l + 3\kappa_f v_l a_f + 3 v_f v_l \dot{\kappa}_f + 3\kappa_f v_f a_l - 3\kappa_l v_l a_l\right) \sin\theta_{e,long} \\
&+ \left(-3\kappa_f^2 v_f^2 v_l - 3\kappa_f \kappa_l v_f v_l^2 + \kappa_l^2 v_l^3 + \frac{1}{\tau}\left[u_l - a_l\right]\right) \cos\theta_{e,long} + \kappa_f^2 v_f^3 + \frac{1}{\tau}\left(a_f - u_f\right).
\end{aligned} \tag{3.31}
$$

The input ξ in $\dot{e}_3$ is the input for linearizing the error dynamics using feedback linearization and is defined as

$$
\xi := h\dot{u}_f + u_f. \tag{3.32}
$$

For input-output linearization, the relative degree of the error dynamics is determined with the output $e(t)$ and the input $\xi(t)$. First the error dynamics is rewritten as

$$
\dot{x} = f(x, \kappa_f, \dot{\kappa}_f, \kappa_l, \dot{\kappa}_l, v_f, v_l, a_f, u_l, u_f, u_l) + g(\tau)\xi, \tag{3.33}
$$

with the states $\mathbf{x} = [e_1, e_2, e_3]^T$ and

$$
f(x, \kappa_f, \dot{\kappa}_f, \kappa_l, \dot{\kappa}_l, v_f, v_l, a_f, u_l, u_f, u_l) = \begin{bmatrix} e_2 \\ e_3 \\ \zeta(x, \kappa_f, \dot{\kappa}_f, \kappa_l, \dot{\kappa}_l, v_f, v_l, a_f, u_l, u_f, u_l) \end{bmatrix}, \tag{3.34}
$$

$$
g(\tau) = \begin{bmatrix} 0 \\ 0 \\ -\frac{1}{\tau} \end{bmatrix}. \tag{3.35}
$$

The term $\zeta(x, \kappa_f, \dot{\kappa}_f, \kappa_l, \dot{\kappa}_l, v_f, v_l, a_f, a_l, u_f, u_l)$ is given in Appendix B.4. Using (3.34) and (3.35), the relative degree of the error dynamics is determined, where the output is $h(x) = e_1(t)$. The Lie derivatives are derived in Appendix 3.3 and given by

$$
\begin{aligned}
L_g h(x) &= 0 \\
L_g L_f h(x) &= 0 \\
L_g L_f^2 h(x) &= -\frac{1}{\tau}.
\end{aligned} \tag{3.36}
$$

As a result of that, the relative degree of the error dynamics of the spacing error is three. Because the relative degree is equal to the number of states, the error dynamics can be linearized using input output linearization. The state feedback law for the input $\xi(t)$ is

$$
\xi(t) = \frac{1}{L_g L_f^2 h(x)}\left(-L_f^3 h(x) + \nu\right), \tag{3.37}
$$

where ν is the new input of the linearized error dynamics. The Lie derivative $L_g L_f^2 h(x) = -\frac{1}{\tau}$ and the Lie derivative $L_f^3 h(x)$ is given by

$$
L_f^3 h(x) = \frac{\partial}{\partial x}\left(\frac{\partial L_f^2 h(x)}{\partial x}\right) f(x, \kappa_f, \dot{\kappa}_f, \kappa_l, \dot{\kappa}_l, v_f, v_l, a_f, u_l, u_f, u_l) = \zeta, \tag{3.38}
$$

where ζ is shown in Appendix B.4. Eventually, the state feedback law is

$$
\xi(t) = \tau\left[\zeta - \nu\right]. \tag{3.39}
$$

The input ν is chosen such that the linearized error dynamics is stabilized. The linearized error dynamics are given by

$$\begin{bmatrix}\dot{e}_1\\ \dot{e}_2\\ \dot{e}_3\end{bmatrix} = \underbrace{\begin{bmatrix}0 & 1 & 0\\ 0 & 0 & 1\\ 0 & 0 & 0\end{bmatrix}}_{A_{long}} \begin{bmatrix}e_1\\ e_2\\ e_3\end{bmatrix} + \underbrace{\begin{bmatrix}0\\ 0\\ 1\end{bmatrix}}_{B_{long}} \nu. \tag{3.40}$$

When input ν is chosen as $\nu = -K_{long}e$ with $K_{long} := [k_p, k_d, k_{dd}]$, the closed loop system is given by

$$\begin{bmatrix}\dot{e}_1\\ \dot{e}_2\\ \dot{e}_3\end{bmatrix} = (A_{long} - B_{long}K_{long}) \begin{bmatrix}e_1\\ e_2\\ e_3\end{bmatrix}, \tag{3.41}$$

where the eigenvalues of $A_{long} - B_{long}K_{long}$ are real and negative to achieve a globally exponentially stable (GES) system. With the Routh-Hurwitz stability criterium, the eigenvalues of (3.40) are always negative when $k_p, k_d, k_{dd} > 0$ and $k_d k_{dd} - k_p > 0$.

3.3.2 Simulations

Now the longitudinal controller is derived, the controller is applied to the kinematic model of the follower. The kinematic model of the follower and leader are described by (3.1). Furthermore, the spacing policy transfer function $H(s) = \xi(s)/u_f(s)$, derived from (3.32) is

$$H(s) = hs + 1. \tag{3.42}$$

The input of the spacing policy transfer function is ξ which is determined in (3.39). The output of the spacing policy transfer function is the desired acceleration of the follower. By integration of $u_f(t)$, the desired velocity of the follower $v_f(t)$ is determined.

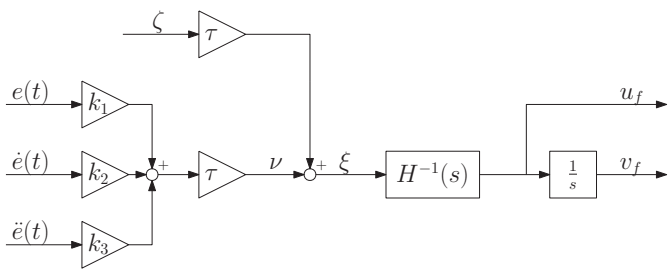

Figure 3.13: The block scheme of the implementation of the longitudinal controller on the follower.

A simulation with lateral controller 1 is performed for driving on a line. The leading vehicle starts 5m in front of the follower, and the follower starts from standstill. The controller gain is chosen as $K_{long} = [3, 3, 3]$. The standstill distance $r = 1m$, the time gap $h = 1s$ and the length of the vehicle $L = 0$. In Figure 3.14 the results of the longitudinal controller are shown. As can be seen in Figure 3.17(a), the velocity of the follower converges to the velocity of the leader. This happens when the estimated intervehicle distance, $x_{e,long}$, slowly converges to the desired intervehicle distance, as shown in Figure 3.17(b). The overshoot of the velocity is large, but the behavior of the system can be affected by changing the controller gains.

Limitations longitudinal controller

The longitudinal controller is designed based on a CACC controller considering a 1D problem. To use this controller in the situation where the leader and follower do not move along the same path, the curvilinear intervehicle distance is estimated by the longitudinal error $x_{e,long}$. In the remainder of this section, situations are discussed where the estimation of the curvilinear intervehicle distance is not correct. The first situation is shown in Figure 3.15, where the leader and follower drive in opposite direction along the same path.

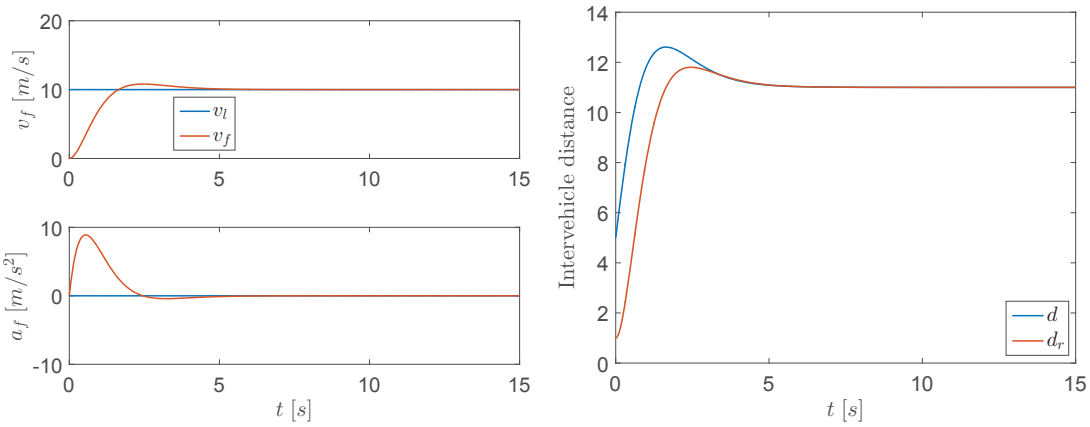

(a) Velocity and acceleration

(b) Intervehicle distance

Figure 3.14: The velocity and acceleration of the follower (blue) and the leader (orange) in a) and in b) the estimated intervehicle distance between the leader and follower (blue) and the desired intervehicle distance (orange)

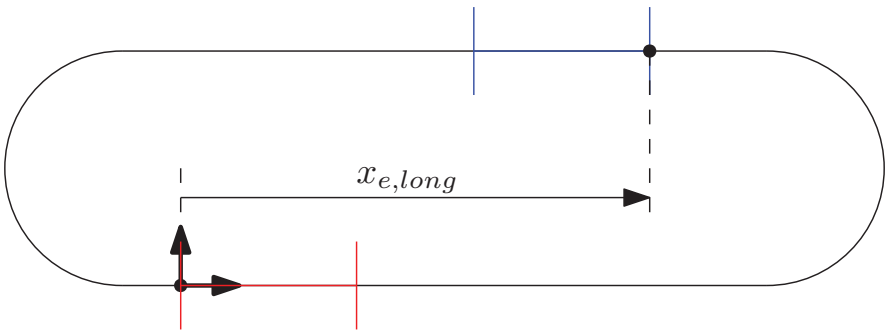

Figure 3.15: Situation 1 that can cause limitations for the longitudinal controller. The follower is displayed in red and the leader in blue. The vehicles drives counter-clockwise.

The simulation results for the first situation are shown in Figure 3.16. As can be seen, the expected results are confirmed. First the follower accelerates to achieve the desired intervehicle distance. Because the leader moves towards the follower, the intervehicle distance becomes smaller than desired and the follower starts accelerating backwards to achieve again the desired intervehicle distance. Eventually the follower moves backwards with the the velocity $-v_l(t)$.

In the second situation, the vehicles drive behind each other on the same path with a desired intervehicle distance. When the vehicles drive along a straight line, the estimated intervehicle distance $x_{e,long}$ is equal to the curvilinear intervehicle distance. Then the vehicles start turning with a constant radius and the estimated intervehicle distance changes. This effect is investigated. The initial condition of the leader is $[x_l(0), y_l(0), \theta_l(0)] = [1, 0, 0]$ and the initial condition of the follower is $[x_l(0), y_l(0), \theta_l(0)] = [0, 0, 0]$. Both the follower and leader have an initial velocity of $10m/s$. The length of the vehicle $L = 0$, the time gap $h = 1s$ and the standstill distance $r = 1m$. The gains of longitudinal controller are $K_{long} = [100, 20, 10]$.

The results of the simulation for the second scenario are shown in Figure 3.17. For driving on a straight line, the intervehicle distance is as desired. When the leader starts turning, the intervehicle distance decreases shortly. When also the follower begins to turn, the intervehicle distance increases again and remains constant while both vehicles are turning. When the leader drives on the straight line again but the follower is still turning, the intervehicle distance slightly increases until the follower also drives on the straight line.

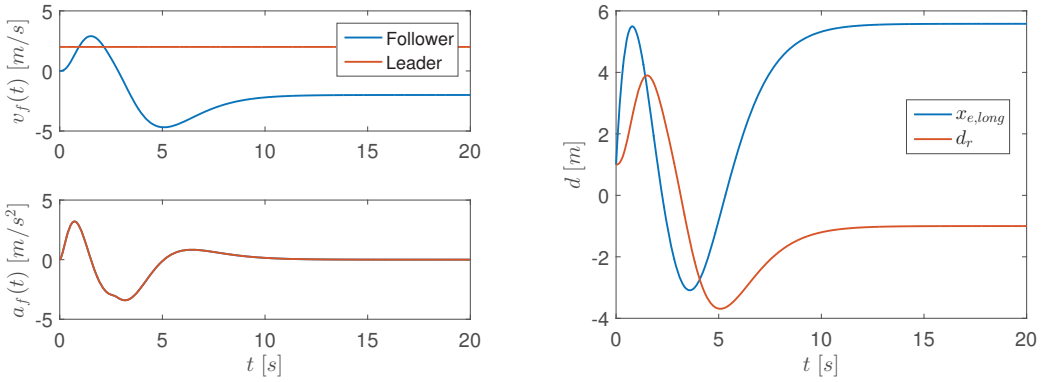

(a) Velocity and acceleration

(b) Intervehicle distance

Figure 3.16: The velocity and acceleration of the follower (blue) and the leader (orange) in a) and in b) the estimated intervehicle distance between the leader and follower (blue) and the desired intervehicle distance (orange)

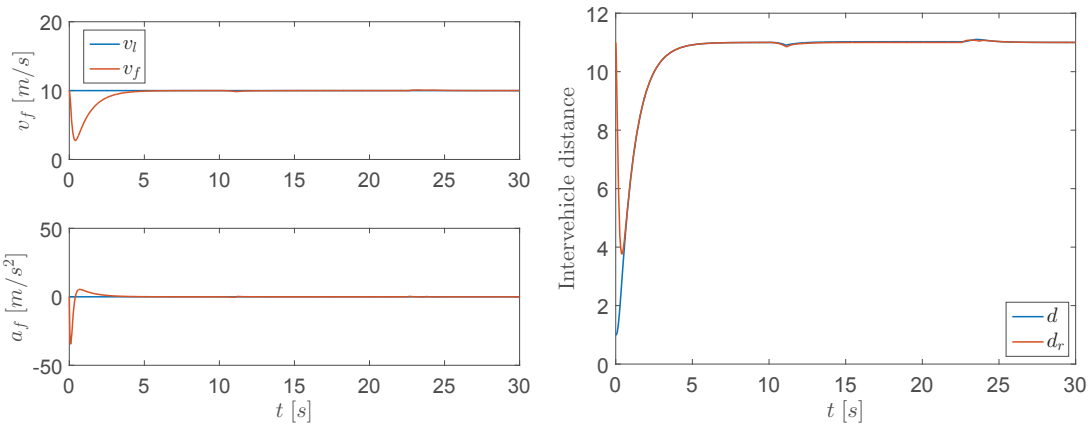

(a) Velocity and acceleration

(b) Intervehicle distance

Figure 3.17: The velocity and acceleration of the follower (blue) and the leader (orange) in a) and in b) the estimated intervehicle distance between the leader and follower (blue) and the desired intervehicle distance (orange)

3.4 Observer

The lateral and longitudinal controllers are derived and applied on the follower. During experiments several parameters are measured for both vehicles and they are transmitted between the different vehicles. Because not all desired parameters are measured, an observer is derived to estimate the orientation and velocity of the leading vehicle. As a positive side issue, the observer reduces the measurement noise. An nonlinear observer is derived, based on the observable canonical form for a multi-input multi-output (MIMO) system. This approach is used to derive an observer for a continuous time observer. For more details of the observer are given in [44]. The model (3.1) cannot be transformed to the observable canonical form. Therefore, an integrator is added for the input v resulting in the following model:

$$\begin{bmatrix} \dot{x} \\ \dot{y} \\ \dot{\theta} \\ \dot{v} \end{bmatrix} = \begin{bmatrix} v\cos\theta \\ v\sin\theta \\ \omega \\ \dot{v} \end{bmatrix}, \tag{3.43}$$

where the inputs are ω and $\dot{v}$ and the outputs are x and y. The states of the new model are given by

$$x = \begin{bmatrix} x \\ y \\ \theta \\ v \end{bmatrix} = \begin{bmatrix} x_1 \\ x_2 \\ x_3 \\ x_4 \end{bmatrix}. \tag{3.44}$$

This results in the vehicle model given by

$$\begin{bmatrix} \dot{x}_1 \\ \dot{x}_2 \\ \dot{x}_3 \\ \dot{x}_4 \end{bmatrix} = \begin{bmatrix} x_4\cos x_3 \\ x_4\sin x_3 \\ u_2 \\ u_1 \end{bmatrix}. \tag{3.45}$$

To derive the observer, (3.45) is transformed into a block triangular block form. A general description of this structure is given by

$$\begin{aligned} \dot{z} &= Az + B(z,u) \\ y &= Cz, \end{aligned} \tag{3.46}$$

where $z = [z_1, z_2, z_3, z_4]^T$ are the states. Here, the matrix $A = diag(A_1, A_2)$, where A_1 and A_2 are

$$A_1 = \begin{bmatrix} 0 & 1 \\ 0 & 0 \end{bmatrix} \qquad A_2 = \begin{bmatrix} 0 & 1 \\ 0 & 0 \end{bmatrix},$$

and matrix $C = diag(C_1, C_2)$, where $C_1 = [1, 0]$ and $C_2 = [1, 0]$. Using the coordinate transformation $z = \Phi(x)$, the new coordinates are

$$z = \begin{bmatrix} h_1(z) \\ L_f h_1(z) \\ h_2(z) \\ L_f h_2(z) \end{bmatrix} = \begin{bmatrix} x_1 \\ x_4\cos x_3 \\ x_2 \\ x_4\sin x_3 \end{bmatrix}, \tag{3.47}$$

with the necessary condition that the Jacobian of $\Phi(x)$ is nonsingular such that $\Phi(x)$ is a diffeomorphism on the region $Z \subset \mathbb{R}^4$ which contains the origin. The determinant of the Jacobian of $\Psi(x)$ is given by

$$\det\left(\mathcal{J}(\Phi(x))\right) = \begin{vmatrix} 1 & 0 & 0 & 0 \\ 0 & 0 & -x_4\sin x_3 & \cos x_3 \\ 0 & 1 & 0 & 0 \\ 0 & 0 & x_4\cos x_3 & \sin x_3 \end{vmatrix} = x_4\cos^2 x_3 + x_4\sin^2 x_3 = x_4. \tag{3.48}$$

Consequently, the Jacobian is nonsingular when the state x_4, i.e. the velocity, is nonzero. The transformed system is given by

$$\dot{z} = \begin{bmatrix} x_4\cos x_3 \\ \dot{x}_4\cos x_3 - x_4\dot{x}_3\sin x_3 \\ x_4\sin x_3 \\ \dot{x}_4\sin x_3 + x_4\dot{x}_3\cos x_3 \end{bmatrix}. \tag{3.49}$$

The output of the system are the states x_1 and x_2 and the orientation x_3 and velocity x_4 are not measured and thus unknown. Therefore, these states are determined by

$$x_3 = \arctan\left(\frac{z_4}{z_2}\right) \tag{3.50a}$$

$$x_4 = \sqrt{z_2^2 + z_4^2}. \tag{3.50b}$$

The state x_4 can be determined when z_2 is nonzero. Eventually, (3.49) is transformed into the form of (3.46) using (3.50) and is given by

$$\dot{z} = \left[\begin{array}{cc|cc} 0 & 1 & 0 & 0 \\ 0 & 0 & 0 & 0 \\ \hline 0 & 0 & 0 & 1 \\ 0 & 0 & 0 & 0 \end{array}\right] z + \begin{bmatrix} 0 \\ \frac{1}{\sqrt{1+\left(\frac{z_4}{z_2}\right)^2}} u_1 - \sqrt{z_2^2 + z_4^2} \frac{z_4}{z_2\sqrt{1+\left(\frac{z_4}{z_2}\right)^2}} u_2 \\ 0 \\ \frac{z_4}{z_2\sqrt{1+\left(\frac{z_4}{z_2}\right)^2}} u_1 + \sqrt{z_2^2 + z_4^2} \frac{1}{\sqrt{1+\left(\frac{z_4}{z_2}\right)^2}} u_2 \end{bmatrix} \tag{3.51a}$$

$$y = \left[\begin{array}{cc|cc} 1 & 0 & 0 & 0 \\ \hline 0 & 0 & 1 & 0 \end{array}\right] z \tag{3.51b}$$

3.4.1 Observer structure

Now the vehicle model is transformed to the required form, the observer is constructed. It is assumed that the states $z(t)$ and inputs $\dot{v}(t)$ and $\omega(t)$ are bounded. The observer estimates the four different states of z. Using (3.51) an estimation of these states is determined and a correction term is added based on the error between the measured and estimated output. By adjusting S, the importance of the measurement can be adjusted. The observer is given by

$$\begin{bmatrix} \dot{\hat{z}}_1 \\ \dot{\hat{z}}_2 \end{bmatrix} = \begin{bmatrix} \hat{z}_2 \\ 0 \end{bmatrix} + \begin{bmatrix} 0 \\ \cos\hat{\theta} u_1 - \hat{v}\sin\hat{\theta} u_2 \end{bmatrix} - S_1^{-1} \begin{bmatrix} 1 \\ 0 \end{bmatrix} (\hat{z}_1 - y_1) \tag{3.52a}$$

$$\begin{bmatrix} \dot{\hat{z}}_3 \\ \dot{\hat{z}}_4 \end{bmatrix} = \begin{bmatrix} \hat{z}_4 \\ 0 \end{bmatrix} + \begin{bmatrix} 0 \\ \sin\hat{\theta} u_1 + \hat{v}\cos\hat{\theta} u_2 \end{bmatrix} - S_2^{-1} \begin{bmatrix} 1 \\ 0 \end{bmatrix} (\hat{z}_3 - y_2) \tag{3.52b}$$

Here, S_1 and S_2 are unique solutions of the Lyapunov equation

$$M^T S + SM + Q = 0. \tag{3.53}$$

Here, $M = -\frac{1}{2}c_i I - A_i$ with the controller gain $c_i > 0$, and $Q = C^T C$ which is symmetric. An unique solution of (3.53) exist if $-\frac{1}{2}c_i I - A_i$ is Hurwitz and if $(-\frac{1}{2}c_i I - A_i, C_i)$ is observable. Because of the form of A_i, M is an upper triangular matrix and the poles are negative when $c_i > 0$. Consequently, the matrix $-\frac{1}{2}c_i I - A_i$ is Hurwitz. To determine if $(-\frac{1}{2}c_i I - A_i, C_i)$ is observable, the observability matrix is given by

$$\mathcal{O} = \begin{bmatrix} 1 & 0 \\ -\frac{1}{2}c_i & -1 \end{bmatrix}. \tag{3.54}$$

The rank of the observability matrix is two, so $(-\frac{1}{2}c_i I - A_i, C_i)$ is observable. Eventually, this results in the Lyapunov equation

$$0 = -\theta_1 S_1 - S_1 A_1 - A_1^T S_1 + C_1^T C_1, \tag{3.55a}$$

$$0 = -\theta_2 S_2 - S_2 A_2 - A_2^T S_2 + C_2^T C_2. \tag{3.55b}$$

According [44, Theorem 3], when choosing c_1 and c_2 sufficient large such that

$$1 \leq c_1 \text{ and } c_1 \leq c_2, \tag{3.56}$$

the estimates $\hat{z}(t)$ of the observer converges exponentially to the true state $z(t)$ of the plant for any initial $\hat{z}(0)$. Because the velocity and orientation are needed for the observer and are not measured during the experiments, the estimated $\hat{v}$ and $\hat{\theta}$ are given by

$$\hat{v} = \sqrt{\hat{z}_2^2 + \hat{z}_4^2} \tag{3.57a}$$

$$\hat{\theta} = \arccos\left(\frac{\hat{z}_2}{\sqrt{\hat{z}_2^2 + \hat{z}_4^2}}\right) \tag{3.57b}$$

The final observer is given by

$$\begin{bmatrix} \dot{\hat{z}}_1 \\ \dot{\hat{z}}_2 \end{bmatrix} = \begin{bmatrix} \hat{z}_2 \\ 0 \end{bmatrix} + \begin{bmatrix} 0 \\ \frac{z_2}{\sqrt{\hat{z}_2^2+\hat{z}_4^2}} u_1 - |\hat{z}_4| u_2 \end{bmatrix} - S_1^{-1} \begin{bmatrix} 1 \\ 0 \end{bmatrix} (\hat{z}_1 - y_1) \tag{3.58a}$$

$$\begin{bmatrix} \dot{\hat{z}}_3 \\ \dot{\hat{z}}_4 \end{bmatrix} = \begin{bmatrix} \hat{z}_4 \\ 0 \end{bmatrix} + \begin{bmatrix} 0 \\ \sqrt{1 - \frac{z_2^2}{\hat{z}_2^2+\hat{z}_4^2}} u_1 + \hat{z}_2 u_2 \end{bmatrix} - S_2^{-1} \begin{bmatrix} 1 \\ 0 \end{bmatrix} (\hat{z}_3 - y_2) \tag{3.58b}$$

3.4.2 Simulation Results

The designed observer is implemented for the leading vehicle and different simulations are performed for two trajectories: driving in a circle and driving in a straight line. The measured x and y position of the leader contains measurement noise. The observer is implemented such that the measured position of the leader is filtered and the orientation and velocity is estimated. Moreover, these signals are sent to the follower. The initial condition of the leader is $[x_l(0), y_l(0), \theta_l(0)] = [0, 0, 0]$ and of the follower $[x_f(0), y_f(0), \theta_f(0)] = [-1, -1, \pi/3]$. There reference vehicle has the same initial condition as the leader. The radius of the circular path is $R = 5m$. The leader drives with a velocity of $v_l(t) = 2m/s$. The measurement noise has a mean equal to zero and the variance is 0.1. The observer is implemented on lateral controller 1.
Figure 3.18 shows the results of simulations for the two trajectories where the measured output of the leader is compared with the estimated output, and the actual velocity is compared with the estimated velocity. As can be seen, the observer estimates the position and the velocity of the leader correctly. Furthermore, measurement noise of the measured output is filtered by the observer and a smoother output signal is obtained which is sent to the reference and following vehicles.

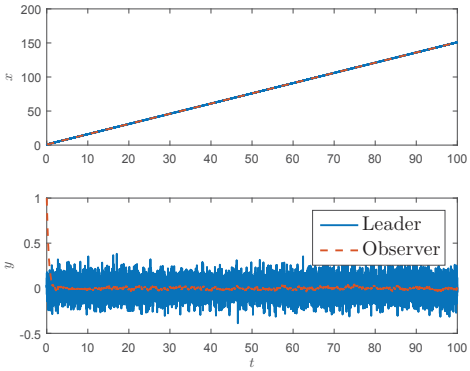

(a) Position, straight line

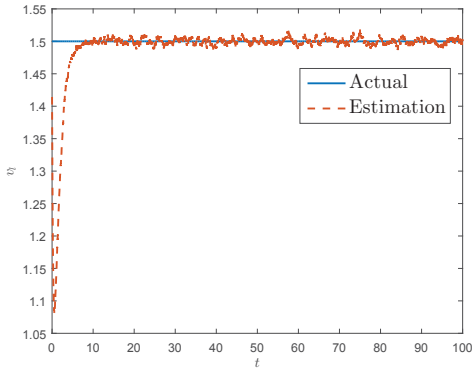

(b) Velocity, straight line

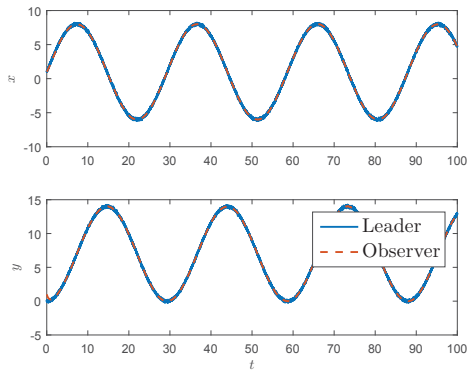

(c) Position, circular path

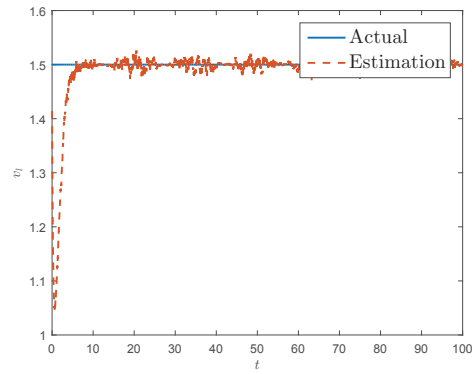

(d) Velocity, circular path

Figure 3.18: The estimation of the x and y position and the velocity of the leader determined with the observer for two different trajectories.

3.5 Summary

In this chapter two lateral controllers, a longitudinal controller and an observer are derived. The lateral controllers are designed based on a path following problem. By parameterizing the path of the leader, the position of the leader does not depend on time but on the traveled distance of the leader. For both controllers it is achieved that the curvature of the follower's path does not depend on the velocity of the following vehicle. A difference between the the two controllers is noticed when simulations are performed with large initial lateral errors. For the second lateral controller the motion of the reference vehicle is restricted. As a result of this, the follower moves directly towards the leader's path compared with the first lateral controller.
The longitudinal controller is derived such that the follower follows the leader with a constant time gap policy. The longitudinal error is used to estimate the intervehicle distance when the leader and follower are not driving along the same path. Using input-output linearization the error dynamics of the spacing error are linearized. A drawback of the longitudinal controller is the estimation of the curvilinear intervehicle distance along the follower's path. Two simple situations are discussed where the estimation of the curvilinear distance were incorrect.
To estimate the velocity and orientation of the vehicle when only measuring the position of the vehicle, an observer is designed. As a result of simulations, the velocity and orientation are estimated correctly and the measurement noise is reduced.

In chapter 4 the two lateral and the longitudinal controllers are tuned such that desired performance is achieved.

Chapter 4

Performance

In the previous section two lateral controllers and a longitudinal controller are designed. The controllers are derived and the controller gains are determined to stabilize the error dynamics. During this derivation of different controllers, the performance is not taken into account. Simulations in chapter 3 show that the behavior of different systems with the lateral and longitudinal controller is not as desired when gains are chosen, e.g. overshoot was present. In this chapter the controller gains are tuned such that the desired behavior, i.e. no collisions and comfort, is achieved.
This chapter is organized as follows. Section 4.1 presents a definition of the desired performance in order to tune the different controllers. In section 4.2, the error dynamics of the lateral controllers are linearized in order to determine the controller gains using pole placement in section 4.3. Moreover, the controller gains of the lateral controllers are determined using time simulation in section 4.3. In section 4.4, the controller gains of the longitudinal controller are determined using pole placement. Section 4.5 presents simulation results of the tuned controllers. This chapter ends with summary in section 4.6

4.1 Performance definition

The lateral and longitudinal controllers are tuned by adjusting the various controller gains. It is important that the controllers are tuned such that good performance, i.e. safety, comfort and tracking performance, is achieved. Consequently, the following three criteria are reviewed;

- Safety: here is looked to the safety of the individual vehicle. Important is that the vehicle stays in the lane to prevent that it cuts corners and also collisions with vehicles in other lanes. Furthermore, the intervehicle distance must be large enough the prevent collisions with vehicles in the same lane.

- Comfort: considering the comfort of the passengers, there are limits for the acceleration and deceleration of the vehicle. Moreover, the vehicle must drive smooth towards the desired trajectory, i.e. no oscillations around the trajectory or undesired motions before the vehicle drives along the leader's trajectory.

- Tracking: to achieve good tracking performance, the tracking errors between the follower and the leader and the follower and reference vehicle are small, for the longitudinal and lateral controller respectively. When these errors converge to zero the follower converges to the leader's path and it follows the leader with the desired intervehicle distance.

To investigate the effect of the different controller gains on the performance criteria, the following scenario's are considered:

- Velocity: two different velocities of the leader are considered. The leader drives with a low velocity ($30km/h$) and a high velocity ($130km/h$).

- Initial condition: two different initial conditions of the follower with respect to the initial conditions of the leader are considered. The follower starts close and far from the leader.
- Trajectory: two different trajectories of the leading vehicle are considered. The first trajectory is a straight line and the second a circular path.

In total eight different combinations are possible with these scenario's.

To tune the controller gains of the lateral and longitudinal controller, two methods are used. Pole placement is the first method, which is used for the longitudinal controller and the linearized system of the lateral controller. The second method, specifically for the lateral controller, is to find the gains in a iterative manner by performing time simulations. The three criteria; safety, comfort and tracking performance do not appear as a direct outcome of these two methods. The solution is to translate them into the performance criteria that can be measured, i.e. rise time, settling time, overshoot and total variation.

To achieve a safe performance of the individual vehicle the rise time should be small, since then the error converges fast to its steady state solution. Also the settling time should be small in order to minimize the oscillations around the steady state solution. Both overshoot and total variation should be as small as possible. The overshoot should be as close as possible to zero, to prevent that the vehicle moves outwards it lane. A small total variation results in fast convergence and minimized the peaks in the time response.
For the comfort for the individual vehicle the rise time cannot be too low as a small rise time results in large accelerations. The settling time is desired to be small to prevent large oscillations around the steady state solution. It is also desired that there is no overshoot. A small total variation results in fast convergence and minimized the peaks in the time response which positively effects the comfort.
In order to achieve good tracking performance, the rise time must be small to converge fast to the steady state solution. To avoid large oscillations around the steady state solutions, the settling time must be small. For a good tracking performance, some overshoot is allowed but it needs to be reasonable with regards to the other two criteria, safety and comfort. Total variation needs to be small to achieve fast convergence to the steady state solution.
In Table 4.1 the desired values of the four different performance criteria are listed. In general it is important to take the acceleration into account. Probably the acceleration is the bottleneck to achieve good safety and tracking behavior, because it can not be too high.

Table 4.1: The desired values for the four performance criteria

	Safety	**Comfort**	**Tracking**
Rise time	Small value	Higher value	Small value
Settling time	Small value	Small value	Small value
Overshoot	Small as possible	No overshoot	Small value
Total variation	Small as possible	Small value	Small value

4.2 Linearisation Of The Error Dynamics

In the previous section different methods are discussed to determine the performance of the lateral and longitudinal controllers. For using the linear techniques, the error dynamics of the lateral controllers are linearized. The error dynamics of the longitudinal is already linearized by input-output linearization. When the error dynamics of the lateral controllers are linearized around the origin, the performance of the controllers is determined for when the tracking errors are small.
To linearize the error dynamics, the states are chosen as

$$\mathbf{x}(t) = [x_e(t), y_e(t), \theta_e(t)]^T, \tag{4.1}$$

and the inputs of the linearized systems are chosen as

$$u_1(t) = \kappa_f(t) - \kappa_l(t) \tag{4.2a}$$
$$u_2(t) = v_l(t) - v_f(t), \tag{4.2b}$$

such that the inputs converges to zero when the error dynamics converge to zero. With the chosen states and inputs, the two lateral controllers are linearized the equilibrium point

$$\mathbf{x}^*(t) = [0, 0, 0]^T \tag{4.3a}$$
$$\mathbf{u}^*(t) = [0, 0]^T. \tag{4.3b}$$

For readability, the time argument t is dropped in the remaining of this section.

4.2.1 Lateral controller 1

The error dynamics of lateral controller 1, derived in Appendix B.1 and B.3, are given by

$$\dot{x}_e = v_f \kappa_f y_e + v_f \tilde{v}_r \cos\theta_e - v_f \tag{4.4a}$$
$$\dot{y}_e = -v_f \kappa_f x_e + v_f \tilde{v}_r \sin\theta_e \tag{4.4b}$$
$$\dot{\theta}_e = v_f \tilde{v}_r \tilde{\kappa}_l - v_f \kappa_f. \tag{4.4c}$$

The input $u(t)$ and the controller $\kappa_f(t)$ are substituted into (4.4). The error dynamics are given by

$$\dot{x}_e = [v_l + u_2]\,[u_1 + \kappa_l]\, y_e + [v_l + u_2]\,\frac{1 - k_1 x_e}{\cos\theta_e}\cos\theta_e - [v_l + u_2] \tag{4.5a}$$
$$\dot{y}_e = -\,[v_l + u_2]\,[u_1 + \kappa_l]\, x_e + [v_l + u_2]\,\frac{1 - k_1 x_e}{\cos\theta_e}\sin\theta_e \tag{4.5b}$$
$$\dot{\theta}_e = [v_l + u_2]\left[\tilde{\kappa}_l\left(\frac{1 - k_1 x_e}{\cos\theta_e} - 1\right) - u_1\right]. \tag{4.5c}$$

The last step is to linearize (4.5) around the equilibrium point x^* and u^*. The matrices A_{c_1} and B_{c_1} are determined as

$$A_{c1} = \frac{\partial f(x,u)}{\partial \mathbf{x}}\bigg|_{x^*} \qquad B_{c1} = \frac{\partial f(x,u)}{\partial \mathbf{u}}\bigg|_{u^*}, \tag{4.6}$$

with $f(x,u) = \left[\dot{x}_e, \dot{y}_e, \dot{\theta}_e\right]^T$. The linearized error dynamics are given by

$$\begin{bmatrix} \dot{x}_{e,l} \\ \dot{y}_{e,l} \\ \dot{\theta}_{e,l} \end{bmatrix} = \begin{bmatrix} -k_1 v_l & v_l \tilde{\kappa}_l & 0 \\ -\tilde{\kappa}_l v_l & 0 & v_l \\ -k_1 \tilde{\kappa}_l v_l & 0 & 0 \end{bmatrix} \begin{bmatrix} x_{e,l} \\ y_{e,l} \\ \theta_{e,l} \end{bmatrix} + \begin{bmatrix} 0 & 0 \\ 0 & 0 \\ -v_l & 0 \end{bmatrix} \begin{bmatrix} u_{1,l} \\ u_{2,l} \end{bmatrix}, \tag{4.7}$$

where $u_{1,l}$ and $u_{2,l}$ are the linearized inputs of input u_1 and u_2, respectively. There is assumed that the velocity of the leader $v_l(t)$ and the curvature of the leader $\tilde{\kappa}_l(t)$ are constant. This results in a time invariant linear system.

4.2.2 Controller 2

For the second lateral controller, the error dynamics is linearized with the same approach as discussed for lateral controller 1. The error dynamics of the second controller are given by

$$\dot{x}_e = v_f\left(1 + ax_e\right)\tilde{\kappa}_l y_e + v_f \cos\theta_e - v_f\left(1 + ax_e\right) \tag{4.8a}$$
$$\dot{y}_e = -v_f\tilde{\kappa}_l\left(1 + ax_e\right)x_e + v_f \sin\theta_e \tag{4.8b}$$
$$\dot{\theta}_e = v_f\kappa_f - v_f\left(1 + ax_e\right)\tilde{\kappa}_l. \tag{4.8c}$$

Also here the inputs $u_1(t)$ and $u_2(t)$ are substituted into (4.8). The error dynamics is given by

$$\dot{x}_e = \left[v_l + u_2\right]\left(1 + ax_e\right)\tilde{\kappa}_l y_e + \left[v_l + u_2\right]\cos\theta_e - \left[v_l + u_2\right]\left(1 + ax_e\right) \tag{4.9a}$$
$$\dot{y}_e = -\left[v_l + u_2\right]\tilde{\kappa}_l\left(1 + ax_e\right)x_e + \left[v_l + u_2\right]\sin\theta_e \tag{4.9b}$$
$$\dot{\theta}_e = \left[v_l + u_2\right]\left[\tilde{\kappa}_l + u_1\right] - \left[v_l + u_2\right]\left(1 + ax_e\right)\tilde{\kappa}_l. \tag{4.9c}$$

Using the Jacobian in (4.6), the error dynamics is linearized around the equilibrium x^* and u^*. The linearized error dynamics are given by

$$\begin{bmatrix}\dot{x}_{e,l}\\ \dot{y}_{e,l}\\ \dot{\theta}_{e,l}\end{bmatrix} = \begin{bmatrix}-av_l & v_l\tilde{\kappa}_l & 0\\ -\tilde{\kappa}_l v_l & 0 & v_l\\ -a\tilde{\kappa}_l v_l & 0 & 0\end{bmatrix}\begin{bmatrix}x_{e,l}\\ y_{e,l}\\ \theta_{e,l}\end{bmatrix} + \begin{bmatrix}0 & 0\\ 0 & 0\\ v_l & 0\end{bmatrix}\begin{bmatrix}u_{1,l}\\ u_{2,l}\end{bmatrix}. \tag{4.10}$$

Also here the linear system is time invariant because there is assumed that $v_l(t)$ and $\tilde{\kappa}_l(t)$ are constant.

4.3 Performance of the lateral controllers

In this section the lateral controllers are tuned such that the performance criteria are satisfied. The three performance criteria, i.e. safety, comfort and tracking, are discussed and the effect of the controller gains of the different controllers on the criteria is investigated. For the lateral controller, both the linearized and nonlinear model are used to tune.

4.3.1 Pole placement

A method to determine the controller gains is to apply pole placement to the linearized state space model. The state feedback closed loop systems is determined by substituting the input $u_{1,l} = -K\mathbf{x}$ into the linearized system, resulting in

$$\dot{x}(t) = \underbrace{(A - BK)}_{A_{cl}}x. \tag{4.11}$$

For a stable closed loop system, the eigenvalues of A_{cl} must be negative. The inputs of the linearized system are already determined in (4.2). The input $u_1(t)$ differs for the two derived lateral controllers. For lateral controller 1, the input is

$$u_1^{c_1}(t) = \frac{1 - k_1\bar{x}_e}{\cos\bar{\theta}_e}\tilde{\kappa}_l(t) - \tilde{\kappa}_l(t) + k_2 y_e(t) - k_1 k_2 x_e(t) y_e(t) + k_3\theta_e(t) \tag{4.12}$$

and for controller 2

$$u_1^{c_2}(t) = a\tilde{\kappa}_l(t)x_e(t) - k_4\frac{\cos\theta_e(t) - 1}{\theta_e(t)}x_e(t) - k_4\frac{\sin\theta_e(t)}{\theta_e(t)}y_e(t) - k_5\theta_e(t). \tag{4.13}$$

To substitute the inputs into the linearized system, the inputs are linearized around the origin of the lateral error. The inputs $u_1(t)$ are linearized as

$$u_{1,l}^{c_1}(t) = -k_1\tilde{\kappa}_l x_{e,l}(t) + k_2 y_{e,l}(t) + k_3\theta_{e,l}(t) \tag{4.14a}$$
$$u_{1,l}^{c_2}(t) = a\tilde{\kappa}_l x_{e,l}(t) - k_4 y_{e,l}(t) - k_5\theta_{e,l}(t). \tag{4.14b}$$

Taking into account that the input of the closed loop system is $\mathbf{u} = -K\mathbf{x}$, the controller K for lateral controller 1 is simplified to

$$K_{c_1} = \begin{bmatrix} k_1\tilde{\kappa}_l & -k_2 & -k_3 \\ 0 & 0 & 0 \end{bmatrix}, \tag{4.15}$$

and for lateral controller 2

$$K_{c_2} = \begin{bmatrix} -a\tilde{\kappa}_l & k_4 & k_5 \\ 0 & 0 & 0 \end{bmatrix}. \tag{4.16}$$

With the determined controllers, the closed loop system is determined using (4.11). The linearized closed loop system for controller 1 is given by

$$A_{c_1}^{cl} = \begin{bmatrix} -k_1 v_l & \tilde{\kappa}_l v_l & 0 \\ -\tilde{\kappa}_l v_l & 0 & v_l \\ 0 & -k_2 v_l & -k_3 v_l \end{bmatrix} \tag{4.17}$$

and for controller 2 by

$$A_{c_2}^{cl} = \begin{bmatrix} -a v_l(t) & \tilde{\kappa}_l v_l & 0 \\ -\tilde{\kappa}_l v_l & 0 & v_l \\ 0 & -k_4 v_l & -k_5 v_l \end{bmatrix} \tag{4.18}$$

The two closed loop matrices are identical when $k_1 = a$, $k_2 = k_4$ and $k_3 = k_5$. For the remaining of this section there is no distinction between the lateral controller 1 and 2.

Now the linearized closed systems are established, the controller gains can be determined using pole placement. The characteristic polynomial of is given by

$$\det\left(\lambda I_3 - A_{c1}^{cl}\right) = \lambda^3 + (k_1 + k_3)\, v_l \lambda^2 + \left(\tilde{\kappa}_l^2 + k_1 k_3 + k_2\right) v_l^2 \lambda + \left(k_3 \tilde{\kappa}_l^2 + k_1 k_2\right) v_l^3 = 0. \tag{4.19}$$

The poles of the closed loop system are chosen based on some requirements; stability, safety, comfort and tracking performance. To achieve a stable closed loop system, the poles must be negative. When placing the poles far in the left half plane, fast convergence is achieved but results also in a larger overshoot and a large control effort. For tracking performance the poles can be placed further in the left half plane, but for safety and comfort the larger overshoot in undesired. When choosing the poles close to zero, this results in less overshoot and a smaller control effort. However, this results in slow convergence of the vehicle to the leader's path, which is positive for the comfort criterion. From this, the poles are chosen as $\lambda_1 = -20$, $\lambda_2 = -20$ and $\lambda_3 = -20$.
Now, the poles are chosen, but the controller gains are not immediately determined. In Appendix B.5 the controller gains are determined for the desired poles. The gains depend on the leader's velocity and the curvature of the leader's path. To see how the controller gains are effect by these two variables, the controller gains are presented for the range $\kappa_l = -0.5$ - 0.5 with steps of 0.1 and $v_l = 30$ - $130 km/h$ with steps of $10 km/h$. The chosen curvature corresponds with circles with a minimum radius of $2m$. Moreover, the vehicle drives both in clockwise and anti-clockwise direction over the path. The results are shown in Figure 4.1. The effect of the leader's velocity and curvature is large for all the controller gains. The controller gains decreases when the velocity increases. For k_2, k_3, k_4 and k_5 the gains increase when the curvature increases. The opposite happens for k_1 and a where the gain decreases when the curvature increases. A remark is made for k_1 and a. For large velocities and large curvature, the gains are negative and based on the stability proof of the lateral controller unstable.
Based on these findings, the controller gains are determined. When the leader drives along a circular path, i.e. $\kappa_l = 0$, the controller gains are chosen as $k_1 = a = 0.9$, $k_2 = k_4 = 0.81$ and $k_3 = k_5 = 1.8$. Because the gains are affected by the leader's velocity, an average velocity of $80 km/h$ is chosen. When te leader's path is circular, it is preferred that different controller gains are chosen. Now, not only for the leader's velocity by also for κ_l the average value is chosen. The controller gains are $k_1 = a = 0.24$, $k_2 = k_4 = 1.79$ and $k_3 = k_5 = 2.46$.

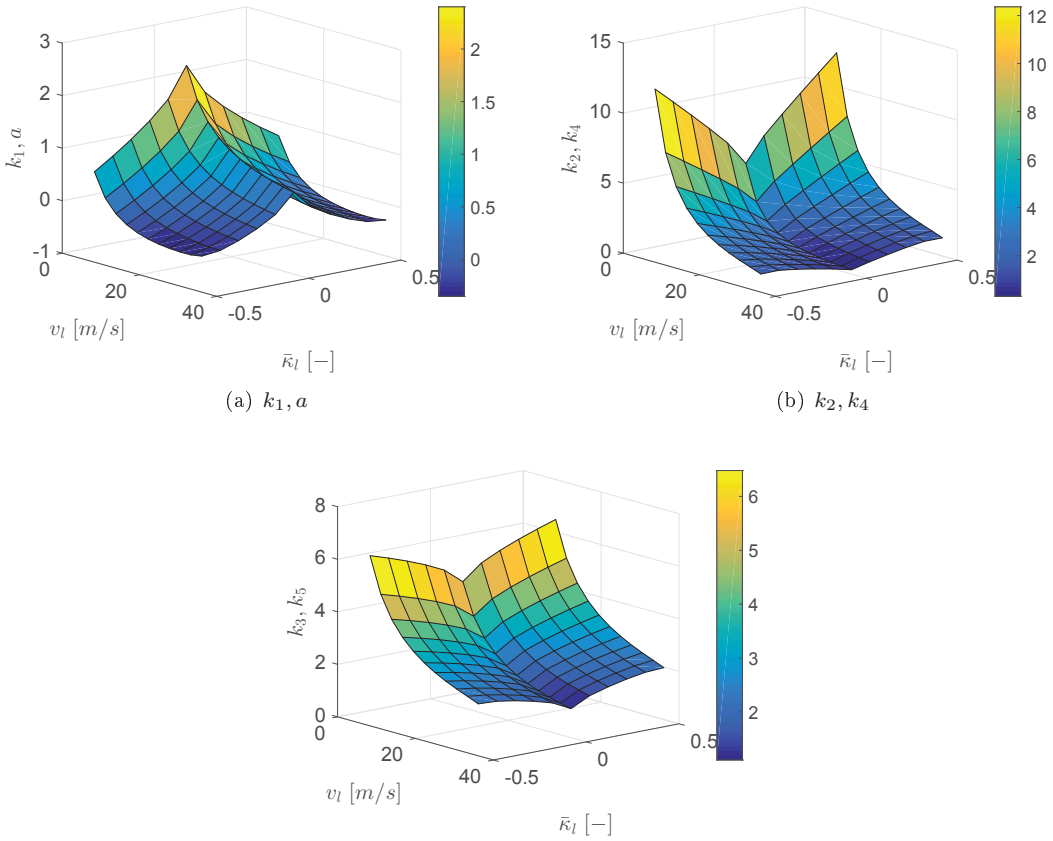

(a) k_1, a

(b) k_2, k_4

(c) k_3, k_5

Figure 4.1: Simulation results of the effect of $\bar{\kappa}_l(t)$ and $v_l(t)$ on the controller gains of the two lateral controllers

4.3.2 Tuning nonlinear error dynamics

In the previous subsection the controller gains are determined by placing the poles of the linearized closed loop error dynamics. In this subsection a second method is discussed. For each controller gain there is investigated what the effect is on performance criteria, i.e. overshoot, settling time, total variation and rise time. For each lateral controller, three gains are investigated by varying one gain each time and keeping the other gains constant. Based on the performance criteria defined in section 4.1, the gains are chosen such that the desired performance is achieved.

In Appendix C the effect of each gain is shown for the different scenario's discussed in section 4.1. In Table 4.2 the results of the different simulations are summarized. Here the effect of the controller gains are shown for driving on a line and circle. Also controller gains are suggested for a general situation.

Remark 1 By investing the effect of a certain gain, the other gains are kept constant. By using this approach, only the edges of the area with possible settings is investigated. Furthermore, the interaction between the different controller gains is not taken into account.

Table 4.2: Effect of the controller gains

		Overshoot	**Settling time**	**Rise time**	**Total Variation**
$\mathbf{k_1}$	Line	Small	Small	Large	Small
	Circle	$k_1 = 1 - 2$	$k_1 = 1$	Small	$k_1 = 1 - 1.8$
	General	$k_1 = 0.9$	$k_1 = 0.5 - 1$	$k_1 = 0.9$	$k_1 = 1$
$\mathbf{k_2}$	Line	Large	Large	Large	Large
	Circle	Large	Large	Large	Large
	General	Large	Large	Large	Large
$\mathbf{k_3}$	Line	$k_3 > 2$	$k_3 = 1.4 - 1.6$	Small	$k_3 > 2$
	Circle	$k_3 > 2$	$k_3 = 1 - 1.2$	Small	$k_3 > 2$
	General	$k_3 > 2$	$k_3 = 1 - 1.6$	Small	$k_3 > 2$
$\mathbf{a}$	Line	Small	Large	Large	Small
	Circle	around $a = 3$	$a = 1.3$	Not affected	$a = 3$
	General	$a = 1 - 2$	$a = 2$	Large	$a = 2$
$\mathbf{k_4}$	Line	Large	Large	Large	Large
	Circle	Large	Large	Large	Large
	General	Large	Large	Large	Large
$\mathbf{k_5}$	Line	$k_5 > 2$	$k_5 = 1.4 - 1.5$	Small	$k_5 > 2$
	Circle	$k_5 > 3$	$k_5 = 1.7$	Small	$k_5 > 2$
	General	$k_5 > 3$	$k_5 = 1.4 - 1.7$	Small	$k_5 > 2$

4.3.3 Comparing the controller gains

The controller gains of the lateral controllers are determined using two separate methods. In Table 4.3 the obtained gains are given. The values for k_3 and k_5 correspond for both methods. It is notable that for pole placement the controller gains k_1 and a decreases when the curvature increases, where for the time domain simulation the opposite behavior is observed. The configurations obtained by both methods are implemented in simulations performed in section 4.5

Table 4.3: Comparison of the controller gains for the two different methods

	Pole placement		Time simulations	
Gains	Line	Circle	Line	Circle
k_1	0.9	0.24	0.5	1
k_2	0.81	1.79	3	3
k_3	1.8	2.46	2	2
a	0.9	0.25	0.7	2
k_4	0.81	1.79	3	3
k_5	1.8	2.46	2	2

4.4 Performance of the longitudinal controller

The error dynamics of the longitudinal controller is already linearized by the chosen controller. The linearized error dynamics of the spacing error e is given in (3.40) where the input is chosen as $\nu = -K_{long}e$. According to the Routh-Hurwitz stability criterion, GES is achieved when $k_p, k_d, k_{dd} > 0$ and $k_d k_{dd} - k_p > 0$ as already discussed in section 3.3.

The performance criteria of the longitudinal controller is that the intervehicle distance between the vehicles is such that the vehicle does not collide with its predecessor. For the driver's comfort, two aspects are considered. First the acceleration of the vehicle can not be too high. Secondly, no overshoot is desired such that the intervehicle distance converges to the desired intervehicle distance without oscillations around the steady state solution.

To avoid collisions of the vehicle with its predecessor, the spacing error converges fast to zero and the overshoot is reduced. By increasing the poles, a faster decay ratio is achieved but the overshoot increases. A trade-off is made between fast convergence and overshoot. Some overshoot is allowed because the intervehicle distance is always larger then zero due to the standstill distance r. The first state of the error dynamics is important for tuning the longitudinal controller because it is the spacing error.
The poles are chosen based on the desired behavior as described above and placed more in the left half plane to achieve faster convergence to the desired intervehicle distance. Fast convergence results in large accelerations, which cannot be too high to achieve the comfort criterion. It is desired that the overshoot is small such that no accident can occur with the predecessor. At last, when the eigenvalues are placed far from the open loop eigenvalue, in this case $\lambda_{1,2,3} = 0$, the control effort is large. Based on these observation the poles are chosen as $\lambda_1 = -5$, $\lambda_2 = -5$ and $\lambda_3 = -5$, resulting in the gains $k_p = 125$, $k_d = 75$ and $k_{dd} = 15$. Figure 4.2 shows the time response of the error dynamics for four different initial conditions. As said before, the state $e_1(t)$ is important. The overshoot of the signals are small and the ∞-norm is given in Table 4.4. The spacing error is critically damped and no oscillations around the steady state solution appear as desired.

Table 4.4: The ∞-norm of $e(t)$ for the different initial conditions.

Initial condition	$\|e(t)\|_\infty$
$[1, 1, 1]^T$	1.0889
$[7, 7, 7]^T$	7.6224
$[5, -5, 5]^T$	5
$[10, 5, -5]^T$	10.2959

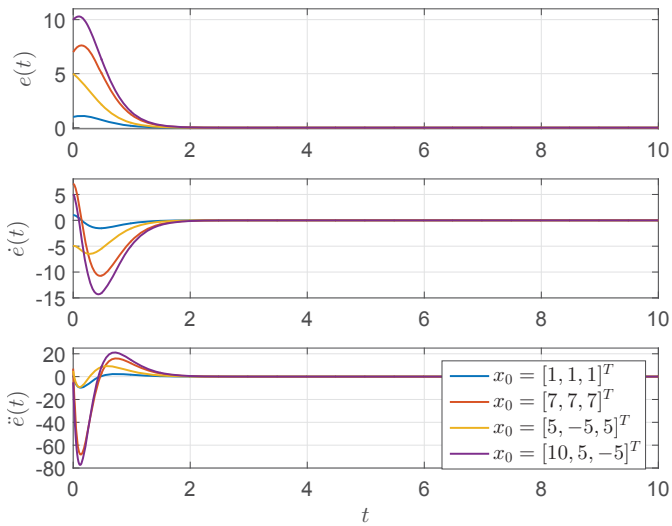

Figure 4.2: The time response of the error dynamics of the longitudinal controller.

It is more difficult to satisfy the condition of comfort. The error dynamics are GES and the system converges exponentially to the origin. When the initial longitudinal error is large, it is possible that the acceleration is larger than desired. To saturate the acceleration such that the performance criteria is satisfied, a different controller must be derived.

4.5 Simulation results

In the previous section the controller gains of the two lateral and the longitudinal controllers are determined. In this section simulations are performed with these different controller gains to

determine the performance and effectiveness of the different settings. The vehicles drive along two trajectories, namely driving along a straight line and along a circular path. The radius of the circular path is $R = 40m$. The leading vehicle drives at the minimum velocity of $30km/h$. After 10 seconds the velocity makes a step to the maximum velocity of $130km/h$ and stays constant.
For the lateral controllers, the controller gains are determined using two approaches, pole placement by the linearized model and using time simulations of the nonlinear model. In Table 4.5 three different configurations are given for the controller gains of the two different lateral controllers. Configuration 1 are the controller gains determined with pole placement. Configuration 2 and 3 are determined using time simulations. The gains of the longitudinal controller are chosen as $k_p = 125$, $k_d = 75$ and $k_{dd} = 15$. Furthermore, the standstill distance $r = 1m$, the time gap $h = 1s$ and the length of the vehicle $L = 0$.

Table 4.5: Different configurations of the controller gains of the lateral controllers

	Configuration 1	Configuration 2	Configuration 3
k_1	0.6	1	0.5
k_2	1.3	3	3
k_3	2.15	2	3
a	0.6	1	3
k_4	1.3	3	3
k_5	2.15	2	3

The initial condition of the leader is $[x_l(0), y_l(0), \theta_l(0)] = [0, 1, 0]$. The initial condition of the reference vehicle is the same as the leader. The initial velocity of the follower is $v_f(0) = 0$ and its initial position is $[x_f(0), y_f(0), \theta_f(0)] = [0, 0, \pi/3]$.

4.5.1 Lateral controller

For the two lateral controllers, the lateral error for a straight line and circular path are shown in Figure 4.3 and Figure 4.4 for controller 1 and 2, respectively. The three different configurations are compared for both controllers. Comparing the two lateral controllers is difficult because the lateral error is defined in two different frames. Therefore, the energy of the follower and the reference vehicle is determined in

$$P = \frac{1}{T}\int_0^T \left((x - x_r)^2 + (y - y_r)^2 + (\theta - \theta_r)^2\right) dt. \tag{4.20}$$

The results are shown in Table 4.6. The differences between the two paths are small. That is an advantage because the controller gains can be determined for a more general setting. For controller 1, the best settings for the lateral controller is configuration 3. For controller 2, the best results are obtained with configuration 1.

Table 4.6: Comparison of the two lateral controllers

	Configuration 1		Configuration 2		Configuration 3	
Gains	Controller 1	Controller 2	Controller 1	Controller 2	Controller 1	Controller 2
Straight line	-0.0210	-0.0252	-0.0240	-0.0345	-0.0199	-0.0277
Circular path	-0.0208	-0.0247	-0.0234	-0.0335	-0.0197	-0.0271

In Figure 4.3 the lateral error for lateral controller 1 is shown. The same as noticed in Table 4.6 the difference between the different configurations are small. As can be seen, configuration has some overshoot in y direction, which is undesired. In Figure 4.4 the lateral error for lateral controller 2 is shown. Here, the same observations are done as for lateral controller 1.

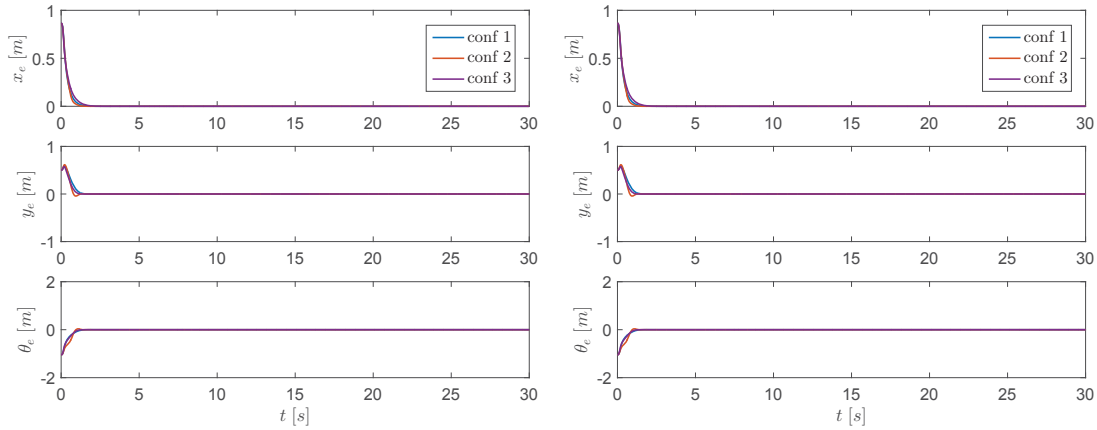

(a) Straight line (b) Circular path

Figure 4.3: The lateral error for lateral controller 1

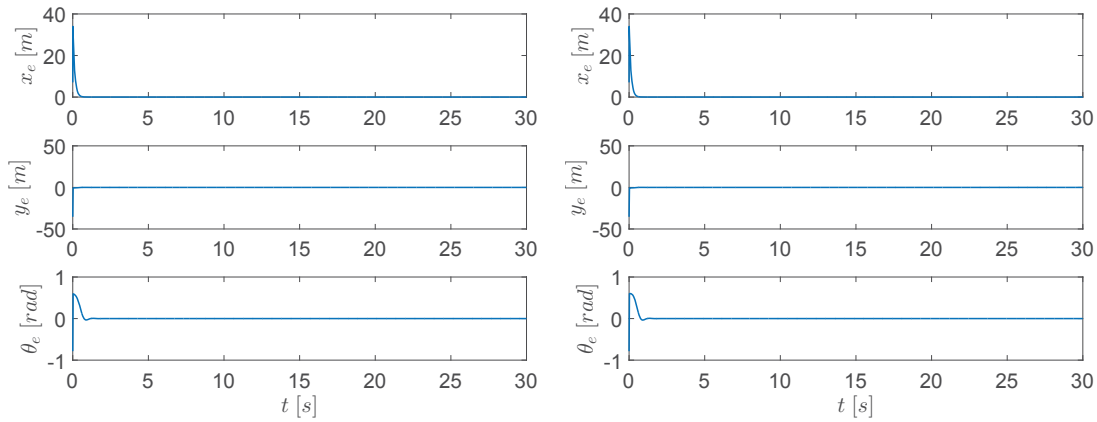

(a) Straight line (b) Circular path

Figure 4.4: The lateral error for lateral controller 2

Large initial lateral error

In the previous chapter the time response of the two vehicles was discussed for a large initial error. There was concluded that the first lateral error moves towards the path with a detour, where the second controller moves directly towards the path. In this section the same simulations are performed, but now the tuned controller gains are implemented. The initial condition of the follower is $[x_f(0), y_f(0), \theta_f(0)] = [-20, 0, \pi/3]$ and the leaders initial conditions are $[x_l(0), y_l(0), \theta_l(0)] = [0, 1, 0]$. Both the leader and the follower drives with the velocity $v_f = 10m/s$ and two different trajectories are considered, i.e. a straight line and a circular path with the radius $R = 20m$. The reference vehicle has the same initial conditions as the leader. The controller gains are $k_1 = 3$, k_2 and $k_3 = 3$, and $a = 0.6$, $k_4 = 1.3$ and $k_5 = 2.15$, for the first and second lateral controller, respectively.
Figure 4.5 shows the simulation results of the two lateral controllers with the tuned controller gains and a large initial lateral error. Comparing the paths of the two controllers, there can be concluded that path of the second lateral controller is more desirable. The same was concluded in the previous chapter. Therefore, only the second lateral controller is used in the remaining of this report.

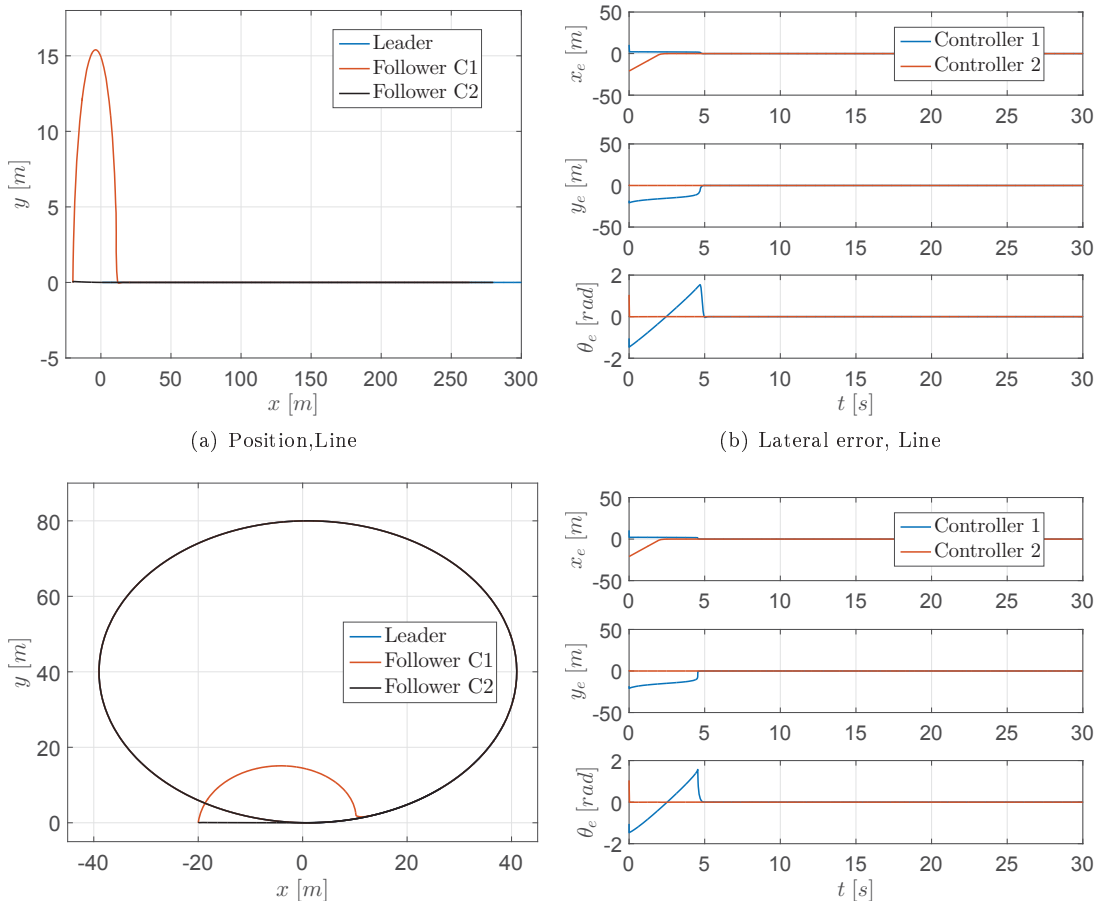

(a) Position,Line

(b) Lateral error, Line

(c) Position, Circle

(d) Lateral error, Circle

Figure 4.5: (a) and (c) show the position of the leader and followers for the two different paths. (b) and (d) show the lateral error between the followers and the reference vehicle.

4.5.2 Longitudinal controller

The simulation results for the longitudinal controller are shown in Figure 4.6 and Figure 4.7. As can be seen in Figure 4.6 the velocity of the follower converges towards the leader's velocity without overshoot and oscillations around the steady state solutions. When the leader starts to accelerate, the follower waits before it also accelerates, which happens with a certain time delay. The comfort criteria is not satisfied because the acceleration in the begin is the too high. In Figure 4.7 the intervehicle distance between the leader and the follower is shown. For the circular path a difference between the actual and desired intervehicle distance is noticed for a high velocity. Because the follower drives with a large velocity, the intervehicle distance is larger and the estimation of intervehicle distance is less accurate.

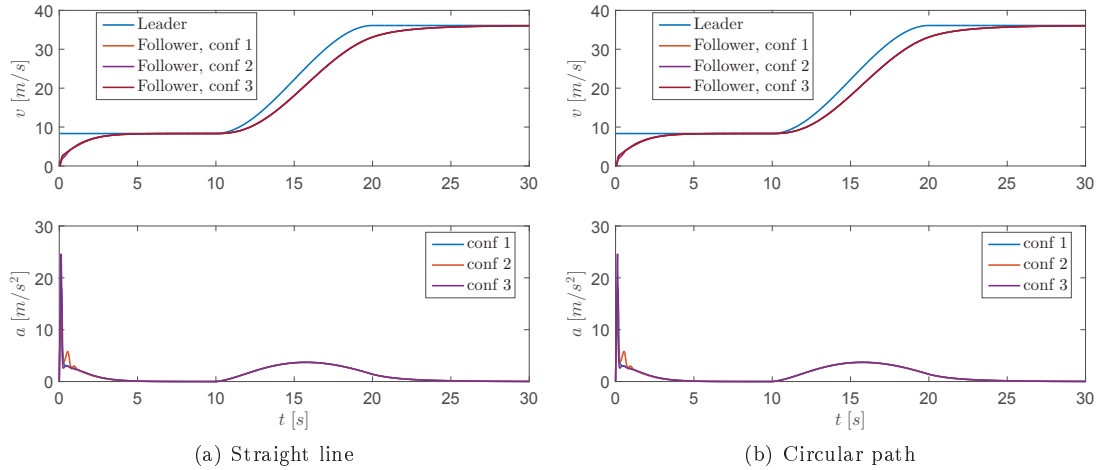

(a) Straight line (b) Circular path

Figure 4.6: The velocity and acceleration of the vehicles

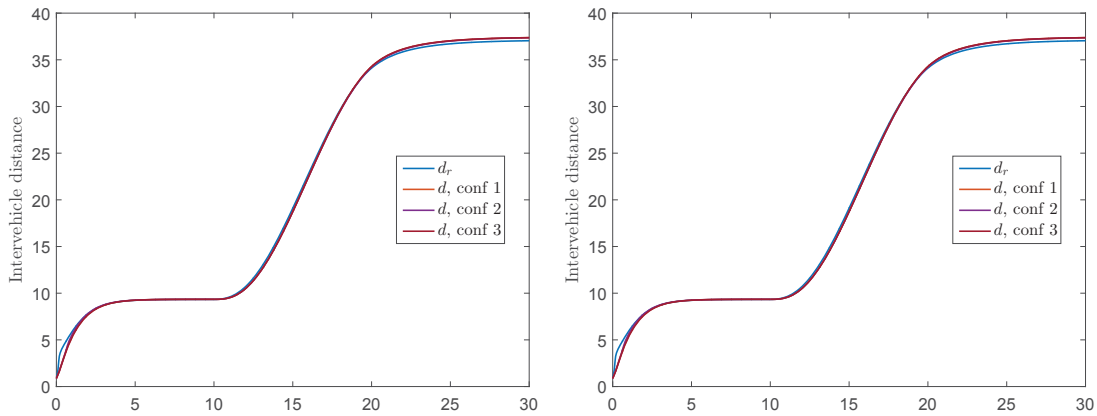

(a) Straight line (b) Circular path

Figure 4.7: The desired intervehicle distance and the actual vehicle distances.

4.6 Summary

In this chapter the lateral and longitudinal controller are tuned to achieve the desired behavior according the performance criteria safety, tracking and comfort. The lateral controllers are tuned using pole placement and performing time simulation to investigate the effect of each controller gain. To apply pole placement, the error dynamics of both lateral controllers are linearized. The gains are tuned considering two different trajectories, i.e. a straight line and a circular path. From both methods, different values for the controller gains are obtained. To compare them, simulations are performed where all the chosen controller gains satisfy the defined criteria.
For the longitudinal controller the controller gains are determined using pole placement. The error dynamics of the spacing error is already linear by the choice of the longitudinal controller. Gains are obtained that satisfy the desired behavior according to the performance criteria.

In the next chapter the controller gains are investigated when the leading vehicle drives a more complex trajectory.

Chapter 5

Simulation Results

In the previous chapters, lateral and longitudinal controllers have been proposed and the suitable controller gains have been determined. Different simulations have been performed already for simple trajectories, i.e. lines and circles, to observe if the controllers are stable. In this chapter, simulations are performed where the vehicles drive along more challenging trajectories. Furthermore, different control laws are compared to verify if the desired behavior, i.e. following the leading vehicle in a safe and comfortable way, is achieved by the derived controllers. At last, the derived controllers are implemented on a more realistic dynamic model, i.e. the Moving Base. In the remainder of this chapter, simulations are performed with the designed lateral and longitudinal controllers. Insection 5.1 the kinematic model is simulated with the controller gains obtained in the previous section for a more challenging trajectory. In section 5.2 the derived controllers in this report are compared with a tracking controller. In section 5.3 the results of the simulations with the Moving base are presented and discussed. Finally, a summary is given in section 5.4

5.1 Kinematic model with lateral and longitudinal controllers

The trajectory is a combination of two half circles and two straight lines, as shown in Figure 5.1(a). The radius of the circle is $R = 40m$ and the length of the straight lines are $900m$. In the previous chapters there is assumed that the leader drives with a constant velocity for the linearization of the error dynamics of the lateral controllers. For the simulations performed in this chapter, the velocity of the leader varies according to the velocity profile shown in Figure 5.1(b).

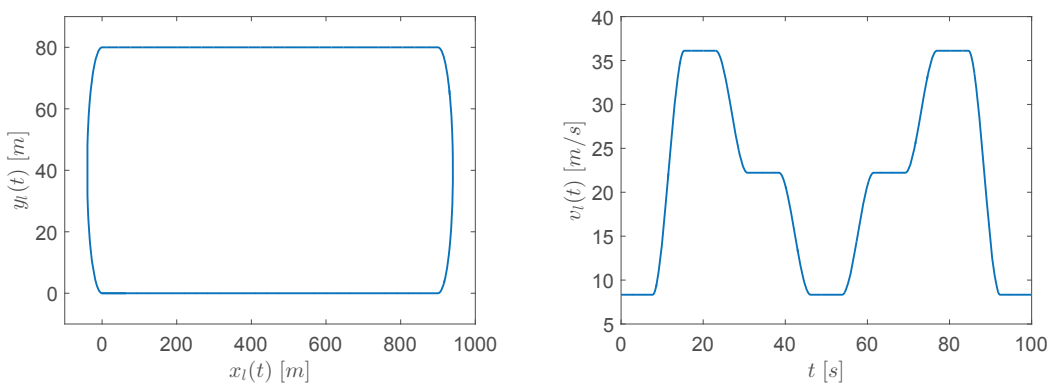

(a) Combined path

(b) Velocity Profile

Figure 5.1: The path and velocity profile for the simulations.

The first simulations are performed with the kinematic model of a mobile robot. A lateral and a longitudinal controller are implemented. The initial condition of the leader is $(x_l(0), y_l(0), \theta_l(0)) = (0, 0, 0)$ and the follower starts from $(x_f(0), y_f(0), \theta_f(0)) = (-1, -1, \pi/4)$. The controller gains for the second lateral controller, determined in chapter 4, are $a = 0.6$, $k_4 = 1.3$ and $k_5 = 2.15$. For the longitudinal controller the controller gains are given by $k_p = 125$, $k_d = 75$ and $k_{dd} = 15$. For the longitudinal controller the standstill distance $r = 1m$, the time gap $h = 1s$ and the length of the vehicle $L = 0$.

In Figure 5.2 the simulation results for lateral controller 2 and the longitudinal controller are shown when the leader drives along the combined path. In Figure 5.2(a) the position of the leader and follower in the $x-y$ plane are shown. The follower drives along the same path as the leader and stays on this path. In Figure 5.2(b) the lateral errors are plotted. The lateral error converges to zero, but in the error in y-direction some ripples appear when the curvature of the path changes. Figure 5.2(c) shows the velocity and acceleration of the leader and follower and Figure 5.3(d) shows the intervehicle distance between the leader and the follower. In the first couple of seconds, the follower adjusts its velocity to realize the desired intervehicle distance. As can be seen, four moments stand out and are distinguished in Figure 5.3(d) where a difference appears between d and d_r. This happens when there is switched in curvature because the vehicle goes from the straight line to the circular path or vise versa. Because of the curve of the path, the estimated intervehicle distance changes suddenly and causes an abrupt change in velocity. Another noticeable element is that the velocity of the follower is shifted to the right compared to the leader's velocity. This time delay appears because the intervehicle distance must be maintained.

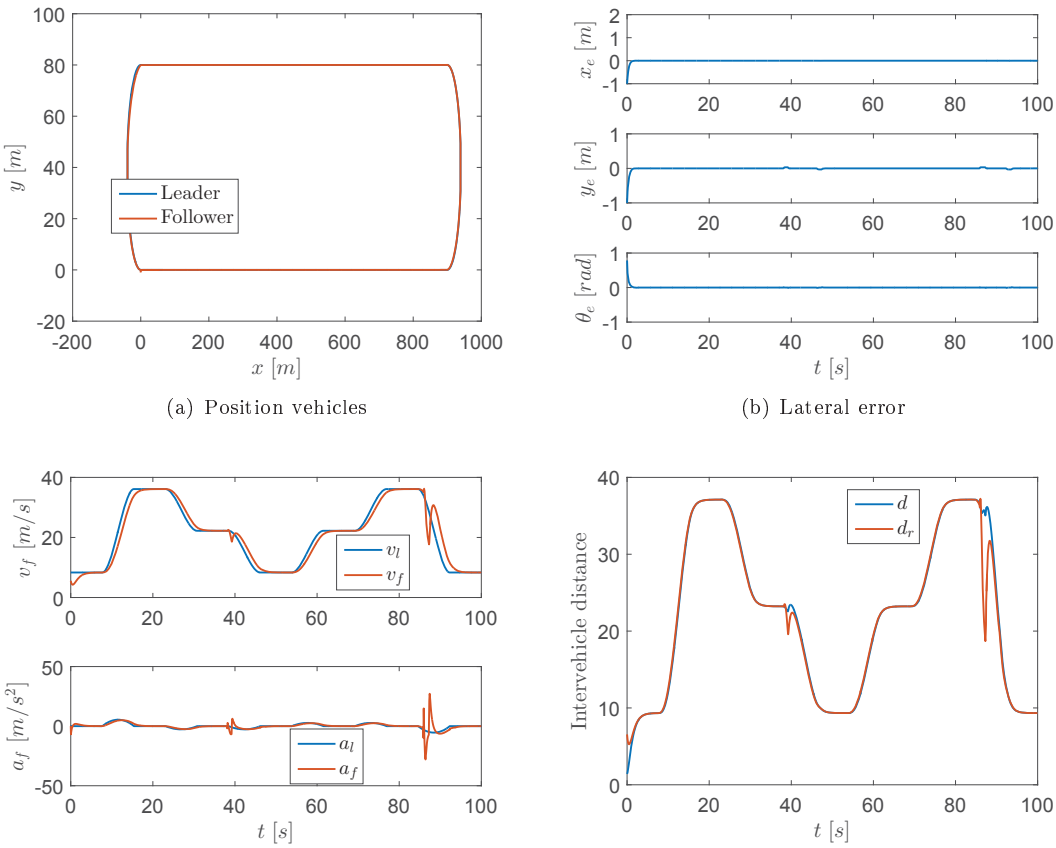

(a) Position vehicles

(b) Lateral error

(c) Velocity and acceleration

(d) Intervehicle distance

Figure 5.2: The simulation results for lateral controller 2 and combined trajectory.

5.2 Comparison with tracking controller

For the problem discussed in this thesis, different controllers have been derived in the past. The derived lateral controller (3.23) and longitudinal controller (3.39) are compared with a tracking controller proposed in [18]. Consider a wheeled mobile robot described by

$$\begin{aligned} \dot{x} &= v\cos\theta \\ \dot{y} &= v\sin\theta \\ \dot{\theta} &= \omega, \end{aligned} \tag{5.1}$$

where v and ω are considered as inputs and the forward and angular velocity, respectively. The proposed tracking controllers in [18] are given by

$$\omega_f(t) = \omega_l(t) + v_l(t)y_e(t)\frac{\sin\theta_e(t)}{\theta_e(t)} + c_1\theta_e(t) \tag{5.2a}$$

$$v_f(t) = v_l(t)\cos\theta_e(t) + c_2x_e(t), \tag{5.2b}$$

where $c_1, c_2 > 0$. The error dynamics

$$\dot{x}_e = \omega_f(t)y_e(t) - v_f(t) + v_l(t)\cos\theta_e(t) \tag{5.3a}$$

$$\dot{y}_e = -\omega_f(t)x_e(t) + v_l(t)\sin\theta_e(t) \tag{5.3b}$$

$$\dot{\theta}_e = \omega_l(t) - \omega_f(t) \tag{5.3c}$$

are globally asymptotically stabilized when $v_l(t)$ and $\omega_l(t)$ are uniformly continuous and bounded and either $v_l(t)$ or $\omega_l(t)$ does not converge to zero. To compare the derived lateral controllers with the tracking controller, first the error dynamics of the tracking controller are linearized. When the linearized error dynamics of the lateral controllers and the trajectory controllers are equal, a fair comparison can be made. The states of the linearized error dynamics are $x(t) = [x_e(t), y_e(t), \theta_e(t)]^T$. Substituting the control law (5.2) into the error dynamics and linearizing the error dynamics around the origin results in

$$\begin{bmatrix} \dot{x}_e(t) \\ \dot{y}_e(t) \\ \dot{\theta}_e(t) \end{bmatrix} = \begin{bmatrix} -c_2 & \omega_l & 0 \\ -\omega_l & 0 & vl \\ 0 & -v_l & -c_1 \end{bmatrix}. \tag{5.4}$$

It is assumed that $\omega_l(t)$ and $v_l(t)$ are constant to obtain a LTI system. Comparing (5.4) with the linearized error dynamics of the lateral controller (4.18), the systems are identical when $c_1 = k_5v_l$, $c_2 = av_l$ and $k_4 = 1$, for the second lateral controller. The controller gains of the lateral controller are chosen as $a = 1$, $k_4 = 1$ and $k_5 = 1$. Because the controller gain c_2 of the tracking controller depends on v_l, the leaders velocity is constant to obtain a constant gain and is chosen as $v_l = 30km/h$. Because the linearized error dynamics are identical, simulations with small lateral error will result in similar results for the derived lateral controller and the tracking controller. To investigate the difference between the controllers, a large initial lateral error are chosen large. The initial condition of the leader is $(x_l(0), y_l(0), \theta_l(0)) = (0, 0, 0)$ and of the follower $(x_f(0), y_f(0), \theta_f(0)) = (-30, 20, \pi/4)$. Because the tracking controller is compared with the lateral controllers, the following vehicle drives with a constant velocity of $30km/h$.
In Figure 5.3 the simulation results of the tracking controller and the lateral controllers are shown. For the two different trajectories, the same can be concluded for the trajectory of the tracking controller and the path of lateral controller 2. The tracking controller moves as fast as possible towards the leader's trajectory without considering the already traveled trajectory by the leader. Whereas the lateral controller 2 takes the traveled path of the leader into account. Because the following vehicle of the second lateral controller converges to the reference vehicle, which has the freedom to move along the leader's path, the follower converges close to the initial position of the leader. The path of the lateral controller is more desirable than the trajectory of the tracking controller, because it is possible that corners are cut with the tracking controller.

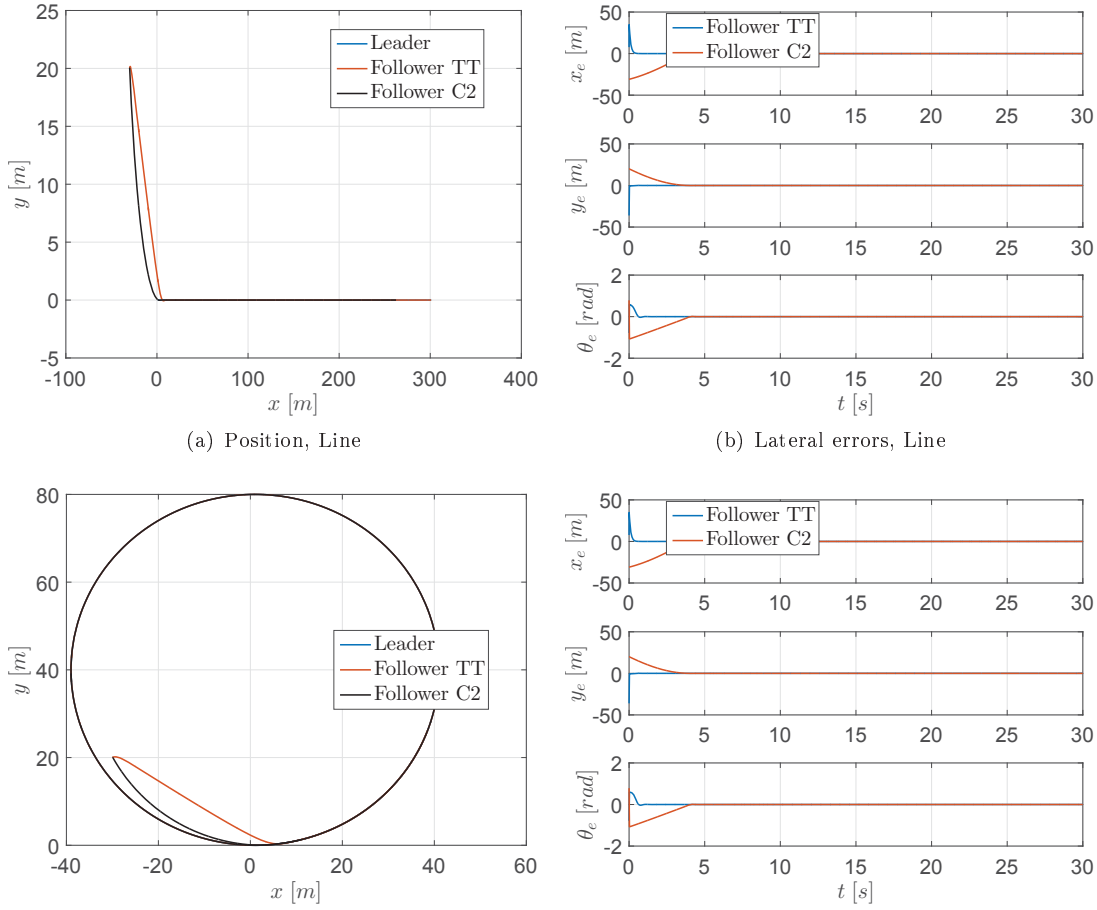

(a) Position, Line

(b) Lateral errors, Line

(c) Position, Circle

(d) Lateral errors, Circle

Figure 5.3: The simulation results of the tracking and the lateral controllers with a large initial lateral error.

5.3 Moving base model

The lateral and longitudinal controllers in this report are derived for a kinematic model of a mobile robot. To derive this model, the assumption is made that the wheels do not slip. In a more realistic situation, this assumption does not hold. Therefore, the controllers are implemented on a complex wheeled mobile robot, i.e. the Moving Base (MB). The MB is designed by TNO Automotive in Helmond and is discussed in more detail in [40]. A schematic figure of the MB is shown in Figure 5.4, where L_{MB} is the length, W_{MB} the width of the MB and Ψ the orientation of the MB. The position of the center of the MB with respect to the inertial frame is given by (x, y) and the corresponding velocity $(\dot{x}, \dot{y})$. The velocity of the center of the moving base with respect to the body fixed frame is given by $(\dot{x}_l, \dot{y}_l)$. It is assumed that the moving base only moves in longitudinal direction, thus $\dot{y}_l = 0$. The MB has eight actuators, four steering and four driving motors. The control objective of the MB is to let the center follow a reference trajectory.

To realize the desired position and orientation of the center of the MB, a decentralized tracking problem is considered. Here, each wheel is controlled separately and needs to follow its own reference trajectory. Therefore, the reference position of the center of the mobile robot needs to be converted to the reference positions x_{ijref} and y_{ijref}, where $i = f(ront), r(ight), j = l(eft), (r(ight))$, for each corner. The reference positions of each wheel are given by

$$x_{fl} = x_{ref} + L_d \cos\left(\theta + \arctan\left(\frac{W_{MB}}{L_{MB}}\right)\right) \tag{5.5a}$$

$$y_{fl} = y_{ref} + L_d \sin\left(\theta + \arctan\left(\frac{W_{MB}}{L_{MB}}\right)\right) \tag{5.5b}$$

$$x_{fr} = x_{ref} + L_d \cos\left(\arctan\left(\frac{W_{MB}}{L_{MB}}\right) - \theta\right) \tag{5.5c}$$

$$y_{fr} = y_{ref} - L_d \sin\left(\arctan\left(\frac{W_{MB}}{L_{MB}}\right) - \theta\right) \tag{5.5d}$$

$$x_{rl} = x_{ref} - L_d \cos\left(\arctan\left(\frac{W_{MB}}{L_{MB}}\right) - \theta\right) \tag{5.5e}$$

$$y_{rl} = y_{ref} + L_d \sin\left(\arctan\left(\frac{W_{MB}}{L_{MB}}\right) - \theta\right) \tag{5.5f}$$

$$x_{rr} = x_{ref} - L_d \cos\left(\theta + \arctan\left(\frac{W_{MB}}{L_{MB}}\right)\right) \tag{5.5g}$$

$$y_{rr} = y_{ref} - L_d \sin\left(\theta + \arctan\left(\frac{W_{MB}}{L_{MB}}\right)\right). \tag{5.5h}$$

The reference orientations Ψ_{ijref} are calculated using kinematics and are determined using

$$\Psi_{ijref} = \arctan\left(\frac{\dot{y}_{ijref}}{\dot{x}_{ijref}}\right), \tag{5.6}$$

where $\dot{x}_{ijref}$ and $\dot{y}_{ijref}$ are calculated by taking the time-derivative of (5.5).

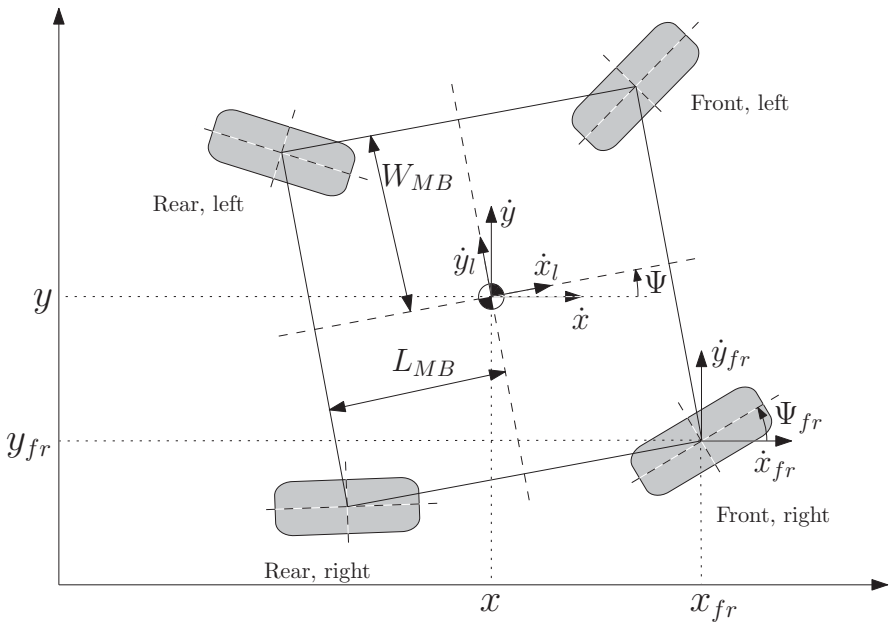

Figure 5.4: A schematic figure of the Moving Base

As noticed before, the MB model has for each wheel two inputs, i.e. the torque of the steering and driving motor. Consequently, the outputs of the lateral and longitudinal controllers cannot be implemented directly, because the outputs are the curvature $\kappa_f(t)$ and velocity $v_f(t)$. Figure 5.5 shows the control scheme how the controllers are implemented on the MB. The mobile robot is placed in the center of the MB, such that the trajectory which the mobile robot travels is the reference trajectory of the MB. This reference trajectory is converted to a reference position and orientation of each wheel using (5.5) and (5.6). The required torque T for each actuator is

determined using PID controllers. The difference between the measured velocity and orientation and the reference velocity and orientation are calculated to determine the input of the MB. The position and orientation of the MB are used to determine v_f and κ_f with the longitudinal and lateral controller, respectively.

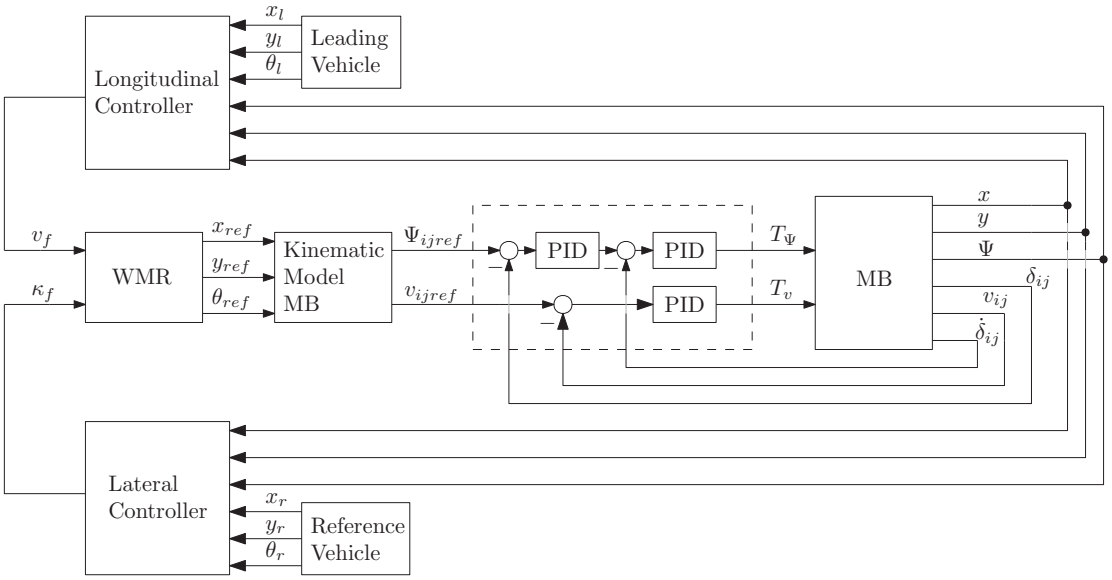

Figure 5.5: The control scheme for implementing the lateral and longitudinal controller on the Moving Base

The MB has a maximum velocity of $50km/h$ and a maximum acceleration of $10m/s^2$ in all directions. Therefore another velocity profile is used, as shown in Figure 5.6. To reduce the large acceleration and sharp cornering, the MB is positioned on the leader's path so the lateral errors are small. Also to prevent large accelerations, the leader is positioned such that the desired intervehicle distance and the actual intervehicle distance are equal. Both the MB and the leader have an initial velocity of $10km/h$. The length of the vehicle $L = 0$, the time gap $h = 1s$ and the standstill distance $r = 1$. Based on these setting, the initial conditions of the leading vehicle are $[x_l(0), y_l(0), \theta_l(0)] = [3.7778, 0, 0]$. The MB and the mobile robot have the same initial conditions $[x_f(0), y_f(0), \theta_f(0)] = [0, 0, 0]$. The orientation of the wheels of the MB are $\Psi_{ij} = 0$. The controller gains of the PID controller for the velocity are $k_p = 40$, $k_d = 0$ and $K_I = 30$. For the orientation $k_p = 20$, $k_d = 0$ and $K_I = 1$ and for the angular velocity $k_p = 10$, $k_d = 0$ and $K_I = 1$.
In Figure 5.7 the results are presented for the simulations with the MB where the leader drives along a straight line. Figure 5.7(a) shows the position of the leader, the reference of the center of the MB, i.e. the WMR, and the MB itself. As can be seen, the MB remains on the leader's path. The same is observed in Figure 5.7(b) where the lateral error between the MB and the reference vehicle converges to zero. In Figure 5.7(c) the velocity and acceleration of the leader, WMR and MB. Similar as observed with the simulation of the kinematic model in section 5.1, the MB starts to accelerate and decelerate with a certain time delay. In the beginning, the acceleration of the MB is large, because the velocity of the MB drops which is caused by the PID controller. After a few seconds, the error between the measured and reference velocity for each wheel is zero and the accelerations are small. Consequently, the MB follows the leader with an intervehicle distance which is equal to the desired intervehicle distance, as shown in Figure 5.7(d).

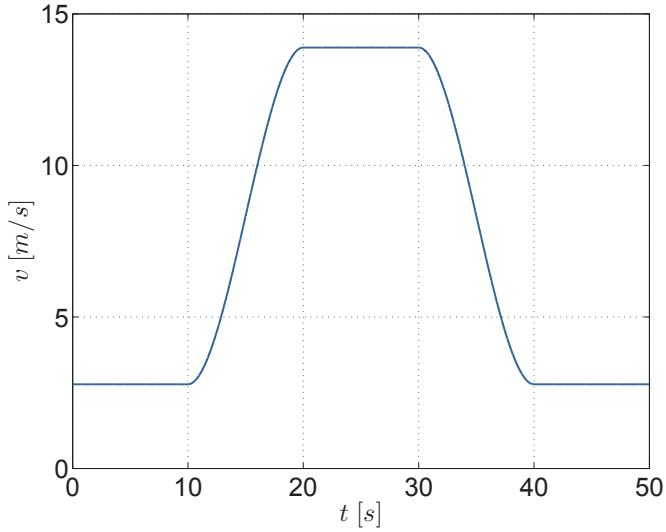

Figure 5.6: The velocity profile for the simulation with the moving base

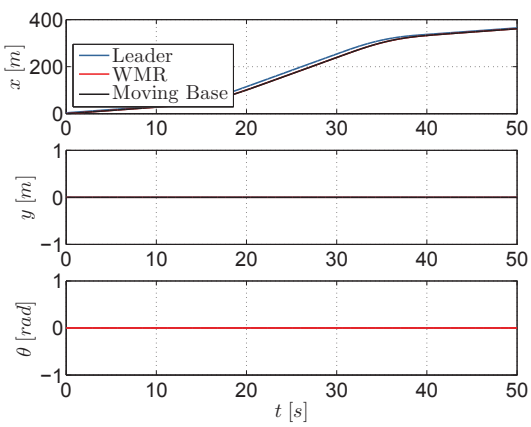

(a) Position vehicles

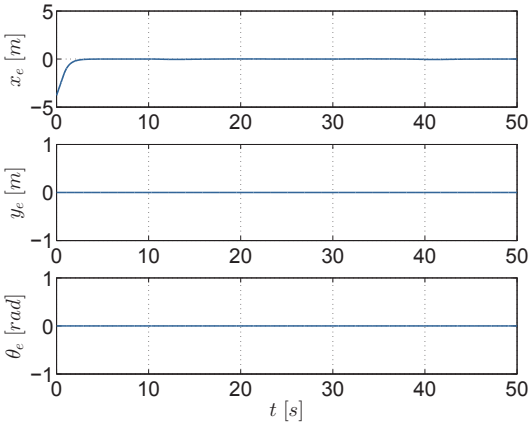

(b) Lateral error

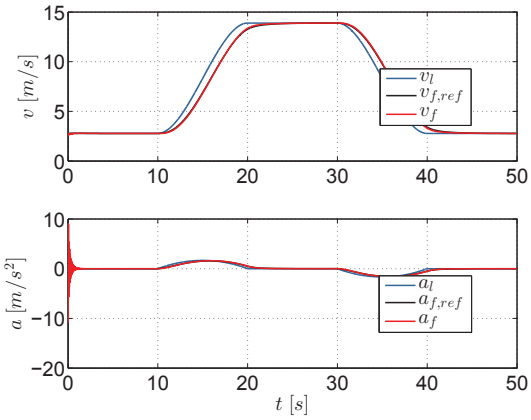

(c) Velocity and acceleration

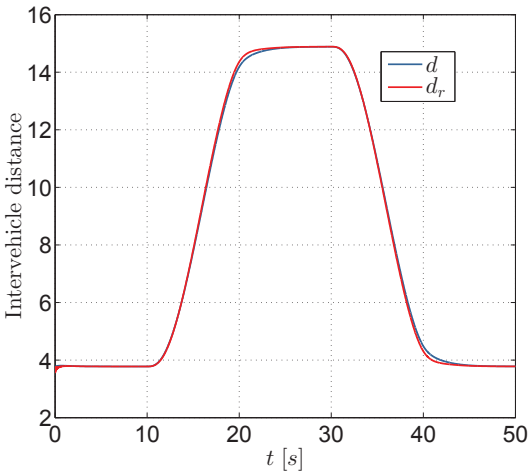

(d) Intervehicle distance

Figure 5.7: The simulation results for the Moving Base while driving along a straight line.

5.4 Summary

Simulations are performed for the lateral and longitudinal controller. The controller gains obtained in chapter 4 are implemented. The main results are that the follower converges smooth to the leader's path. Moreover, the follower follows the leader with a desired intervehicle distance also when the leader changes its velocity. Large errors in the intervehicle distance appear when the leader changes from a straight line to a circle and vise versa. Because suddenly the intervehicle distance is smaller than desired, the follower adapts its velocity as fast as possible to obtain the desired intervehicle distance. This is caused by the choice that is made to estimate the intervehicle distance.

Further, the second lateral controller is compared with a tracking controller. To make a fair comparison between the two controllers, the controller gains are chosen such that the linearized error dynamics are identical. The tracking controller converges as fast as possible to the position of the leading vehicle without considering the already traveled trajectory of the leader. While the path following controller does take the path of the leader into account while converging towards the it.

Finally, the lateral and longitudinal controller are implemented on the MB. Considering that the leading vehicle drives along a straight line, the MB follows the leader with a desired intervehicle distance. The lateral error between the MB and the reference vehicle converges to zero and remains stable.

Chapter 6

Conclusion and Recommendations

In this chapter the main conclusions are summarized and recommendations are given for future research in this topic.

6.1 Conclusion

The goal of this research was to develop a lateral and longitudinal controller such that the following vehicle follows the path of the leading vehicle with a desired constant time intervehicle distance. The vehicles are modeled using a kinematic model of a mobile robot with rear wheel drive and front wheel steering. It is assumed that no slip is present and mobile robot moves in the plane. The inputs of the model are the curvature and the velocity of the vehicle. The problem is divided into two separate control problems, i.e. achieve convergence towards the trajectory of the leader and follow the leader in longitudinal direction with a constant time spacing policy.

In section 3.1, a lateral controller is derived in the spatial domain using a Lyapunov candidate and based on the kinematic model of a mobile robot. The following vehicle follows the same path as the leading vehicle based on the curvature of the path which the leading vehicle travels. The advantage of this controller is that the path towards the leader's trajectory does not change when the follower drives with different velocities. To implement this controller, an extra step is made to transform the controller into the time domain.

A second lateral controller is derived in section 3.2 using the same approach as the first lateral controller. Compared with the first derived lateral controller, this controller is directly derived in the time domain and could be implemented immediately. Furthermore, the velocity of the reference vehicle is saturated. This has as result that the path of the follower directly converges to the leader's path for large initial lateral error.

In section 3.3, a longitudinal controller is derived based on a CACC controller. Using input-output linearization, the error dynamics of the spacing error is linearized. The spacing error is defined as the difference between the actual and desired intervehicle distance. Because the following and leading vehicle not necessary drive along the same path, the intervehicle distance is determined in the plane along the path of the follower. The intervehicle distance is estimated and the accuracy depends on the curvature of the follower's path.

The controller gains for the two lateral and the longitudinal controller are determined in chapter 4 using commonly used techniques, i.e. pole placement. Performance is defined as the safety of the individual vehicle, comfort of the driver and small tracking errors. The error dynamics for the longitudinal controller are linearized using input-output linearization and stability is determined using the Routh-Hurwitz stability criterion. Using pole placement the controller gains are determined to achieve good performance. For the lateral controllers two different techniques are

used to achieve good performance. For the first approach, the error dynamics are linearized and using pole placement the controller gains are determined. For the second approach time simulations are performed and for various controller gains the time characteristics, i.e. overshoot, rise time, settling time and total variation, are investigated. For the different trajectories and approaches, the controller gains are similar and one configuration is chosen for different trajectories.

In section 5.1, simulations are performed with the derived longitudinal and lateral controllers. The controller gains obtained in chapter 4 are implemented. The follower converges smooth to the leader's path and also follows the leader with a desired intervehicle distance. When the leader changes its velocity, with a certain time delay, the follower also starts to accelerate to maintain the desired intervehicle distance. Limitations of the estimation of the intervehicle distance are revealed. When the curvature of the path changes, sudden changes in the intervehicle distance appear which causes aggressive action of the longitudinal controller. Furthermore, the acceleration of the following vehicle is too large. It is not possible for real vehicles to achieve these large accelerations and also it is not desired for the driver's comfort.
In section 5.2, a tracking controller is compared with the lateral controller. To make a fair comparison, the controller gains are chosen such that the linearized error dynamics are the same. Different behavior is noticed for large initial lateral error. The tracking controller moves as fast as possible towards the leader, which can result in cutting corners. The lateral controller takes the previous path of the leader into account because it converges towards the reference vehicle which moves along the leaders path.
At last, simulations are performed with a complex wheeled mobile robot, i.e. the Moving base, in section 5.3. Here a simple path is considered, i.e. a straight line, where the leading vehicle moves along this path with a certain velocity profile. The Moving Base follows the leading vehicle at a desired intervehicle distance and the lateral error converges to zero and remains stable.

6.2 Recommendations

For the designed controllers, a kinematic model of a mobile robot is used. There is assumed that there is no slip which is not realizable in practice. A more advanced dynamical model is suggested. The mobile robot has the curvature and velocity as input. It is desired that the input of the mobile robot is the acceleration such that this input could be saturated. With that saturation, the problem of too high acceleration could be avoided. By extending the model, more complex lateral and longitudinal controllers are derived, but the approach is the same.

The definition of the curvilinear intervehicle distance between the leader and follower in the plane is an estimation of the actual intervehicle distance. The accuracy of this estimation depends on the curvature of the path of the follower. When the curvature is zero or small, the estimation is accurate. If the curvature becomes larger, the accuracy decreases and results in larger or smaller intervehicle distances than desired. A small intervehicle distance, results in dangerous situations. When the intervehicle distance is larger, the advantages of driving closer behind each other are neutralized. In further research a more accurate definition of the intervehicle distance must be defined which takes the curvature of the follower's path into account.

String stability is not considered in this thesis in neither lateral nor longitudinal direction. The longitudinal controller is derived based on a CACC controller, but there is not proved that it is string stable. If considering string stability for this controller, it must be considered in both lateral and longitudinal direction. Therefore, multivariable string stability must be considered.

The controllers are implemented in simulations for a not realistic kinematic model, but also for a more realistic dynamical model, i.e. the Moving Base, which is verified by experiments. A first step is to perform more simulations with this model considering more challenging trajectories and larger lateral and longitudinal error. A next step is to perform experiments with the moving base and implementation of the derived controllers.

Bibliography

[1] B. Bamieh, F. Paganini, and M. A. Dahleh. Distributed control of spatially invariant systems. IEEE Transactions on automatic control, 47(7):1091–1107, 2002.

[2] A. Banaszuk and J. Hauser. Feedback linearization of transverse dynamics for periodic orbits. Systems & Control Letters, 26(2):95 – 105, 1995.

[3] R. W. Brockett et al. Asymptotic stability and feedback stabilization. Defense Technical Information Center Virginia, 1983.

[4] S. Bus. Cooperative control of a platoon via feedback linearization. Master's thesis, Eindhoven University of Technology, 2015. Dynamics & Control, DC 2015.095.

[5] A. Chaibet, L. Nouveliere, S. Mammar, and M. Netto. Backstepping control synthesis for automated low speed vehicle. In Proceedings of the 2005, American Control Conference, 2005., pages 447–452, June 2005.

[6] O. H. Dagci, U. Y. Ogras, and U. Ozguner. Path following controller design using sliding mode control theory. In American Control Conference, 2003. Proceedings of the 2003, volume 1, pages 903–908 vol.1, June 2003.

[7] C. C. De Wit and O. J. Sørdalen. Exponential stabilization of mobile robots with nonholonomic constraints. Automatic Control, IEEE Transactions on, 37(11):1791–1797, 1992.

[8] J. P. Desai, J. Ostrowski, and V. Kumar. Controlling formations of multiple mobile robots. In Robotics and Automation, 1998. Proceedings. 1998 IEEE International Conference on, volume 4, pages 2864–2869 vol.4, May 1998.

[9] A. W. Divelbiss and J. T. Wen. Trajectory tracking control of a car-trailer system. IEEE Transactions on Control Systems Technology, 5(3):269–278, May 1997.

[10] K. D. Do and J. Pan. Nonlinear formation control of unicycle-type mobile robots. Robotics and Autonomous Systems, 55(3):191 – 204, 2007.

[11] W. B. Dunbar and D. S. Caveney. Distributed receding horizon control of vehicle platoons: Stability and string stability. IEEE Transactions on Automatic Control, 57(3):620–633, March 2012.

[12] M. I. El-Hawwary and M. Maggiore. Global path following for the unicycle and other results. In 2008 American Control Conference, pages 3500–3505, June 2008.

[13] R. Ghabcheloo, A. Pascoal, C. Silvestre, and I. Kaminer. Coordinated path following control of multiple wheeled robots with directed communication links. In Proceedings of the 44th IEEE Conference on Decision and Control, pages 7084–7089, Dec 2005.

[14] A. Ghasemi, R. Kazemi, and S. Azadi. Stability analysis of bidirectional adaptive cruise control with asymmetric information flow. Proceedings of the Institution of Mechanical Engineers, Part C: Journal of Mechanical Engineering Science, 229(2):216–226, 2015.

[15] Y. Hayakawa, R. White, T. Kimura, and G. Naito. Driver-compatible steering system for wide speed-range path following. IEEE/ASME Transactions on Mechatronics, 9(3):544–552, Sept 2004.

[16] J. K. Hedrick, D. McMahon, V. Narendran, and D. Swaroop. Longitudinal vehicle controller design for ivhs systems. In American Control Conference, 1991, pages 3107–3112, June 1991.

[17] Z. P. Jiang, A. A. J. Lefeber, and H. Nijmeijer. Saturated stabilization and tracking of a nonholonomic mobile robot. Systems & Control Letters, 42(5):327 – 332, 2001.

[18] Z. P. Jiang and H. Nijmeijer. Tracking control of mobile robots: A case study in backstepping. Automatica, 33(7):1393 – 1399, 1997.

[19] H.K. Khalil. Nonlinear Systems. Pearson, third edition edition, 2002.

[20] M. E. Khatir and E. J. Davison. A decentralized lateral-longitudinal controller for a platoon of vehicles operating on a plane. In 2006 American Control Conference, pages 6 pp.–, June 2006.

[21] G. Klančar, D. Matko, and S. Blažič. A control strategy for platoons of differential drive wheeled mobile robot. Robotics and Autonomous Systems, 59(2):57 – 64, 2011.

[22] E. Lefeber. Path following : a new idea. Internal document, 2016.

[23] E. Lefeber. Some thoughts about a path following approach. Internal document, 2016.

[24] E. H. M. Lim and J. K. Hedrick. Lateral and longitudinal vehicle control coupling for automated vehicle operation. In American Control Conference, 1999. Proceedings of the 1999, volume 5, pages 3676–3680 vol.5, 1999.

[25] G. Lu and M. Tomizuka. A practical solution to the string stability problem in autonomous vehicle following. In American Control Conference, 2004. Proceedings of the 2004, volume 1, pages 780–785 vol.1, June 2004.

[26] M. Lu, K. Wevers, and R. V. D. Heijden. Technical feasibility of advanced driver assistance systems (adas) for road traffic safety. Transportation Planning and Technology, 28(3):167–187, 2005.

[27] J. P. Maschuw, G. C. Keßler, and D. Abel. Lmi-based control of vehicle platoons for robust longitudinal guidance. IFAC Proceedings Volumes, 41(2):12111 – 12116, 2008. 17th IFAC World Congress.

[28] A. Micaelli and C. Samson. Trajectory tracking for unicycle-type and two-steering-wheels mobile robots. PhD thesis, INRIA, 1993.

[29] P. Morin and C. Samson. Motion control of wheeled mobile robots. In Springer Handbook of Robotics, pages 799–826. Springer, 2008.

[30] A. Morro, A. Sgorbissa, and R. Zaccaria. Path following for unicycle robots with an arbitrary path curvature. IEEE Transactions on Robotics, 27(5):1016–1023, Oct 2011.

[31] G. J. L. Naus, J. Ploeg, R. P. A. Vugts, M. J. G. van de Molengraft, and M. Steinbuch. Cooperative adaptive cruise control, design and experiments. 2010 American Control Conference, 1(1):6145–6150, 2010.

[32] G. J. L. Naus, R. P. A. Vugts, J. Ploeg, M. J. G. van de Molengraft, and M. Steinbuch. String-stable cacc design and experimental validation: A frequency-domain approach. IEEE Transactions on Vehicular Technology, 59(9):4268–4279, Nov 2010.

[33] C. Nielsen and M. Maggiore. Output stabilization and maneuver regulation: A geometric approach. Systems & Control Letters, 55(5):418 – 427, 2006.

[34] S. Öncü, J. Ploeg, N. van de Wouw, and H. Nijmeijer. Cooperative adaptive cruise control: Network-aware analysis of string stability. IEEE Transactions on Intelligent Transportation Systems, 15(4):1527–1537, 2014.

[35] I. Papadimitriou, G.g Lu, and M. Tomizuka. Autonomous lateral following consideration for vehicle platoons. In Advanced Intelligent Mechatronics, 2003. AIM 2003. Proceedings. 2003 IEEE/ASME International Conference on, volume 1, pages 401–406 vol.1, July 2003.

[36] P. Petrov and O. Boumbarov. Nonlinear adaptive control of a two-vehicle autonomous convoy using a look-ahead approach. In Proceedings of the 7th WSEAS International Conference on Signal Processing, Robotics and Automation, pages 55–60. World Scientific and Engineering Academy and Society (WSEAS), 2008.

[37] J. Ploeg. Analysis and design of controllers for cooperative and automated driving. PhD thesis, Eindhoven University of Technology, 2014.

[38] J. Ploeg, D. P. Shukla, N. van de Wouw, and H. Nijmeijer. Controller synthesis for string stability of vehicle platoons. IEEE Transactions on Intelligent Transportation Systems, 15(2):854–865, April 2014.

[39] J. Ploeg, N. van de Wouw, and H. Nijmeijer. Lp string stability of cascaded systems: Application to vehicle platooning. IEEE Transactions on Control Systems Technology, 22(2):786–793, March 2014.

[40] J. Ploeg, J. P. M. Vissers, and H. Nijmeijer. Control design for an overactuated wheeled mobile robot. IFAC Proceedings Volumes, 39(16):127–132, 2006.

[41] R. Rajamani and C. Zhu. Semi-autonomous adaptive cruise control systems. IEEE Transactions on Vehicular Technology, 51(5):1186–1192, Sep 2002.

[42] W. Ren and R. W. Beard. A decentralized scheme for spacecraft formation flying via the virtual structure approach. In American Control Conference, 2003. Proceedings of the 2003, volume 2, pages 1746–1751, June 2003.

[43] C. Samson. Time-varying feedback stabilization of nonholonomic car-like mobile robots. PhD thesis, INRIA, 1991.

[44] H. Shim, Y. I. Son, and J. H. Seo. Semi-global observer for multi-output nonlinear systems. Systems & Control Letters, 42(3):233 – 244, 2001.

[45] S. Shladover, J. VanderWerf, M. A. Miller, N. Kourjanskaia, and H. Krishnan. Development and performance evaluation of avcss deployment sequences to advance from today's driving environment to full automation. California Partners for Advanced Transit and Highways (PATH), 2001.

[46] R. Skjetne and T. I. Fossen. Nonlinear maneuvering and control of ships. In MTS/IEEE Oceans 2001. An Ocean Odyssey. Conference Proceedings (IEEE Cat. No.01CH37295), volume 3, pages 1808–1815 vol.3, 2001.

[47] R. Skjetne, S. Moi, and T. I. Fossen. Nonlinear formation control of marine craft. In Decision and Control, 2002, Proceedings of the 41st IEEE Conference on, volume 2, pages 1699–1704 vol.2, Dec 2002.

[48] D. Soetanto, L. Lapierre, and A. Pascoal. Adaptive, non-singular path-following control of dynamic wheeled robots. In Decision and Control, 2003. Proceedings. 42nd IEEE Conference on, volume 2, pages 1765–1770 Vol.2, Dec 2003.

[49] S. Solyom, A. Idelchi, and B. B. Salamah. Lateral control of vehicle platoons. In 2013 IEEE International Conference on Systems, Man, and Cybernetics, pages 4561–4565, Oct 2013.

[50] S. S. Stankovic, M. J. Stanojevic, and D. D. Siljak. Decentralized overlapping control of a platoon of vehicles. IEEE Transactions on Control Systems Technology, 8(5):816–832, Sep 2000.

[51] D. Swaroop and J. K. Hedrick. String stability of interconnected systems. IEEE Transactions on Automatic Control, 41(3):349–357, Mar 1996.

[52] D. V. A. H. G. Swaroop and J. K. Hedrick. Constant spacing strategies for platooning in automated highway systems. Journal of dynamic systems, measurement, and control, 121(3):462–470, 1999.

[53] A. Vahidi and A. Eskandarian. Research advances in intelligent collision avoidance and adaptive cruise control. IEEE Transactions on Intelligent Transportation Systems, 4(3):143–153, Sept 2003.

[54] P. Venhovens, K. Naab, and B. Adiprasito. Stop and go cruise control. International journal of automotive technology, 1(2):61–69, 2000.

[55] R. White and M. Tomizuka. Autonomous following lateral control of heavy vehicles using laser scanning radar. In American Control Conference, 2001. Proceedings of the 2001, volume 3, pages 2333–2338. IEEE, 2001.

[56] X. Xiang, L. Lapierre, B. Jouvencel, and O. Parodi. Coordinated path following control of multiple nonholonomic vehicles. In OCEANS 2009 - EUROPE, pages 1–7, May 2009.

[57] Y. Zheng, S. Eben Li, J. Wang, D. Cao, and K. Li. Stability and scalability of homogeneous vehicular platoon: Study on the influence of information flow topologies. IEEE Transactions on Intelligent Transportation Systems, 17(1):14–26, Jan 2016.

[58] Y. Zheng, S. Eben Li, J. Wang, L. Y. Wang, and K. Li. Influence of information flow topology on closed-loop stability of vehicle platoon with rigid formation. 2014 IEEE 17th International Conference on Intelligent Transportation Systems (ITSC), pages 2094 – 2100, 2014.

Appendix A

Proofs

In this chapter the stability of the designed lateral controllers in section 3.1 and section 3.2 are discussed. The nontrivial definitions that are used for this stability analysis are recalled. A useful tool for showing asymptotic stability for a certain signal is:

Lemma A.1 (Barbalat, [19], Lemma 8.2) Let $f : R \to R$ be a uniformly continuous function on $[0, \infty)$. Suppose that $\lim_{t\to\infty} \int_0^t f(\tau)\, d\tau$ exists and is finite. Then,

$$\lim_{t\to\infty} f(t) = 0.$$

An extension on Barbalat's lemma of a function $f(t)$ that is not uniformly continuous was presented in [28].

Lemma A.2 (Micaelli and Samson, [28], Lemma 1) Let $f : \mathcal{R}_+ \to R$ be any differentiable function. If $f(t)$ converges to zero as $t \to \infty$ and its derivative satisfied

$$\dot{f}(t) = f_0(t) + \eta(t) \quad t \leq 0$$

where f_0 is a uniformly continuous function and $\eta(t)$ tends to zero as $t \to \infty$, then $\dot{f}(t)$ and $f_0(t)$ tens to zero as $t \to \infty$.

These two lemmas are used for a Lyapunov based stability analysis for nonlinear time-varying systems, where the derivative of the Lyapunov candidate function is semi-negative definite. With these lemmas the asymptotic convergence of a signal can be determined.

A.1 Proof of Proposition 1 and Proposition 2

A.1.1 Proof of Proposition 1

The Lyapunov function candidate is defined as

$$V(s_f) = \frac{1}{2}\bar{x}_e(s_f)^2 + \frac{1}{2}\bar{y}_e(s_f)^2 + \frac{1}{2k_2}\bar{\theta}_e(s_f)^2, \tag{A.1}$$

where $k_2 > 0$. The derivation of (A.1) with respect to s_f of (A.1) using (3.11) and (3.12), and substituting the proposed control law (3.13), results in

$$\frac{d}{ds_f}V(s_f) = -k_1\bar{x}_e^2(s_f) - k_3\bar{\theta}_e^2(s_f) \leq 0, \tag{A.2}$$

where $k_1 > 0$ and $k_3 > 0$. This implies that $V(s_f)$ has a bounded limit for $t \to \infty$ and consequently, the errors $\bar{x}_e(s_f)$, $\bar{y}_e(s_f)$ and $\bar{\theta}_e(s_f)$ are bounded. It is assumed that $\tilde{v}_r(s_f)$ and $\tilde{\kappa}_l(s_f)$ are bounded. Hence, from (3.13) can be concluded that $\bar{\kappa}_f(s_f)$ is bounded and from (3.11) there is concluded that $\frac{d}{ds_f}\bar{x}_e(s_f)$, $\frac{d}{ds_f}\bar{y}_e(s_f)$ and $\frac{d}{ds_f}\bar{\theta}_e(s_f)$ are bounded. This implies that $\bar{x}_e(s_f)$,

$\bar{y}_e(s_f)$ and $\bar{\theta}_e(s_f)$ are uniformly continuous functions of $s_f(t)$. Since (A.2) is a uniformly continuous function, Lemma A.1 is applied using (A.1) and (A.2), it is concluded that $\lim_{s_f \to \infty} \bar{x}_e = 0$ and $\lim_{s_f \to \infty} \bar{\theta}_e = 0$.

What remains, is to prove that $\bar{y}_e$ tends to zero as $t \to \infty$. Therefore, Lemma A.2 is applied to (3.11c) and (3.13). Substituting (3.13) into (3.11c) results in

$$\frac{d}{ds_f}\bar{\theta}_e(s_f) = k_2\bar{y}_e\left(1 - k_1\bar{x}_e\right)\frac{\tan\bar{\theta}_e}{\bar{\theta}_e} + k_3\bar{\theta}_e. \tag{A.3}$$

Because $k_3\bar{\theta}_e$ tends to zero as $t \to \infty$ and $k_2\bar{y}_e\left(1 - k_1\bar{x}_e\right)\frac{\tan\bar{\theta}_e}{\bar{\theta}_e}$ is uniformly continuous, it can be concluded that $\lim_{s_f \to \infty} \bar{y}_e = 0$. Therefore, the error dynamics are asymptotically stable.

It is assumed that $\tilde{v}_r$ is bounded, but this is only the case when $|\bar{\theta}_e| < \frac{\pi}{2}$. Because (A.2) is semi-negative definite, $V(0)$ is the maximum value of (A.1). This property is useful to prevent that $\bar{\theta}_e$ becomes larger or equal to $\pi/2$. To guarantee that $\tilde{v}_r$ is bounded, the initial conditions must satisfy

$$k_2x_e^2(0) + k_2y_e^2(0) + \theta_e^2(0) < \frac{\pi^2}{4}. \tag{A.4}$$

A.1.2 Proof of Proposition 2

The proof of Proposition 2 is derived in a simular fashion as the proof of Proposition 1. Consider the Lyapunov function candidate proposed in [23]

$$V(s_f) = \frac{1}{2}\bar{x}_e^2(s_f) + \frac{1}{2}\bar{y}_e^2(s_f) - \frac{1}{k_2}\int_0^{\bar{\theta}_e} \tan\theta d\theta, \tag{A.5}$$

for $|\bar{\theta}_e| < \pi/2$ and $k_2 > 0$. The derivative of (A.5) with respect to $s_f(t)$ using (3.11) and (3.12) and substituting the control law (3.14), is given by

$$\frac{d}{ds_f}V(s_f) = -k_1\bar{x}_e^2(s_f) - k_3\tan\bar{\theta}_e(s_f)\bar{\theta}_e(s_f) \leq 0. \tag{A.6}$$

Because (A.6) is semi-negative definite, (A.5) has a bounded limit for $t \to \infty$. Consequently, $\bar{x}_e(s_f)$, $\bar{y}_e(s_f)$ and $\bar{\theta}_e$ are bounded, which implies that $|\theta_e| < \pi/2$. It is assumed that $\tilde{\kappa}_r(s_f)$ is bounded, and to guarantee that $\tilde{v}_r(s_f)$ is bounded, the initial conditions must satisfy (A.4). From (3.14) it is concluded that $\bar{\kappa}_f(s_f)$ is bounded, and $\frac{d}{ds_f}x_e(s_f)$, $\frac{d}{ds_f}y_e(s_f)$ and $\frac{d}{ds_f}\theta_e(s_f)$ are bounded using (3.11). This implies that $x_e(s_f)$, $y_e(s_f)$ and $\theta_e(s_f)$ are uniformly continuous functions of $s_f(t)$. Since (A.6) is a uniformly continuous function, Lemma A.1 is applied on (A.5) and (A.6). It is concluded that $\lim_{s_f \to \infty} \bar{x}_e = 0$ and $\lim_{s_f \to \infty} \bar{\theta}_e = 0$.

To prove that $\bar{y}_e$ tends to zero when $t \to 0$, Lemma A.2 is applied to (3.11c) and (3.14). Substituting (3.14) into (3.11c), resulting in

$$\frac{d}{ds_f}\bar{\theta}_e(s_f) = -k_2\bar{y}_e(s_f)\left(1 + k_1\bar{x}_e(s_f)\right) - k_3\bar{\theta}_e(s_f) \tag{A.7}$$

Because $-k_3\bar{\theta}_e(s_f)$ tends to zero when $t \to 0$, and $-k_2\bar{y}_e(s_f)\left(1 + k_1\bar{x}_e(s_f)\right)$ is uniformly continuous, it can be concluded that $\lim_{s_f \to \infty} \bar{y}_e = 0$. Therefore, the error dynamics are asymptotically stable.

A.2 Proof of Proposition 3

Consider the Lyapunov function candidate with $k_4 > 0$

$$V(t) = \frac{1}{2}x_e^2(t) + \frac{1}{2}y_e^2(t) + \frac{1}{2k_4}\theta_e^2(t). \tag{A.8}$$

Taking the derivative of (A.8) and substituting (3.20), (3.21) and (3.23), where the time argument t is omitted for readability, results in

$$\dot{V} = -v_f x_e \sigma(x_e) - \frac{k_5}{k_4} v_f \theta_e^2 \leq 0. \tag{A.9}$$

where $k_5 > 0$ and $v_f \geq \epsilon > 0$. This implies that (A.8) has a bounded limit for $t \to \infty$ and consequently, $x_e(t)$, $y_e(t)$ and $\theta_e(t)$ are bounded. Assuming that $\kappa_l(s_f)$ is bounded, it can be concluded using (3.23) that $\kappa_f(t)$ is bounded. Therefore, $\dot{x}_e(t)$, $\dot{y}_e(t)$ and $\dot{\theta}_e(t)$ are bounded according to (3.20). This implies that $x_e(t)$, $y_e(t)$ and $\theta_e(t)$ are uniformly continuous functions of t. Since (A.9) is a uniformly continuous function, Lemma A.1 is applied using (A.8) and (A.9). Consequently, it is concluded that $\lim_{t\to\infty} \bar{x}_e = 0$ and $\lim_{t\to\infty} \bar{\theta}_e = 0$.

To prove that $\bar{y}_e$ tends to zero as $t \to \infty$, Lemma A.2 is applied to (3.20c) and (3.23). Substituting (3.23) into (3.20c) results in

$$\dot{\theta}_e(t) = -k_4 v_f(t)\frac{\cos\theta_e(t) - 1}{\theta_e(t)} x_e(t) - k_4 v_f(t)\frac{\sin\theta_e(t)}{\theta_e(t)} y_e(t) - k_5 v_f(t)\theta_e(t). \tag{A.10}$$

Because $-k_5 v_f(t)\theta_e(t)$ tends to zero when $t \to 0$, and $-k_4 v_f(t)\frac{\cos\theta_e(t)-1}{\theta_e(t)} x_e(t) - k_4 v_f(t)\frac{\sin\theta_e(t)}{\theta_e(t)} y_e(t)$ is uniformly continuous, it can be concluded that $\lim_{t\to\infty} \bar{y}_e = 0$. Therefore, the error dynamics are asymptotically stable.

Appendix B

Derivation

B.1 Error Dynamics Lateral Controller 1

In section 3.1 a lateral controller is derived to stabilize the error dynamics between the following and reference vehicle. The lateral error of controller 1 is given in (3.17). Because all variables depends on $s_f(t)$, this argument is dropped. Taken the time derivative of (3.17) results in

$$\dot{x}_e = -\sin\theta_f\dot{\theta}_f(x_r - x_f) + \cos\theta_f(\dot{x}_r - \dot{x}_f) + \cos\theta_f\dot{\theta}_f(y_r - y_f) + \sin\theta_f(\dot{y}_r - \dot{y}_f) \tag{B.1a}$$
$$\dot{y}_e = -\cos\theta_f\dot{\theta}_f(x_r - x_f) - \sin\theta_f(\dot{x}_r - \dot{x}_f) - \sin\theta_f\dot{\theta}_f(y_r - y_f) + \cos\theta_f(\dot{y}_r - \dot{y}_f) \tag{B.1b}$$
$$\dot{\theta}_e = \dot{\theta}_r - \dot{\theta}_f \tag{B.1c}$$

Substituting the kinematics models (3.16) of the follower and reference vehicle into (B.1) results in

$$\dot{\bar{x}}_e = v_f(t)\kappa_f\left[-\sin\theta_f(x_r - x_f) + \cos\theta_f(y_r - y_f)\right] - v_f(t)\left[\cos^2\theta_f + \sin^2\theta_f\right] + v_f(t)\tilde{v}_r\left[\cos\theta_f\cos\theta_r + \sin\theta_f\sin\theta_r\right] \tag{B.2a}$$
$$\dot{y}_e = -v_f(t)\kappa_f\left[\cos\theta_f(x_r - x_f) + \sin\theta_f(y_r - y_f)\right] + v_f(t)\tilde{v}_r\left[\cos\theta_f\sin\theta_r - \sin\theta_f\cos\theta_r\right] \tag{B.2b}$$
$$\dot{\theta}_e = v_f(t)\tilde{v}_r\tilde{\kappa}_l - v_f(t)\kappa_f \tag{B.2c}$$

Eventually, this results in the error dynamics of the lateral controller 1 given by

$$\dot{x}_e = v_f(t)\kappa_f\bar{y}_e - v_f(t) + v_f(t)\tilde{v}_r\cos\theta_e \tag{B.3a}$$
$$\dot{y}_e = -v_f(t)\kappa_f\bar{x}_e + v_f(t)\tilde{v}_r\sin\theta_e \tag{B.3b}$$
$$\dot{\theta}_e = v_f(t)\tilde{v}_r\tilde{\kappa}_l - v_f(t)\kappa_f \tag{B.3c}$$

B.2 Error Dynamics Lateral Controller 2

For the lateral controller 2 also the error dynamics is derived in order to derive the lateral controller. The lateral error of the controller is given in (3.19). The time derivatives of the lateral error is given by

$$\dot{x}_e = -\sin\theta_r\dot{\theta}_r\left(x_f - x_r\right) + \cos\theta_r\left(\dot{x}_f - \dot{x}_r\right) + \cos\theta_r\dot{\theta}_r\left(y_f - y_r\right) + \sin\theta_r\left(\dot{y}_f - \dot{y}_r\right) \tag{B.4a}$$
$$\dot{y}_e = -\cos\theta_r\dot{\theta}_r\left(x_f - x_r\right) - \sin\theta_r\left(\dot{x}_f - \dot{x}_r\right) - \sin\theta_r\dot{\theta}_r\left(y_f - y_r\right) + \cos\theta_r\left(\dot{y}_f - \dot{y}_r\right) \tag{B.4b}$$
$$\dot{\theta}_e = \dot{\theta}_f - \dot{\theta}_r \tag{B.4c}$$

Substituting the kinematics models of the follower and reference vehicle into (B.4) results in

$$\dot{x}_e = \dot{s}_r\kappa_l\left(-\sin\theta_r\left[x_f - x_r\right] + \cos\theta_r\left[y_f - y_r\right]\right) + v_f\left(\cos\theta_r\cos\theta_f + \sin\theta_r\sin\theta_f\right) - \dot{s}_r\left(\cos^2\theta_r + \sin^2\theta_r\right) \tag{B.5a}$$

$$\dot{y}_e = -\dot{s}_r\kappa_l x_e + v_f\left(\cos\theta_r\sin\theta_f - \sin\theta_r\cos\theta_f\right) \tag{B.5b}$$

$$\dot{\theta}_e = v_f\kappa_f - \dot{s}_r\kappa_l \tag{B.5c}$$

This result in the error dynamics of lateral controller 2

$$\dot{x}_e = \dot{s}_r\kappa_l y_e + v_f\cos\theta_e - \dot{s}_r \tag{B.6a}$$

$$\dot{y}_e = -\dot{s}_r\kappa_l x_e + v_f\sin\theta_e \tag{B.6b}$$

$$\dot{\theta}_e = v_f\kappa_f - \dot{s}_r\kappa_l \tag{B.6c}$$

B.3 Error Dynamics Longitudinal Controller

In section 3.3 a longitudinal controller is derived with help of the longitudinal error defined in (3.25). The error dynamics in longitudinal direction are given by

$$\dot{x}_{e,long}(t) = -\sin\theta_f\dot{\theta}_f(x_l - x_f) + \cos\theta_f(\dot{x}_l - \dot{x}_f) + \cos\theta_f\dot{\theta}_f(y_l - y_f) + \sin\theta_f(\dot{y}_l - \dot{y}_f) \tag{B.7a}$$

$$\dot{y}_{e,long}(t) = -\cos\theta_f\dot{\theta}_f(x_l - x_f) - \sin\theta_f(\dot{x}_l - \dot{x}_f) - \sin\theta_f\dot{\theta}_f(y_l - y_f) + \cos\theta_f(\dot{y}_l - \dot{y}_f) \tag{B.7b}$$

$$\dot{\theta}_{e,long}(t) = \dot{\theta}_l - \dot{\theta}_f \tag{B.7c}$$

Substituting the kinematics of the leader and follower into (B.7) results in

$$\dot{x}_{e,long}(t) = v_f\kappa_f\left[-\sin\theta_f(x_l - x_f) + \cos\theta_f(y_l - y_f)\right] + \cos\theta_f(v_l\cos\theta_l - v_f\cos\theta_f) + \sin\theta_f(v_l\sin\theta_l - v_f\sin\theta_f) \tag{B.8a}$$

$$\dot{y}_{e,long}(t) = -v_f\kappa_f\left[\cos\theta_f(x_l - x_f) + \sin\theta_f(y_l - y_f)\right] - \sin\theta_f(v_l\cos\theta_l - v_f\cos\theta_f) + \cos\theta_f(v_l\sin\theta_l - v_f\sin\theta_f) \tag{B.8b}$$

$$\dot{\theta}_{e,long}(t) = v_l\tilde{\kappa}_l - v_f\kappa_f \tag{B.8c}$$

Eventually this results in

$$\dot{x}_{e,long}(t) = v_f\kappa_f y_{e,long} - v_f + v_l\cos\theta_{e,long} \tag{B.9a}$$

$$\dot{y}_{e,long}(t) = -v_f\kappa_f x_{e,long} + v_l\sin\theta_{e,long} \tag{B.9b}$$

$$\dot{\theta}_{e,long}(t) = v_l\tilde{\kappa}_l - v_f\kappa_f \tag{B.9c}$$

B.4 Longitudinal error

In section 3.3 the error dynamics of the longitudinal controller are linearized. To apply input-output linearization, the relative degree of the system is determined. The expression of $\zeta(x, \kappa_f, \dot{\kappa}_f, \kappa_l, \dot{\kappa}_l, v_f, v_l, a_f, a_l, u_f, u_l)$ in (3.34) is given by

$$
\begin{aligned}
&\zeta(x,\kappa_f,\dot{\kappa}_f,\kappa_l,\dot{\kappa}_l,v_f,v_l,a_f,a_l,u_f,u_l) = \kappa_f^2 v_f^3 + \frac{u_f}{\tau} + \frac{a_f - u_f}{\tau} \\
&- \sqrt{1 - \frac{p_1^2}{v_l^2}} \left(3a_f\kappa_f v_l - \dot{\kappa}_l v_l^2 + 3a_l\kappa_f v_f - a a_l \kappa_l v_l + 3\dot{\kappa}_f v_f v_l\right) + \frac{h\left(a_f - u_f\right)}{\tau^2} \\
&- \frac{p_1\left(3\tau\kappa_f^2 v_f^2 v_l + 3\tau\kappa_f\kappa_l v_f v_l^2 - \tau\kappa_l^2 v_l^3 + a_l - u_l\right)}{\tau v_l} - 3\kappa_f v_f\left(a_f\kappa_f + \dot{\kappa}_f v_f\right)\left[L + e_1 + r + h v_f\right] \\
&+ \frac{v_l p_2\left[2\kappa_f v_f - \kappa_l v_l\right]^2\left(-\tau\kappa_f v_f + \ddot{\kappa}_f \tau v_f - a_f + u_f + 2a_f\dot{\kappa}_f\tau\right)}{2\tau\left(a_f\kappa_f v_l - a_f\kappa_f v_f + \dot{\kappa}_f v_f v_l\right)^2}
\end{aligned}
\tag{B.10}
$$

where

$$
p_1 = e_2 + v_f + a_f h - \frac{\kappa_f v_f v_l^3 p_2\left(2\kappa_f v_f - \kappa_l v_l\right)^2}{2\left(a_f\kappa_f v_l - a_f\kappa_f v_f + \dot{\kappa}_f v_f v_l\right)^2} \tag{B.11}
$$

$$
p_2 = \kappa_f v_f + v_l \sqrt{\frac{\kappa_f^2 v_f^2}{v_l^2} - \frac{4\left[a_f\kappa_f v_l - a_f\kappa_f v_f + \dot{\kappa}_f v_f v_l\right]^2 \left(\frac{a_f - \frac{h\left(a_f - u_f\right)}{\tau} + \kappa_f^2 v_f^2 (L + e_1 + r + h v_f) - \frac{a_l\left(e_3 + v_f + a_f h\right)}{v_l} + \frac{e_2 + v_f + a_f h}{v_l} - 1}{\kappa_l v_l^2 - 2\kappa_f v_f v_l}\right)}{v_l^2\left[\kappa_l v_l^2 - 2\kappa_f v_f v_l\right]^2}} \tag{B.12}
$$

To determine the relative degree of the error dynamics the Lie derivatives with respect to $f(x,\kappa_f,\dot{\kappa}_f,\kappa_l,\dot{\kappa}_l,v_f,v_l,a_f,a_l,u_f,u_l)$ and $g(\tau)$ are determined. The Lie derivative of $h(x) = e(t)$ with respect to $g(\tau)$ is given by

$$
L_g h(x) = \frac{\partial h(x)}{\partial x} g(\tau) = \begin{bmatrix} 1 & 0 & 0 \end{bmatrix} \begin{bmatrix} 0 \\ 0 \\ -\frac{1}{\tau} \end{bmatrix} = 0. \tag{B.13}
$$

The Lie derivative of $h(x)$ with respect to $f(x,\kappa_f,\dot{\kappa}_f,\kappa_l,\dot{\kappa}_l,v_f,v_l,a_f,a_l,u_f,u_l)$ is given by

$$
L_f h(x) = \frac{\partial h(x)}{\partial x} f(x,\kappa_f,\dot{\kappa}_f,\kappa_l,\dot{\kappa}_l,v_f,v_l,a_f,a_l,u_f,u_l) = \begin{bmatrix} 1 & 0 & 0 \end{bmatrix} \begin{bmatrix} e_2 \\ e_3 \\ \zeta \end{bmatrix} = e_2. \tag{B.14}
$$

This results in

$$
L_g L_f h(x) = \frac{\partial}{\partial x}\left(\frac{\partial L_f h(x)}{\partial x}\right) g(\tau) = \begin{bmatrix} 0 & 1 & 0 \end{bmatrix} \begin{bmatrix} 0 \\ 0 \\ -\frac{1}{\tau} \end{bmatrix} = 0. \tag{B.15}
$$

The Lie derivative of (B.14) with respect to $f(x,\kappa_f,\dot{\kappa}_f,\kappa_l,\dot{\kappa}_l,v_f,v_l,a_f,a_l,u_f,u_l)$ is given by

$$
L_f^2 h(x) = \frac{\partial}{\partial x}\left(\frac{\partial L_f h(x)}{\partial x}\right) f(x,\kappa_f,\dot{\kappa}_f,\kappa_l,\dot{\kappa}_l,v_f,v_l,a_f,a_l,u_f,u_l) = \begin{bmatrix} 0 & 1 & 0 \end{bmatrix} \begin{bmatrix} e_2 \\ e_3 \\ \zeta \end{bmatrix} = e_3. \tag{B.16}
$$

The last Lie derivative is given by

$$
L_g L_f^2 h(x) = \frac{\partial}{\partial x}\left(\frac{\partial L_f^2 h(x)}{\partial x}\right) g(\tau) = \begin{bmatrix} 0 & 0 & 1 \end{bmatrix} \begin{bmatrix} 0 \\ 0 \\ -\frac{1}{\tau} \end{bmatrix} = -\frac{1}{\tau}, \tag{B.17}
$$

and is nonzero. The relative degree of the error dynamics of the spacing error is three.

B.5 Pole Placement

For tuning the lateral controllers in chapter 4 pole placement is applied. For lateral controller 1 and 2 the same approach is used, because the closed loop linearized error dynamics are identical. The desired characteristic polynomial with the poles $\lambda_1 = -20$, $\lambda_2 = -20$ and $\lambda_3 = -20$ is

$$\det\left(sI - A^{cl}\right) = \lambda^3 + 60\lambda^2 + 1200\lambda + 8000. \tag{B.18}$$

The controller gains are determined by solving

$$\left(k_1 + k_3\right) v_l = 60 \tag{B.19a}$$
$$\left(\bar{\kappa}_l^2 + k_1 k_3 + k_2\right) v_l^2 = 1200 \tag{B.19b}$$
$$\left(k_3 \bar{\kappa}_l^2 + k_1 k_2\right) v_l^3 = 8000. \tag{B.19c}$$
$$\tag{B.19d}$$

The controller gains k_1 and k_2, depending on k_3, are determined as

$$k_1 = \frac{60}{v_l} - k_3 \tag{B.20a}$$
$$k_2 = \frac{1200}{v_l^2} - \bar{\kappa}_l^2 - \left(\frac{60}{v_l} - k_3\right) k_3. \tag{B.20b}$$

The gain k_3 is determined by solving the polynomial

$$-v_l^3 k_3^3 + 120 v_l^2 k_3^2 + \left(-4800 v_l + 2\bar{\kappa}_l^2 v_l^3\right) k_3 - 60\bar{\kappa}_l^2 v_l^2 + 64000 = 0. \tag{B.21}$$

The determinant of the polynomial is given by

$$\Delta = 16\bar{\kappa}_l^4 v_l^{10}(2\bar{\kappa}_l^2 v_l^2 - 675). \tag{B.22}$$

Figure B.1 shows the determinant for the range $\kappa_l = -0.5$ - 0.5 and $v_l = 30km/h$ - $130km/h$. As can be seen, $\Delta < 0$ so the polynomial has one real solution and two non-real complex conjugate solutions. Only the real solution is interesting to use to determine the controller gains.

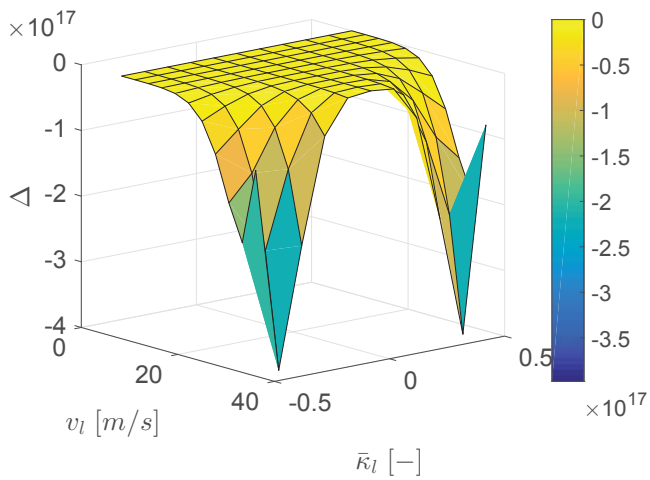

Figure B.1: The determinant of the third order polynomial of k_3.

Using the cubic formula, the controller gain k_3 is given by

$$k_3 = \frac{120 + 2v_l \sqrt[3]{\frac{270\bar{\kappa}_l^2 + 6v_l \sqrt{-6\bar{\kappa}_l^6 + \frac{2025\bar{\kappa}_l^4}{v_l^2}}}{v_l}}}{3v_l}. \tag{B.23}$$

Appendix C

Tuning

C.1 Controller gains with time simulations

To determine the effect of the controller gains of the lateral controller, the effect of these gains on the overshoot, settling time, rise time and total variation are determined using time simulations. The initial conditions are chosen such that when the leader's path is a straight line, the time response can be determined. When the leader drives along a circular path, the position of the follower is transformed to polar coordinates to determine the time response.

C.1.1 Controller 1

In Figure C.1 the effect of k_1 is shown for three different scenario's: driving on a line, in a circle and starting with a large initial condition. All three with a low velocity (30km/h) and high velocity (130km/h). In the figure where determining the settling time, large steps are presents. Also for other gains in this chapter similar behavior appears. The reason for this is that way the settling time is calculated. When a larger step size is used, not the exact value of the settling time is determined and can cause a wiggling behavior

- Overshoot: There is no difference between driving with a high and low velocity.
  - Line: a small k_1 results in less overshoot. The increasing of the overshoot is larger for starting with a large initial condition.
  - Circle: a higher k_1 results in less overshoot. There can be seen that for $k_1 > 1$ the overshoot increases gradually again for a large initial condition and for $k_1 > 1.6$ for starting close to the desired trajectory.
- Settling time: The effect of the controller gain is the same for both velocities.
  - Line: The settling time increases when k_1 increases. For starting with a large initial condition, a very small value of k_1 results in a larger settling time.
  - Circle: the settling time decreases until $k_1 = 1$ and then increases again when k_1 increases.
- Rise time: The effect of the controller gain is the same for both velocities.
  - Line: the rise time decreases when k_1 increases.
  - Circle: the rise time increases when k_1 increases.
- Total variation: No difference between driving with low or high velocity.
  - Line: a small k_1 results in smaller total variation.
  - Circle: a higher k_1 results in smaller total variation. There can be seen that for $k_1 > 1$ the overshoot increases gradually again for a large initial condition and for $k_1 > 1.8$ for starting close to the desired trajectory.

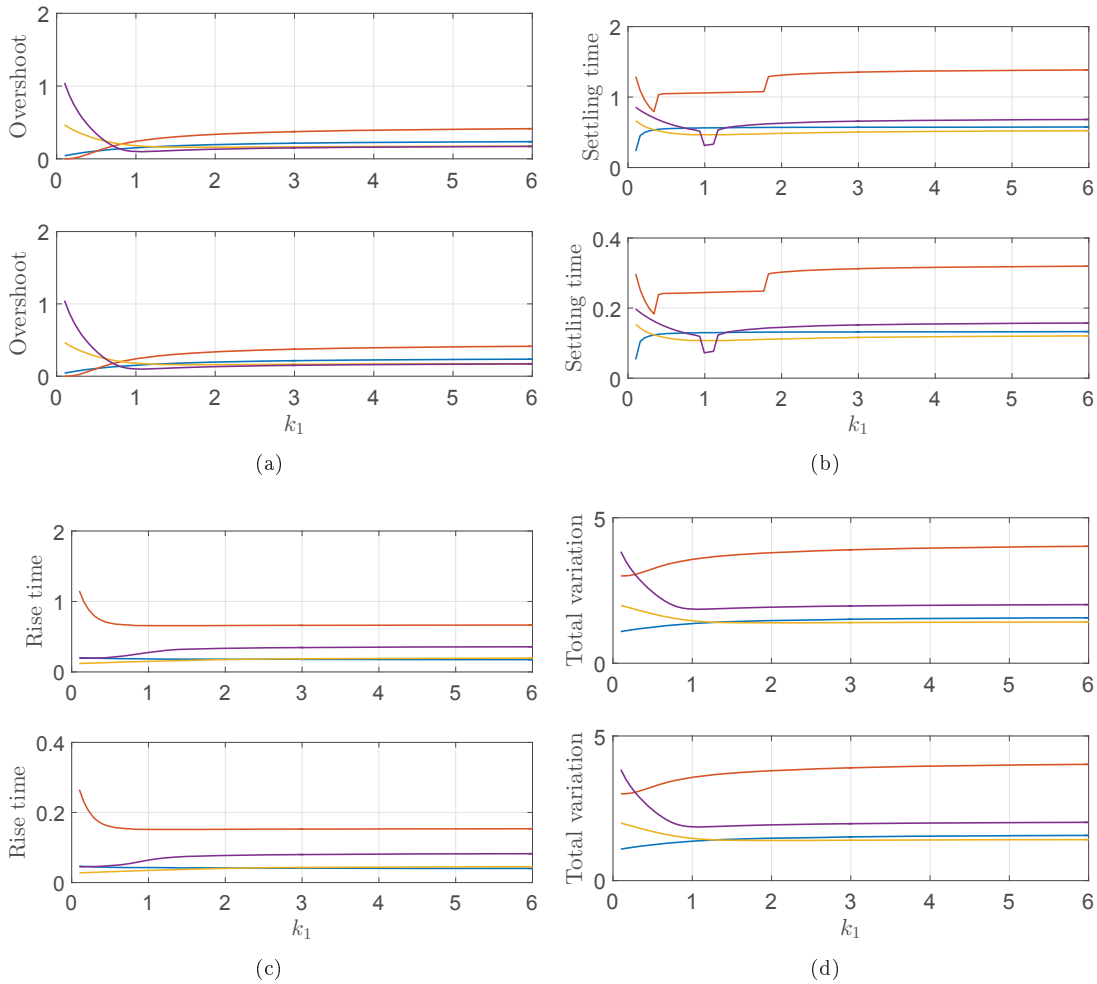

Figure C.1: The effect of k_1 on the performance of controller 1. The overshoot is shown in a), the settling time in b), the rise time in c) and the total variation in d). Different scenario's are considered, driving on a line and starting close to this line (blue) and starting far away from this line (orange). Also driving on a circle and starting close to the circle (yellow) and starting far away from the circle (purple) is considered. In the top figure the follower drives with a low velocity and in the bottom figure with a high figure.

In Figure C.2 the effect of k_2 is shown for the three different scenario's.

- Overshoot: No difference between driving with low or high velocity.
  - Line: the overshoot increases when k_2 increases. When $k_2 > 1.9$ for starting close to the line and when $k_2 > 1.7$ for starting with a large initial condition, the overshoot decreases again.
  - Circle: the overshoot increases when k_2 increases. When $k_2 > 1.9$ for starting close to the circle, the overshoot decreases creases again.
- Settling time: The effect of the controller gain is the same for both velocities.
  - The effect of k_2 is the same for both driving on a line and circle. The settling time decreases for an increase of k_2.
- Rise time: The effect of the controller gain is the same for both velocities.

- No difference between driving on a line and a circle. When k_2 increases, the rise time decreases.

- Total variation: No difference between driving with low or high velocity.
  - Line: the total variation increases when k_2 increases. When $k_2 > 2.8$ for starting close to the line and when $k_2 > 2$ for starting with a large initial condition, the overshoot decreases again.
  - Circle: the overshoot increases when k_2 increases. When $k_2 > 2.8$ for starting close to the circle the overshoot decreases again.

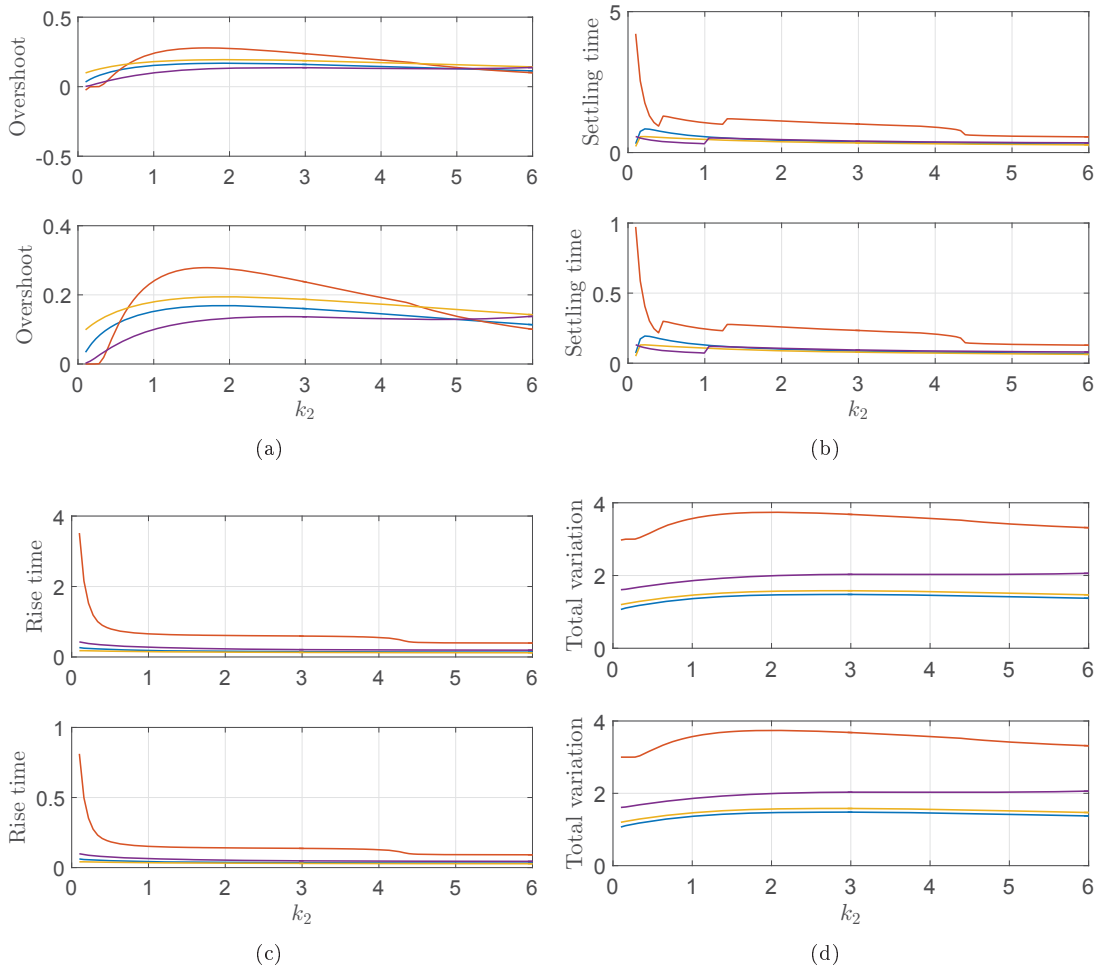

Figure C.2: The effect of k_2 on the performance of controller 1. The overshoot is shown in a), the settling time in b), the rise time in c) and the total variation in d). Different scenario's are considered, driving on a line and starting close to this line (blue) and starting far away from this line (orange). Also driving on a circle and starting close to the circle (yellow) and starting far away from the circle (purple) is considered. In the top figure the follower drives with a low velocity and in the bottom figure with a high figure.

In Figure C.3 the effect of k_3 is shown for the three different scenario's.

- Overshoot: No difference between driving with low or high velocity.
  - Is zero for $k_3 > 2$.

- Settling time: The effect of the controller gain is the same for both velocities.
  - The settling time decreases first and increases again when k_3 increases. The minimum of the settling time differs for the different scenario's. The minimum for driving on a line close to the line is $k_3 = 1.4$ and $k_3 = 1.6$ for a large initial condition. When driving in a circle the minimum is $k_3 = 1.2$ for starting close to the circle and $k_3 = 1$ when starting with a large initial condition.
- Rise time: The effect of the controller gain is the same for both velocities.
  - The rise time increases when k_3 increases.
- Total variation: No difference between driving with low or high velocity.
  - Is minimal for $k_3 > 2$.

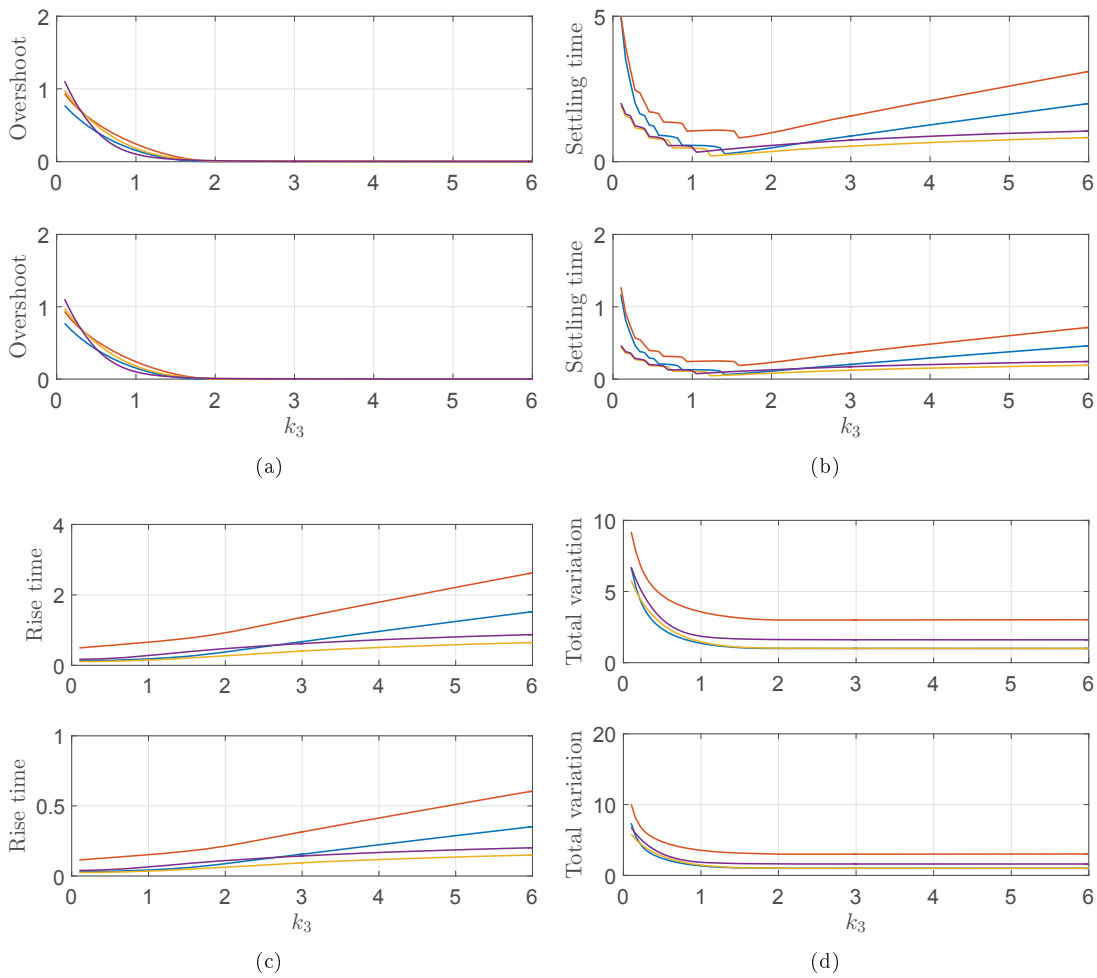

Figure C.3: The effect of k_3 on the performance of controller 1. The overshoot is shown in a), the settling time in b), the rise time in c) and the total variation in d). Different scenario's are considered, driving on a line and starting close to this line (blue) and starting far away from this line (orange). Also driving on a circle and starting close to the circle (yellow) and starting far away from the circle (purple) is considered. In the top figure the follower drives with a low velocity and in the bottom figure with a high figure.

C.1.2 Controller 2

In Figure C.4 the effect of a is shown for the three different scenario's.

- Overshoot: There is no difference between driving with a high and low velocity.
  - Line: a small a results in less overshoot. The increasing of the overshoot is larger for starting with a large initial condition.
  - Circle: a higher a results in less overshoot. There can be seen that for $a > 3$ the overshoot increases gradually again.
- Settling time: The effect of the controller gain is the same for both velocities.
  - Line: The settling time decreases minimal when a increases. When starting close to the line, the settling time is not affected.
  - Circle: the settling time decreases until $a = 1.3$ and then increases again when k_1 increases for starting close to the line. For starting with a large initial condition, the settling time decreases when a increases.
- Rise time: The effect of the controller gain is the same for both velocities.
  - The rise time is only affected for starting with a large initial condition from the line. The rise time decreases when a increases.
- Total variation: No difference between driving with low or high velocity.
  - Line: a small a results in smaller total variation.
  - Circle: a higher a results in smaller total variation. There can be seen that for $a > 3$ the overshoot increases gradually again.

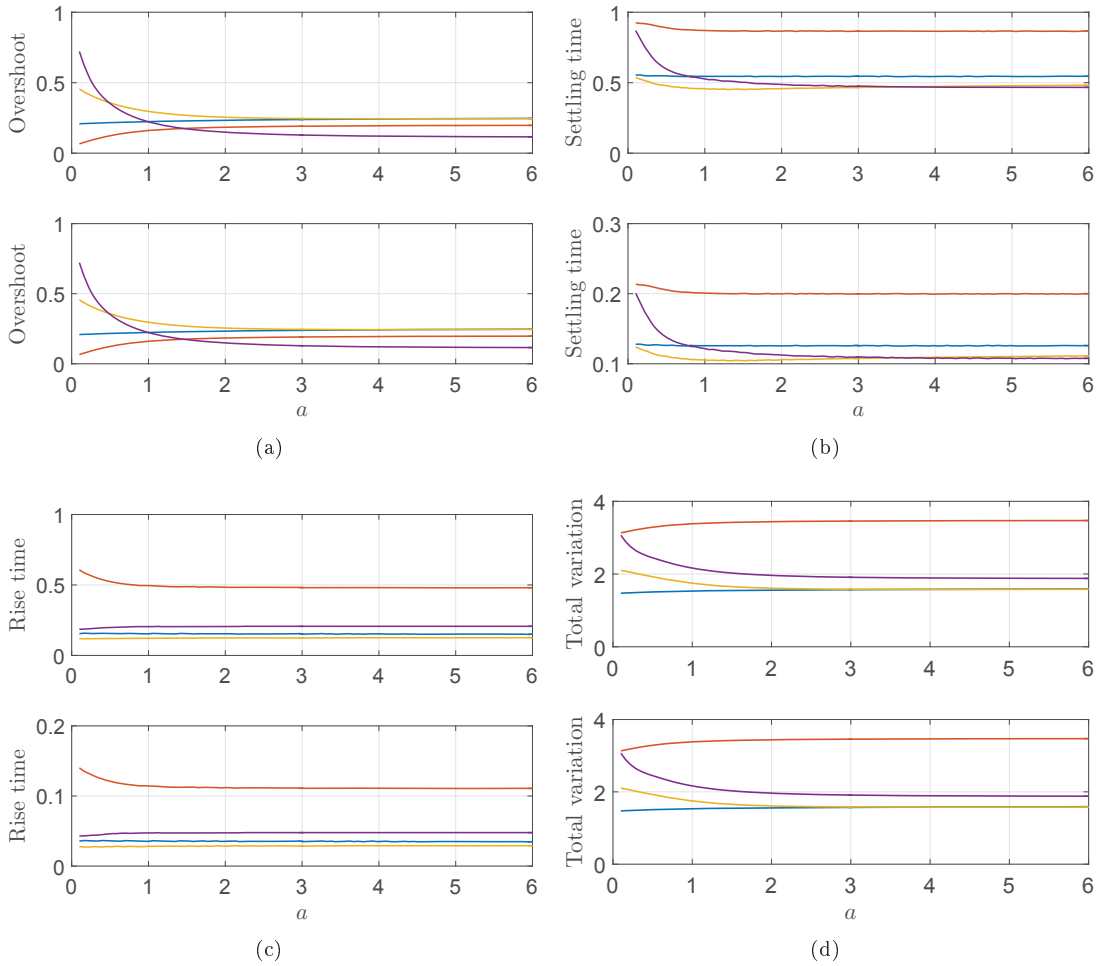

Figure C.4: The effect of a on the performance of controller 1. The overshoot is shown in a), the settling time in b), the rise time in c) and the total variation in d). Different scenario's are considered, driving on a line and starting close to this line (blue) and starting far away from this line (orange). Also driving on a circle and starting close to the circle (yellow) and starting far away from the circle (purple) is considered. In the top figure the follower drives with a low velocity and in the bottom figure with a high figure.

In Figure C.5 the effect of k_4 is shown for the three different scenario's.

- Overshoot: No difference between driving with low or high velocity.
  - Line: the overshoot increases when k_4 increases. When $k_4 > 1.7$ for starting close to the line and when $k_4 > 1.7$ for starting with a large initial condition, the overshoot decreases again.
  - Circle: the overshoot increases when k_4 increases. When $k_4 > 1.4$ for starting close to the circle and $k_4 > 1$ for starting with a large initial condition, the overshoot decreases again.
- Settling time: The effect of the controller gain is the same for both velocities.
  - The effect of k_4 is the same for both driving on a line and circle. The settling time decreases for an increase of k_4.
- Rise time: The effect of the controller gain is the same for both velocities.

- No difference between driving on a line and a circle. When k_4 increases, the rise time decreases.

- Total variation: No difference between driving with low or high velocity.
  - Line: the total variation increases when k_4 increases. When $k_4 > 2.6$ for starting close to the line and when $k_4 > 2.8$ for starting with a large initial condition, the overshoot decreases again.
  - Circle: the overshoot increases when k_4 increases. When $k_4 > 2.6$ for starting close to the circle and $k_4 > 1.7$ when starting with a large initial condition, the overshoot decreases again.

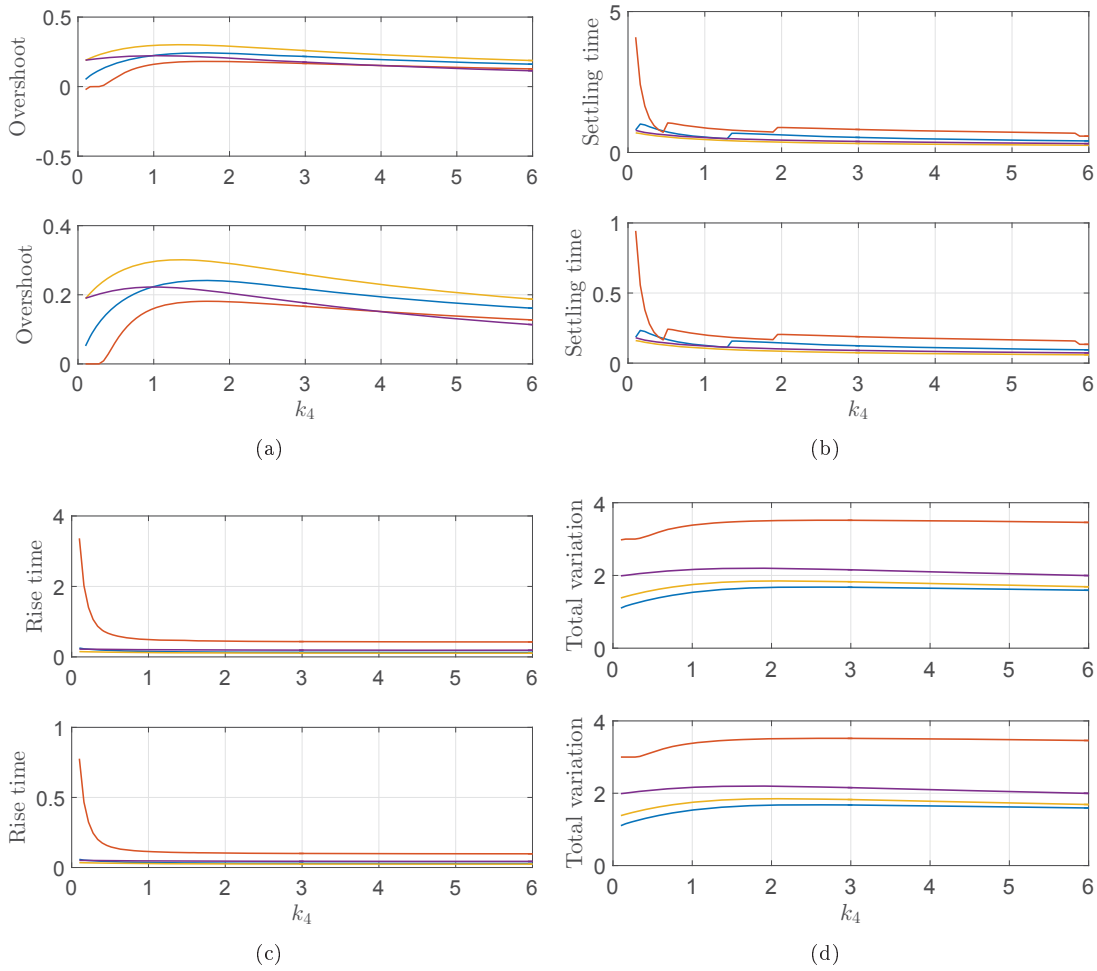

Figure C.5: The effect of k_4 on the performance of controller 1. The overshoot is shown in a), the settling time in b), the rise time in c) and the total variation in d). Different scenario's are considered, driving on a line and starting close to this line (blue) and starting far away from this line (orange). Also driving on a circle and starting close to the circle (yellow) and starting far away from the circle (purple) is considered. In the top figure the follower drives with a low velocity and in the bottom figure with a high figure.

In Figure C.6 the effect of k_5 is shown for the three different scenario's.

- Overshoot: No difference between driving with low or high velocity.
  - Line: Is zero for $k_5 > 2$.

- Circle: Is zero for $k_5 > 3$.

- Settling time: The effect of the controller gain is the same for both velocities.
  - The settling time decreases first and increases again when k_5 increases. The minimum of the settling time differs for the different scenario's. The minimum for driving on a line close to the line is $k_5 = 1.5$ and $k_5 = 1.4$ for a large initial condition. When driving in a circle the minimum is $k_5 = 1.7$ for starting close to the circle and $k_5 = 1.7$ when starting with a large initial condition.

- Rise time: The effect of the controller gain is the same for both velocities.
  - The rise time increases when k_5 increases.

- Total variation: No difference between driving with low or high velocity.
  - Is minimal for $k_5 > 2$.

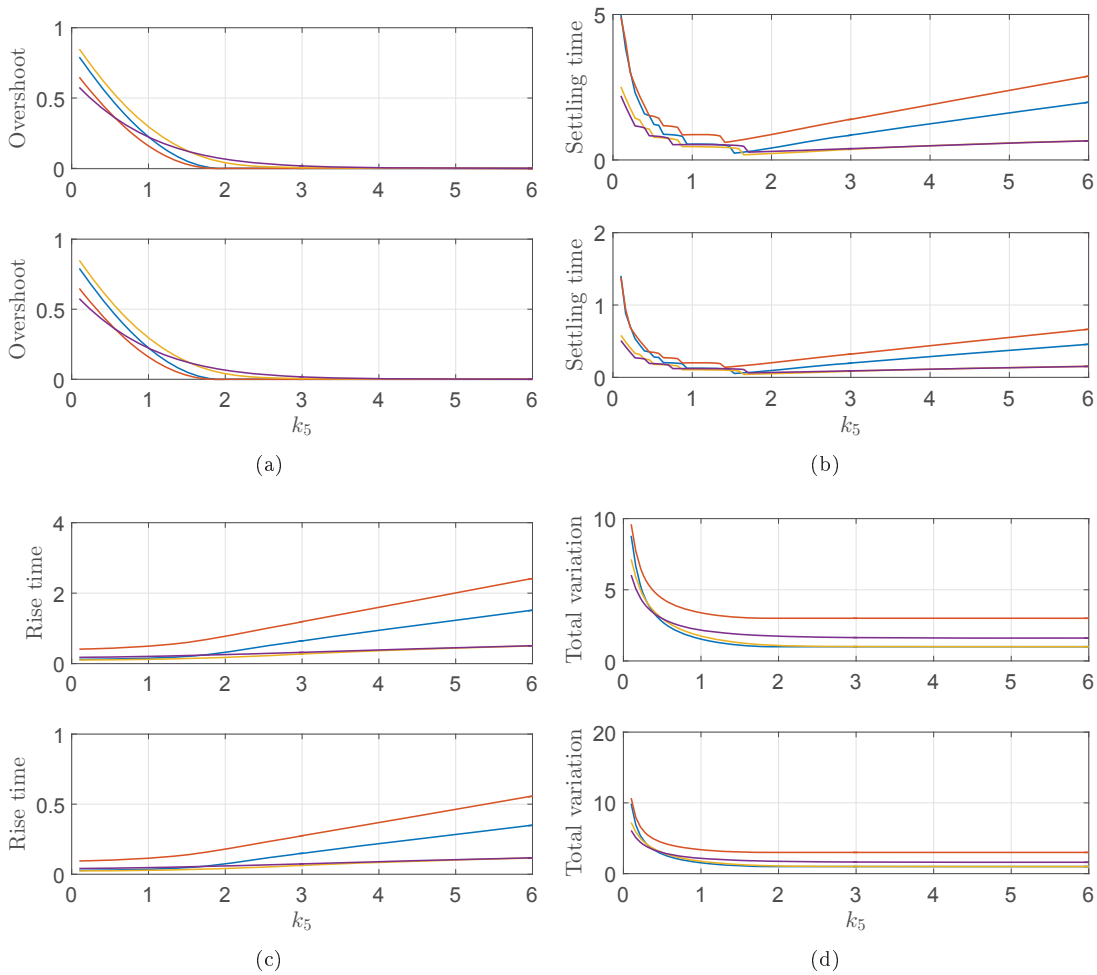

Figure C.6: The effect of k_5 on the performance of controller 1. The overshoot is shown in a), the settling time in b), the rise time in c) and the total variation in d). Different scenario's are considered, driving on a line and starting close to this line (blue) and starting far away from this line (orange). Also driving on a circle and starting close to the circle (yellow) and starting far away from the circle (purple) is considered. In the top figure the follower drives with a low velocity and in the bottom figure with a high figure.